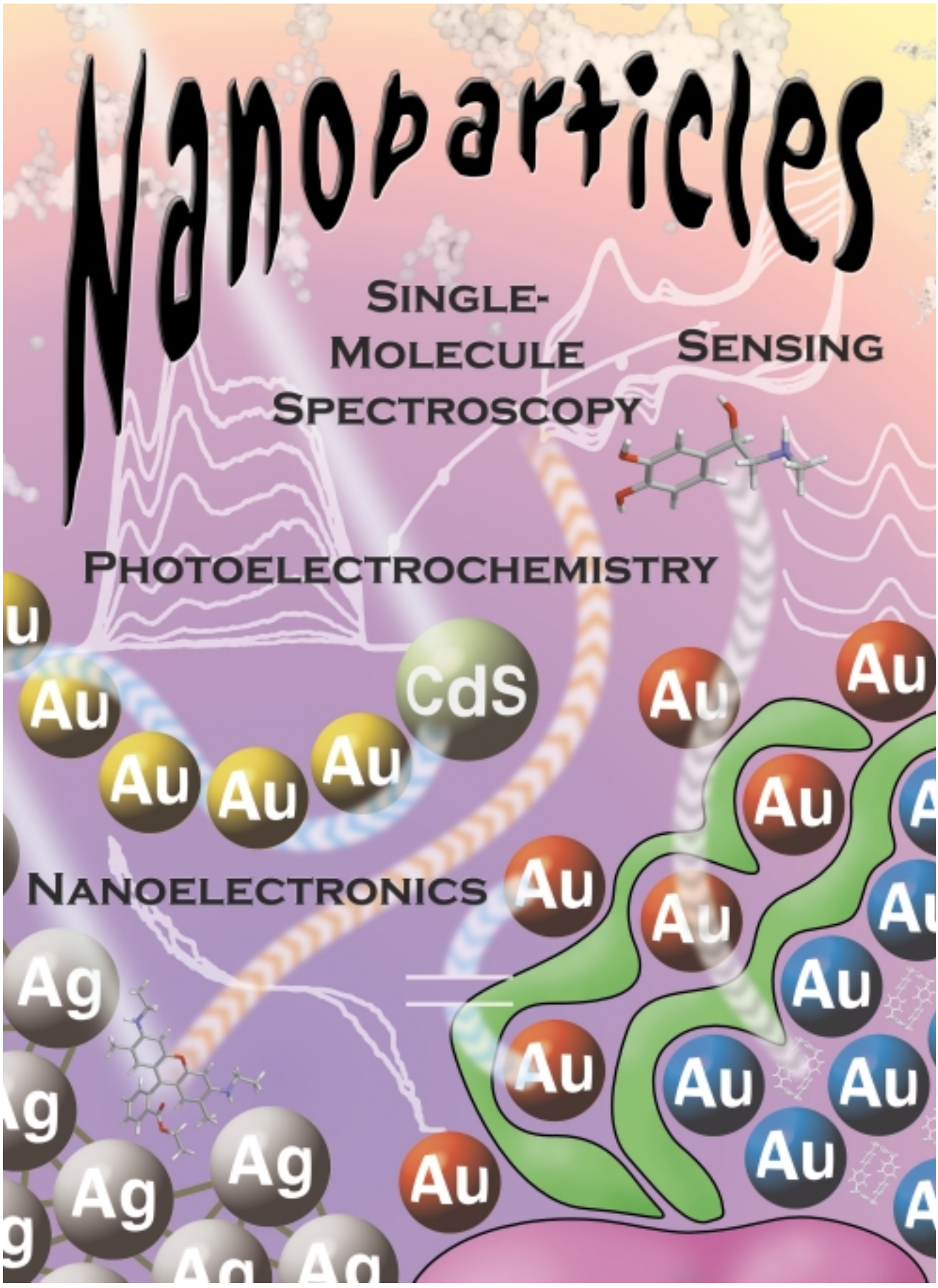

  1439-4235/00/01/01 $ 17.50+.50/0 CHEMPHYSCHEM **2000**, 1, 18 – 52

Nanoparticle Arrays on Surfaces for Electronic, Optical, and Sensor Applications**

Andrew N. Shipway,[a] Eugenii Katz,[a] and Itamar Willner*[a]

Particles in the nanometer size range are attracting increasing attention with the growth of interest in nanotechnological disciplines. Nanoparticles display fascinating electronic and optical properties as a consequence of their dimensions and they may be easily synthesized from a wide range of materials. The dimensions of these particles makes them ideal candidates for the nanoengineering of surfaces and the fabrication of functional nanostructures. In the last five years, much effort has been expended on their organization on surfaces for the construction of functional interfaces. In this review, we address the research that has led to numerous sensing, electronic, optoelectronic, and photoelectronic interfaces, and also take time to cover the synthesis and characterization of nanoparticles and nanoparticle arrays.

KEYWORDS:

colloids · interfaces · monolayers · nanostructures · sensors

1. Introduction

The emerging disciplines of nanoengineering,[1] nanoelectronics,[2] and nanobioelectronics[3] require suitably sized and functional building blocks with which to construct their architectures and devices. This need has encouraged the development of supramolecular,[4] biomolecular,[5] and dendrimer[6] chemistries for engineering substatnces of Ångström and nanoscale dimensions but, even with lithographic techniques now reaching the 100 nm range, the intermediate scale of 10 – 100 nm remains relatively unexploited (Figure 1). The world of colloid and cluster science[7] has risen to this challenge and is beginning to find ways to organize nanometer-sized particles on the micron and submicron scale. Although many of these particles have been known for a substantial time, it is only now that the tools for their engineering and characterization exist, which open the doors to new disciplines of nanoparticle and nanocrystal devices. Nanoparticles are not just convenient structural elements however, but can also display unique functions. They can be fashioned from many materials and have a wide functional diversity very different from bulk materials, with much of their electronic,[8, 9] optical,[7, 10–13] and catalytic[14] properties originating from their quantum-scale dimensions.[15]

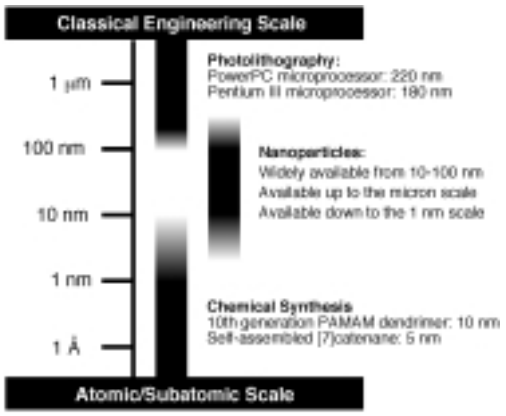

Figure 1. *Bridging the nanometer-size gap between photolithographic and synthetic chemical engineering—colloidal nanoparticles fit the bill.*

In order to tailor the new generation of nanodevices and "smart" materials, ways to organize the nanoparticles into controlled architectures must be found. This conundrum has been addressed to some extent by a large body of recent work describing the construction of colloidal dyads and triads,[16, 17] "strings",[18] clusters,[19] and other architectures[19–22] in solution and at liquid – liquid interfaces. These constructions will not be described in any detail here, since this review is dedicated to surface-bound nanostructures. Likewise, we will not explore the highly active research area of single-nanoparticle electronics in great depth, as excellent reviews already exist.[12, 15, 20] These single-electron devices tap into the quantum properties of nanoparticles for the fabrication of single-electron transistors[23, 24] and similar devices[25–27] from isolated, immobilized nanoparticles. Here, we will focus on efforts to construct organized nanoparticle arrays which perform tangible functions. These superstructures are formed on various solid supports by specific adsorption or self-assembly techniques. Although work on spin-coated, evaporated, or nonspecifically adsorbed nanoparticle films has yielded noteworthy results,[28] these techniques are conceptually macroscopic rather than nanoscopic and so will not be covered here.

The relevance of nanoparticle superstructures to the emerging areas of nanotechnology and nanophotoelectrochemistry, and to the development of nanoelectronics and "smart" materials cannot be underestimated. Colloidal particles offer a

[a] *Prof. I. Willner, Dr. A. N. Shipway, Dr. E. Katz*
Institute of Chemistry
The Hebrew University of Jerusalem
Jerusalem 91904 (Israel)
Fax: (+ 972) 2-6527715
E-mail: willnea@vms.huji.ac.il

[**] *Parts of our studies on nanoparticle arrays are supported by the Israel – U.S. Binational Science Foundation and the German – Israeli program (DIP).*

Itamar Willner

was born in 1947. He completed his Ph.D. studies in chemistry in 1978 at The Hebrew University of Jerusalem. After a postdoctoral stay with M. Calvin at the University of California, Berkeley, from 1978 to 1981 he joined the Institute of Chemistry at the Hebrew University of Jerusalem in 1982. In 1986, he was appointed as Professor at the Hebrew University. He is a fellow of the American Association for the Advancement of Science (AAAS), acts as a member of several editorial boards, and is the recipient of the Kolthoff Award and the Max Planck Research Award. His research interests include light-induced electron transfer processes and artificial photosynthesis, molecular electronics and optoelectronics, bioelectronics and biosensors, optobioelectronics, supramolecular chemistry, nanoscale chemistry, and monolayer and thin-film assemblies.

Eugenii Katz

was born in Moscow in 1952. He completed his Ph.D. in 1983 at the Frumkin Institute of Electrochemistry, Moscow, and acted as senior scientist at the Institute of Photosynthesis, Pushchino, until 1991. In 1991, he undertook postdoctoral research at the Hebrew University of Jerusalem and later (1993), as a recipient of a Humboldt scholarship, he worked at the Technische Universität, Munich. He joined the research group of Itamar Willner at the Hebrew University as Senior Research Associate in 1994. His research interests include electroanalytical chemistry, functionalized monolayers, biosensors and bioelectronics.

Andy Shipway

was born in 1971 in Bristol, UK. He studied for his B.Sc. at the University of Birmingham and stayed on as a Ph.D. student under the supervision of Professor J. Fraser Stoddart with a thesis entitled "Insight into Dendrimers and their Role in Catalysis". He joined the group of Itamar Willner at the Hebrew University in late 1997 as a postdoctoral fellow, coordinating projects inovolving organic synthesis and nanoparticle superstructures.

route to the simple assembly of complex structures and can be used to create a variety of electronic and sensor components. We should note that in this review, we use the terms "nanoparticle" and "colloid" as synonyms for nanosized particles of ambiguous structure, while we consider "nanocrystals" to be necessarily crystalline and "clusters" to have a defined stoichiometry.

2. Synthesis of Nanoparticle Arrays

The construction of nanoparticle arrays on surfaces has only gained significant attention in the last ten years. Nevertheless, the diversity of building blocks, architectures, and construction techniques that have been reported is impressive.[19, 29] This research has also spurred on efforts to synthesize colloids from new materials and with novel surface functionalities. The construction of two-dimensional colloid arrays is well studied. This groundwork has led to methods for the synthesis of much more complex three-dimensional systems and patterned arrays, which may eventually lead to highly functionalized assemblies and composites.

2.1. Synthesis of Colloidal Nanoparticles

Many colloidal nanoparticle syntheses have been known for a considerable amount of time[30, 31] but, more recently, a body of work has grown that is dedicated to nanoparticle syntheses specifically for the construction of devices and nanostructures. These particles may consist of a particular material, be of a particular size, or have specialized surface functionality. It has even become possible to have some degree of control over the nanoparticle shape.[32] Nanoparticles tend to be fairly unstable in solution, so special precautions have to be taken to avoid their aggregation or precipitation. Glassware is cleaned thoroughly, while reagent solutions and solvents are all filtered and of the highest purity. All nanoparticle syntheses also involve the use of a stabilizing agent, which associates with the surface of the particle, provides charge or solubility properties to keep the nanoparticles suspended, and thereby prevents their aggregation.

2.1.1. Reductive Synthesis of Noble Metal Colloids

The simplest and by far the most commonly used preparation for gold nanoparticles is the aqueous reduction of $H[AuCl_4]$ by sodium citrate at reflux.[31, 33] Although sodium citrate is the most common reducing agent, metal nanoparticles can also be synthesized by the use of borohydride and other reducing agents.[31–34] The application of alcohols as reductants for the production of platinum nanoparticles allows control over the size of the particles: Higher alcohols yield larger particles, which indicates that a more rapid reduction rate of the $[PtCl_6]^{2-}$ ions is an important factor for the production of smaller particles.[35]

Particles synthesized by citrate reduction are nearly monodisperse spheres of a size controlled by the initial reagent concentrations (Figure 2 and Table 1).[36] They have a negative surface charge as a consequence of a weakly bound citrate

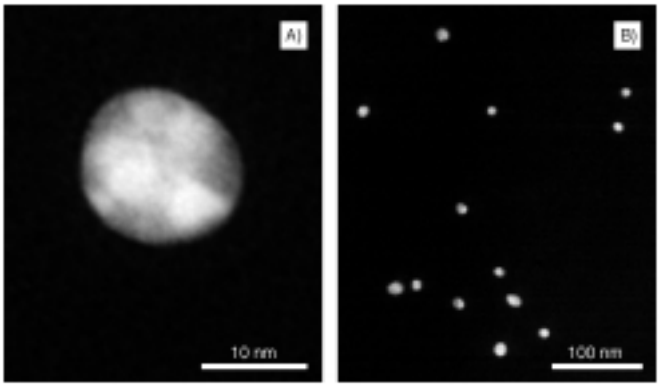

Figure 2. *Gold nanoparticles synthesized by citrate reduction. A) A single particle at high magnification shows its highly spherical shape. B) A region of single nanoparticles at a lower magnification shows the monodispersity of particle sizes.*

Table 1. *The dependence of nanoparticle diameter on citrate concentration in the reductive synthesis of gold nanoparticles.[a]*

Citrate solution added[b] [mL]	Diameter[c] [nm]
1.0	16
0.75	25
0.5	41
0.3	72
0.21	98
0.16	147

[a] Data is taken from reference 34. [b] Trisodium citrate (1% aqueous solution) was added to 50 mL refluxing solution of 0.01% $H[AuCl_4]$. [c] Particle diameters were measured by SEM.

coating and are easily characterized by their plasmon absorbance (at about 520 nm for 15 nm particles; see Section 3.2). Nanoparticles of other noble metals may also be prepared by citrate reduction, such as silver particles from $AgNO_3$, palladium from $H_2[PdCl_4]$, and platinum from $H_2[PtCl_6]$.[37, 38] The similarities in the preparation of these different metal colloids allows the synthesis of mixed-metal particles, which may have functionality different from each individual metal.[30] For example, the reduction of suitable mixtures of noble metal salts can lead to "alloy" or "mixed grain" particles. More interestingly, composite particles can be built up in "shells" by the synthesis of a small colloidal nuclei followed by its enlargement with a different metal: a gold colloid can be covered with silver.[39] Well defined core/shell organosilicon micronetworks with topologically trapped gold particles have also been prepared using a molecular reactor technique.[40] Metallic nanoparticles can be capped with various shells, such as conductive, nonmetallic graphite,[37] or semiconductive CdS.[42] This capping can be done in situ if the reductive formation of nanoparticles is performed in the presence of the shell-forming material[37] or the shell can be organized later through a chemical reaction on the surface of the nanoparticle.[42] The enlargement of a nanoparticle can take place even after the colloidal "seed" particle has been immobilized on a substrate. In such cases, a colloid-functionalized glass substrate is introduced to a gold-[43] or silver-[44] depositing solution, to thereby enlarge the surface-bound nanoparticles and provide a method of control over their size and density. Such "core – shell" particles have been studied extensively because their properties can differ from those of the core or shell materials.[40, 41, 45]

The synthesis of particles that bear surface functionality is desirable for the purpose of nanoparticle handling and the construction of functional architectures. This functionalization of the nanoparticle surface can be accomplished during the nanoparticle synthesis by the addition of a suitable agent to the reaction vessel. As the nanoparticles form, the surface functionalization agent attaches to the nanoparticles, which also imparts an enhanced stability and gives additional control over their size. The borohydride reduction of $H[AuCl_4]$ in the presence of (γ-mercaptopropyl)-trimethoxysilane gives rise to very small (1 – 5 nm) gold nanoparticles which bear a surface silane functionality.[46] Other borohydride reductions in the presence of thiols[47] have produced nanoparticles with a surface functionality from amines to carboxylic acids. Where the surface-functionalization agent is not water soluble, a two-phase synthesis can be used, as in the preparation of long-chain alkanethiol surfaces on gold colloids.[48] The surface-functionalization agent does not even need to bind covalently with the nanoparticle. Nanoparticles have been synthesized in the presence of dendrimeric[49] and polymeric[50–52] stabilizers, and have been formed in the cavities of micelles[53] and silicate sols.[54] Gold and silver nanoparticles functionalized by adsorbed dialkyl disulfides have also been generated in the presence of sodium borohydride.[55] Disulfides offer the advantage that asymmetrical disulfides, that have two distinct functional groups (RSSR'), may be used, which enables the possibility of generating mixed, self-assembled monolayers (SAMs) that possess a homogeneous distribution of functional groups or chain lengths. The use of disulfides also allows the functionalization of nanoparticles with groups such as quinones that are otherwise incompatible with thiols (normally, a thiol would be used rather than a disulfide). The application of different capping materials or the preparation of mixed bimetallic particles allows control of the size and shape of the nanoparticles.[32, 56] For example, platinum nanoparticles with cubic, tetrahedral, polyhedral, or irregular-prismatic shapes could be generated selectively when the initial concentrations of $[PtCl_6]^{2-}$ and polyacrylic acid were varied for the reductive particle formation.[32]

2.1.2. Synthesis of Semiconductor Nanoparticles

The production of semiconductor nanoparticles and their organization on solid supports is of great importance for the fabrication of nanoelectronic devices. The quantum properties of these particles have potential uses in information-processing devices and, in recognition of this, they are often called "Q particles".[15] By far the most studied of these are cadmium sulfide particles.[57] These and related colloidal particles (for example, PbS,[58] Ag_2S,[59] CdSe,[23] and TiO_2[60, 61]) can be prepared relatively easily by using inverse micelles as nanoscale reaction vessels.[62] Firstly, solutions of inverse micelles are prepared, one containing the metal salt (usually as the chloride) and the other containing Na_2S (or Na_2Se for the production of CdSe, and so

forth). These solutions are mixed together and nanoparticles form as the different micelles exchange their contents (Scheme 1). Alternatively, the sulfide can be introduced as H_2S gas. After the particles are formed, they may be stabilized by the addition of a thiol, which bonds to the surface of the nanoparticle and may also contain other functionalities.[63, 64] If a mixture of thiols is used, nanoparticles with a mixture of surface

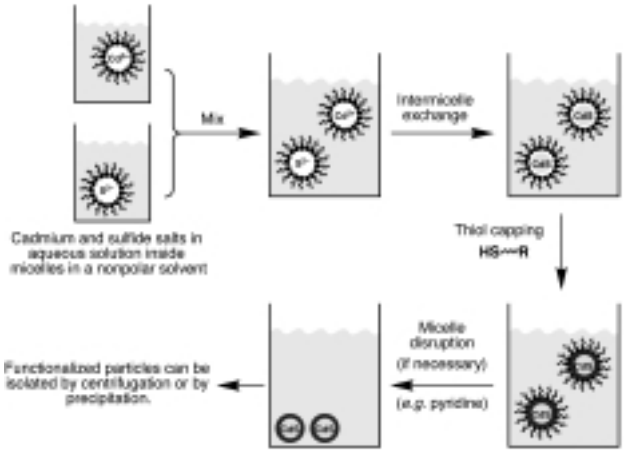

Scheme 1. *The synthesis of CdS particles inside inverse micelles, their capping by thiol molecules, and their recovery from the reaction mixture.*

groups are produced.[65] The particles may be isolated after disrupting the micelles (provided that this has not already taken place in the stabilization step). The synthesis of CdS nanoparticles gives a highly monodisperse product but for some other materials, such as PbS, the procedure gives particles with a much wider size distribution. Several metal-sulfide nanoparticles have also been synthesized by a similar route involving a polymer (rather than micellar) stabilizer,[66] and related cadmium compounds have been synthesized from organometallic reagents.[67, 68] Other semiconductor nanoparticles of interest include gallium nitride[68] and titania; nanoparticles of the latter can be synthesized either by precipitation[61, 69] or in micelles.[60]

2.1.3. Other Techniques for Nanoparticle Synthesis

Smaller nanoparticles may be formed in the gas phase,[70] or by ablation using high peak-power laser pulses,[71, 72] while others have been etched,[73, 74] electrodeposited,[75] or synthesized[76, 77, 79–81] directly onto surfaces, or in Langmuir – Blodgett (LB) layers.[82] These techniques cater for the specialized needs of researchers who require colloids of particular sizes, shapes, or materials. For the cheap and easy synthesis of simple nanoparticles, there is no substitute for solution-state synthesis, which can be used to prepare bulk quantities without the need for specialized laboratory apparatus.

2.2. Assembly of Nanoparticle Monolayers

This Section details the first step in the production of colloid interfaces—their ordered immobilization on a solid support. Nanoparticles have been assembled on a wide variety of substrates, sometimes by highly ingenious means, such as the association of a streptavidin-functionalized colloid to a biotin-functionalized surface,[83] but true nanoengineering requires nanoscale control, namely, control over the morphology of nanoparticle packing on the surface. This requirement is finally becoming a reality with new research into the ordering of adsorbed particles, which brings new applications to light, such as the use of nanoparticles as nanoscale "masks" for the lithography of surfaces.[84, 85] It should be noted, that one should expect some nonideality even from networks of nanoparticles with a very narrow size distribution (variation of less than 10%). Theoretical considerations of nanoparticle lattices using a Hamiltonian based on a Hückel-type, tight-binding approximation concludes that they have a configurational disorder and can never be identical.[86]

2.2.1. Assembly by Adsorption on Glass Substrates

Glass substrates may be conductive (such as indium- or fluorine-doped tin oxide—ITO or "K-glass") or nonconductive (such as quartz or soda glass) but are all characterized by their transparency and the availability of surface -OH functionality. Glass substrates allow simple spectroscopic and electron microscopic characterization of thin films and are also advantageous on account of their high rigidity and low cost. The polymerization of a thin film of a trialkoxysilane on the substrate is usually carried out to produce a useful surface functionality (Scheme 2).[71, 83, 87–90] This is a general method, which can be applied to a variety of surfaces, and has been reviewed in detail.[91, 92] The surface must first be scrupulously clean in order to ensure the maximum number of exposed surface OH groups. This is achieved by oxidative cleaning in acidic solution (often "piranha solution", HCl/HNO_3 3/1) and rinses of various solvents. The clean substrate is then immersed in a solution of the siloxane. The conditions for this reaction vary widely and depend upon the desired properties of the film and the nature of the substrate. While quartz and soda glass are relatively easy to functionalize, K-glass substrates normally require much harsher conditions to obtain a similar silane coverage. For characterization by atomic force microscopy (AFM), a very smooth and flat surface is required, so the minimum amount functionalization is used. For electrochemical analysis, an overly thick siloxane film may also be disadvantageous as it insulates and hampers electrical communication between the electrode and the colloid. At the opposite extreme, if a colloid array is to be characterized only by spectroscopy, a very extensive functionalization is advantageous in order to provide the best possible surface for nanoparticle adsorption.

The functionalized glass surface bears chemical groups that are capable of binding a colloid particle either covalently (for example, a thiol to bind gold colloids) or through electrostatic interactions (for example, an quaternary amine to bind anionic particles). The formation of a colloid monolayer is achieved by placing the surface-functionalized substrate in a solution of the nanoparticle, which adsorbs onto the surface and assembles into a saturated monolayer with time. The monolayer density is

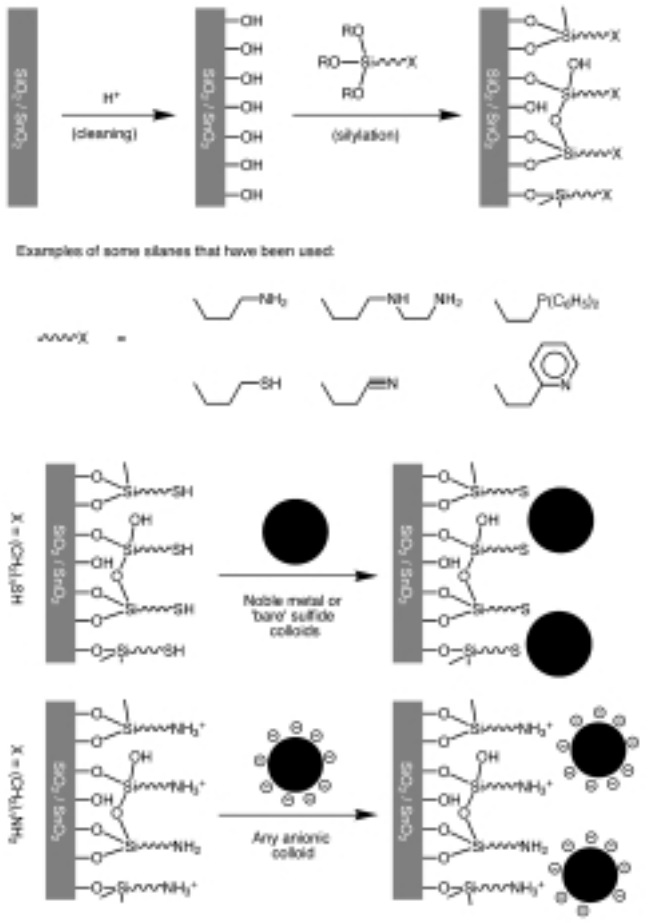

Scheme 2. *The construction of gold-nanoparticle monolayers on glass substrates by adsorption onto a thin film of polymerized siloxane. Top: Modification of the surface of the glass. Middle: A selection of surface-modifying silanes. Bottom: Adsorbtion of the nanoparticles. R = Me, Et.*

dependent on factors such as the size and charge of the particles as well as the attachment method and the substrate.[93] In a study of citrate-stabilized gold nanoparticles assembled on amine- and thiol-functionalized ITO glass surfaces, it was found that 80 nm particles formed layers over 20 times less dense than 15 nm particles (approximately 2×10^9 80 nm particles, as opposed to about 4.5×10^{10} 15 nm particles, per cm^2).[88] This result is supported by an optical reflectometry study of the adsorption of (negatively charged) silica nanoparticles on an aminopropyl silane-functionalized support.[94] The initial rate of nanoparticle adsorption was found to decrease with increasing particle size. Amine-functionalized substrates bind the particles at a slightly higher density than thiol-functionalized substrates. The dynamics of monolayer assembly has been followed directly by quartz-crystal microgravimetry (QCM)[95, 96] and spectroscopy[97] and, for the case of citrate-capped gold particles, occurs over a period of a few hours.

2.2.2. Assembly on Metal Substrates

Assembly of nanoparticles on gold substrates often follows a similar procedure to that for glass substrates, namely, surface modification of the substrate followed by the adsorption of colloidal particles. The modification of the gold surface can be achieved by use of a thiol,[98] which forms a covalent link to the gold surface (Scheme 3). The thiol also bears a group capable of binding to a nanoparticle, for instance, another thiol moiety for CdS or Pt particles,[99] an amine or thiol for Au particles,[100] or a carboxylic acid for TiO_2 particles.[61] Aluminium surfaces are easily functionalized by carboxylic acids (Scheme 3) and thus colloids may be immobilized on them by modification of either the nanoparticles or the surface with a carboxylic acid attached to a colloid-binding group (such as a thiol for gold nanoparticles).[101, 102]

Electrically conductive substrates also allow the possibility of particle adsorption by electrophoretic means.[35, 51, 103] In this procedure, the gold nanoparticle surface is first treated with an alkanethiol in order to lower the surface charge. The particles are then deposited onto the anodic surface under relatively low potentials and are subsequently desorbed if the electrode polarity is reversed. The monolayers formed have extremely regular structures but, since the particles are not truly adsorbed to the substrate, the structures exhibit low stabilities. Real electrocatalyzed adsorption can be accomplished by the use of functionalized nanoparticles. Reduced viologen is known to adsorb strongly to gold electrodes and thus viologen-functionalized gold colloids can be electrochemically activated to form a monolayer on a QCM surface.[104] When the viologen units are subsequently oxidized, the monolayer is released from the electrode surface.

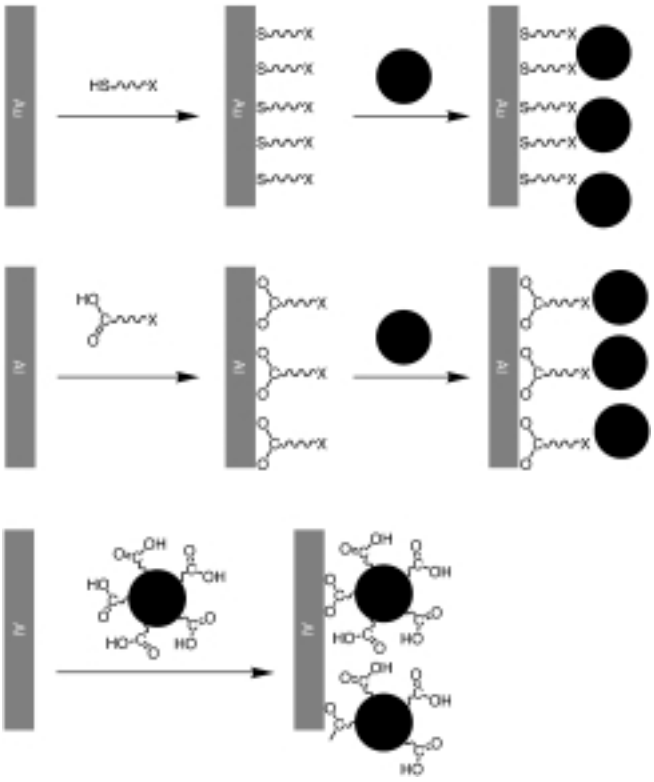

Scheme 3. *The construction of nanoparticle monolayers on Au and Al substrates, accomplished by modification of either the substrate or the nanoparticle.*

2.2.3. Assembly on Carbon Substrates

The electrochemical deposition of metal nanocrystals onto carbon electrodes has been the subject of a large number of investigations,[105, 106] as this type of interface is of great importance to electrocatalysis and as a model system for electroplating. The focus of many of these studies has been on the early stages of electrochemical deposition in order to elucidate the nucleation and growth mechanisms of the metal phase on the substrate (usually a glassy carbon electrode). The mechanisms of electrochemically assisted deposition of metal nanoparticles include the electrochemical reduction of the respective salt (such as $[AuCl_4]^-$ for gold deposition), primary formation of ad-atoms, and the further growth of nanocrystals on the carbon electrode. The overall surface area of gold, as well as the nanocrystal size, density, and surface texture, can be controlled by the variation of deposition conditions (the bulk concentration of the salt and the overpotential applied).[106] A combination of electrochemical and chemical steps allows the formation of sulfur-capped CdS nanocrystals onto a graphite support.[107–109] This procedure includes the electrochemical reduction of Cd^{2+} ions to form metallic Cd^0 precursor particles on the electrode surface. Improved size monodispersity[109] was achieved by the deposition of cadmium precursor particles through a series of 8 – 12 ms deposition voltage pulses separated by 1 – 5 s "mixing" periods during which growth was suspended, instead of a single, long deposition pulse that usually results in a very wide size distribution. After their formation, these metallic particles were electrochemically oxidized to form hydroxylated nanoparticles. Finally, (the chemical step) OH^- anions associated with the nanoparticles were displaced by S^{2-}, to produce CdS capped with a polysulfide shell. These sulfur-capped CdS nanoparticles exhibited photoluminescence emission line widths of 15 – 35 meV at 20 K,[109] which are much narrower than those observed for widely size-distributed CdS particles (125 – 180 meV).[107]

2.2.4. Other Techniques

The assembly of negatively charged nanoparticle layers on adsorbed polycationic polymer films such as poly(ethyleneimine) or poly(diallyldimethylammonium chloride) (PDDA) is of significance. This methodology is very general and yields successful results for metallic,[110, 111] semiconductive,[65, 112] silica,[113] and even mineral[114] nanoparticles. Techniques for the construction of thin polymer films are very well known[115] and allow the construction of nanoparticle arrays almost irrespective of the substrate material. Similarly, nanoparticles have been assembled on polyamidoamine (PAMAM) dendrimer films.[116, 117] Surfaces have also been prepared for nanoparticle organization by the formation of Langmuir – Blodgett films.[118] This method gives very thin and dense sublayers but is not suitable for the large-scale production or shaped substrates. The Langmuir – Blodgett technique and a similar "surface-tension driven" method[119] have also been used for the direct assembly of nanoparticle layers. The nanoparticles can be immobilized at the air – water interface either within a "carrier" monolayer (for instance, negatively charged silver colloids have been immobilized in positively charged fatty amine monolayers)[120] or by virtue of their own properties.[120–122] Langmuir – Blodgett films enable a very high degree of control over the nanoparticle density and ordering, since the monolayer can be manipulated prior to the assembly of the particles on the substrate,[123] but their formation has neither the generality nor the ease of the self-assembly methods.

Other monolayer syntheses are less developed. We have already seen that arrays of nanoparticles can be etched[73, 74] or grown[76, 77, 80] directly on surfaces. It is also possible to synthesize nanoparticles that are prelinked to surface by the immersion of a suitably functionalized substrate in the nanoparticle-generating reaction vessel.[124] If a thiol-functionalized substrate is placed in the reaction vessel during CdS colloid synthesis, then the nanoparticles bind to the surface as they form. This is advantageous, since fully formed CdS particles are usually stabilized by a thiol layer which then inhibits the particle from binding to a substrate. In addition, easy control over the particle size is possible but this method yields only very poor coverage. Finally, there are several examples of nanoparticles that have been assembled on the surface of other, larger nanoparticles.[22, 39, 125–127] The synthetic routes employed are usually analogous to those used for assembly on bulk substrates (such as electrostatic, biotin/avidin,[128] DNA/complementary DNA,[16, 22, 129–131] protein/carbohydrate,[132] or nonbiological host/guest[133] interactions) but the whole process usually proceeds in solution. These solution-state architectures are of great interest to the field of nanoengineering but will not be covered here.

2.2.5. Monolayer Ordering

We have already seen that monolayers formed by electrophoresis can have very regular, close-packed structures. Similar results can be obtained from the evaporation of colloid solutions on substrate surfaces under carefully controlled conditions[134] but other methods of monolayer formation tend to give less organized films with lower coverage. The particle density of electrostatically produced monolayers is dependent on factors such as the particle size[88] and surface charge—the particles in these films are usually well spaced, since their charges prevent close contact with each other. Citrate-stabilized gold nanoparticles normally give around 30% adsorption coverage for 12 nm particles[89, 97] but closer packing can be achieved by the neutralization of their surface charge (Scheme 4). If a thiol-bound monolayer of citrate-stabilized colloids are exposed to a solution of an alkanethiol, then the alkanethiol displaces the citrate and thereby neutralizes the particle's charge (Scheme 4 A). After this procedure, additional nanoparticles can be adsorbed in the spaces between those in the original layer, as electrostatic repulsion no longer inhibits their approach.[97] Continued cycles of neutralization and nanoparticle adsorption leads to a dense monolayer with interparticle spacings controlled by the choice of the alkanethiol.[110] A similar procedure on an amine-functionalized substrate can even coax the nanoparticles into reorganizing themselves (Scheme 4 B).[87] In this case, when the citrate

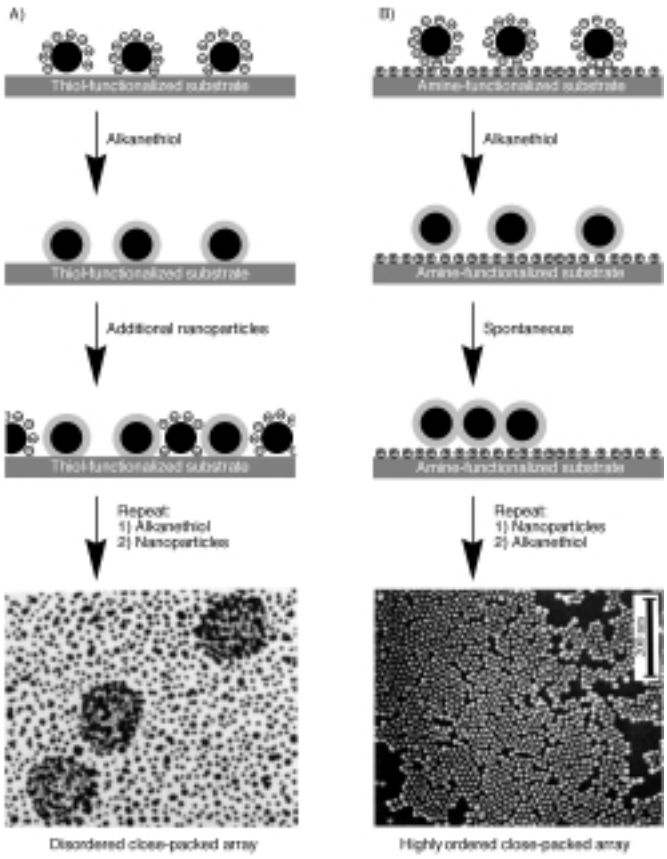

Scheme 4. *Control over interparticle spacing and packing. A) Assembly of a high density monolayer by the neutralization of the nanoparticle surface charge. B) Assembly of a "crystallized" monolayer by loosening the nanoparticle – substrate bond, which allows particle reorganization. Micrographs in (A) and (B) are reproduced from refs. [97] and [87], respectively, with permission.*

layer is removed from the nanoparticles, their electrostatic bond to the substrate is substantially weakened. The freed nanoparticles can then self assemble into highly regular, hexagonally packed structures on the surface, while further neutralization and adsorption cycles give rise to highly ordered surfaces. These monolayers suffer low stabilities, however, as a consequence of the loss of binding between the particles and the surface. Other studies have generated crystallized monolayers through carefully optimized conditions for the colloid deposition[135] or very dense but uneven layers by the aggregation of the colloid solution prior to its deposition.[89] More widely spaced nanoparticle matrices and other superstructures[136] can be constructed with the help of templates. Self-assembled, organized bacterial monolayers have been used as substrates for the adsorption of CdS nanoparticles.[137] The particles only adsorb in the pores between the bacterial subunits, which leads to morphologically controlled wide matrices that are suitable for the construction of addressable device arrays.

2.3. Assembly of Nanoparticle Multilayers

In order to assemble nanoparticle multilayers, a monolayer must be "primed" in some way for the adsorption of the second (and subsequent) particle layers. This priming may be little more than a modification of the surface layer or it may involve its functionalization with another component. The forces used to hold such structures together are either covalent or ionic—although specific interactions, such as DNA duplex formation[16, 22, 129, 130] and biotin/avidin complexation,[128] have been used to form interparticle complexes in solution; such approaches are in their infancy for the construction of a multilayers.[277] Architectures may also be much more complicated than simple alternating layers, and may contain different layers, which consist of different types of nanoparticles[99, 113, 138] or crosslinkers,[131, 139] leading to designed functional materials.

2.3.1. Polymer-Linked Architectures

The polymer-linked nanoparticle multilayer arrays constructed to date have focused on anionic colloidal nanoparticles (usually of gold), although other examples (such as hydroxide-functionalized gold particles crosslinked by titania[141]) do exist. The charge on anionic particles allows them to adsorb onto cationic polymers and vice versa, allowing three-dimensional structures to be built up in a stepwise fashion. Scheme 5 shows how a polymer – colloid multilayer composite can be constructed by

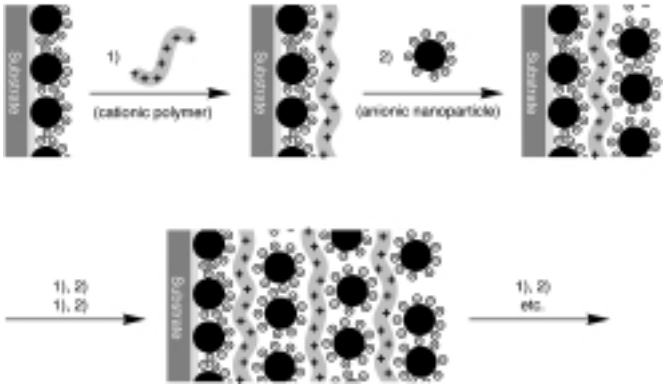

Scheme 5. *The construction of polymer – colloid multilayers by the exploitation of electrostatic interactions between anionic nanoparticles and cationic polymers.*

the exploitation of electrostatic interactions. The base colloid layer has a net negative charge, so facilitates the assembly of a thin film of a polycationic polymer. In turn, the polymer layer leaves a surface positive charge, on which a second colloid layer is assembled; subsequent layers are built likewise. Polymers that have been used include PDDA,[37, 65, 113, 123, 142] among others,[111, 131, 140] and a wide range of colloidal materials, such as gold,[111, 131] silver,[37] semiconductors,[65] and silica,[113, 142] have been utilized. Although these architectures are only stabilized by ionic interactions, they tend to be highly stable in almost any solvent and require physical scratching or chemical reaction to damage them. Polymer – nanoparticle assemblies hold great promise for the construction of nanoscale electronic devices. Polymer layers can be of controllable thickness, which isolates

colloid layers from each other by whatever distance is required, and they may also be conducting, semiconducting, or insulating.

The characteristics of the colloid layers can be controlled by the conditions at which they are adsorbed. A QCM study of PDDA-crosslinked silica colloid (mean 45 nm) grown in layers showed that lower colloid concentrations or the presence of other electrolytes in the colloid solution caused a lower coverage for each layer. These measurements were highly reproducible over many consecutive layers.[113] Careful control over the adsorption time can also prove important. For the same system, sufficient colloid adsorption for a new polymer layer to be laid requires as little as two seconds, even though it requires over ten seconds to achieve colloid saturation.[142]

2.3.2. Other Electrostatically Linked Architectures

The assembly of electrostatically linked nanoparticle arrays is a general method which has been shown to be effective up to micron dimensions.[143] Nanoparticle arrays can be constructed from any charged nanoparticle and an oppositely charged "crosslinker" in an analogous way to the construction of colloid – polymer architectures (Scheme 6). The "crosslinker" may be anything from a small molecule[144] to another nanoparticle[145, 151] but it must bear multiple charges so it can simultaneously interact with the colloid layers both above and below it. Aggregation of gold nanoparticles mediated by C_{60} can be used to construct a C_{60}/Au multilayer with unusual optical and electronic properties.[146] The origin of the interaction between gold particles and fullerene molecules is still unclear but it has been suggested that it involves an electron transfer process between the organic and inorganic components of the array.

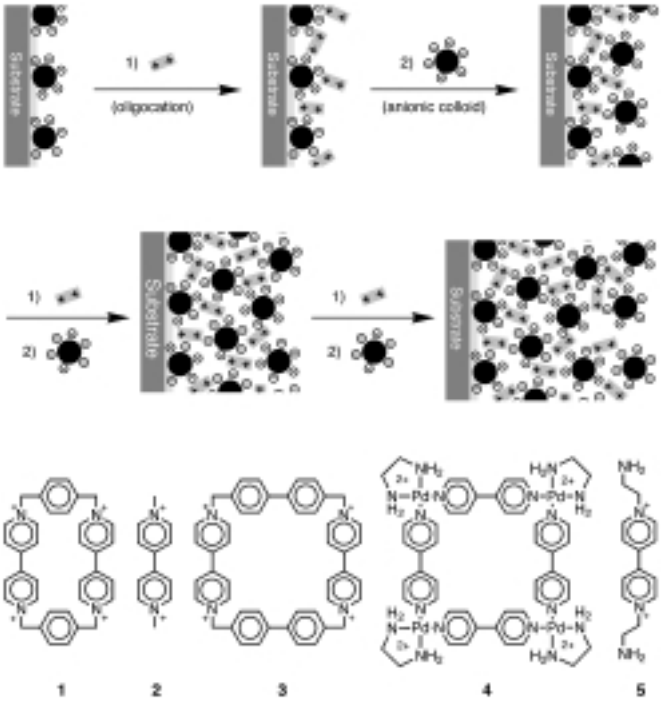

Scheme 6. *The construction of molecular oligocation/anionic colloid multilayers by the exploitation of electrostatic interactions, with examples of some bipyridinium-based oligocations (**1** – **5**).*

Great success has been realized by the use of 4,4′-bipyridinium-based crosslinkers **1** – **5**,[138, 139, 147–150] which also exhibit electrochemical activity as well as other functions (see Section 4). Singly charged species, such as tetrabutylammonium chloride, are able to partially neutralize the colloidal charge, so that greater coverage can be realized, but they cannot be used to assemble true multilayer structures.[151] In fact, not even all oligocations are successful. Those that bind the nanoparticle more strongly than the underlying substrate may destroy the superstructure, while those with a low charge density may not form a superstructure. The oligocationic molecule can be assembled in a variety of solvents but, to achieve efficient coverage, immersion in a fairly concentrated nanoparticle solution (about 10 mM) for at least 30 minutes is usually required. It is very important that the sample is washed very thoroughly before every colloid treatment, as any weakly bound crosslinker can diffuse into the bulk solution and aggregate the colloid.

Like in the construction of polymer-linked structures, treatment of a colloid monolayer with an oppositely charged species results in a surface ready for the assembly of a second colloid layer. In this case, however, the much smaller "crosslinker" means the colloid layers are much closer—even interleaved—such that there can be electrical communication throughout the entire structure.[147] The use of *N*,*N*′-diaminoethyl-4,4′-bipyridine (**5**) as a crosslinker has been used to demonstrate the versatility of the method—gold and silver colloids offer the same assembly characteristics, which allows composite structures to be built.[138]

2.3.3. Covalently Linked Architectures

Covalently linked colloid superstructures can be built analogously to electrostatically linked architectures. This has been accomplished by the use of bisthiol crosslinkers for gold[95, 152–154] and other[99] nanoparticles (Scheme 7) and has been verified by QCM and other techniques. If a gold colloid monolayer is exposed to a solution of a bisthiol, then the crosslinker assembles on the gold surface, which leaves thiol moieties at the nanostructure – solution interface. The assembly of a second colloid layer is thereby possible and the construction can continue in the same way. This method allows some control over

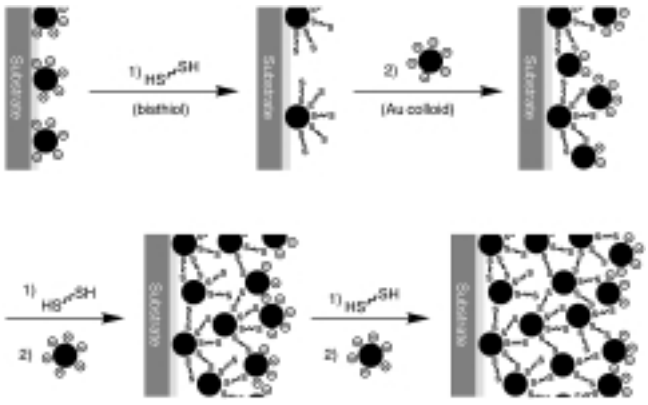

Scheme 7. *The construction of thiol-crosslinked multilayers of gold nanoparticles.*

interparticle spacing by the use of bisthiols with spacers of various lengths[152] and, in turn, the interparticle spacing affects lattice properties such as conductivity (as will be discussed in Section 3.3.2). The conditions required for this assembly are very similar to those for electrostatic assembly but the technique has not yet been extended to include functionally interesting crosslinkers. It should be noted that the reaction of the gold surface with a thiol displaces the negatively charged citrate ions, to leave the thiol – colloid interface uncharged. As is shown in Scheme 7 however, the charge remains at the colloid – solution interface, which leaves a path open for the construction of composite covalent – ionic structures. 2-Mercaptoethylamine has already been used as an interparticle crosslinker.[144]

2.4. Assembly of Patterned Nanoparticle Arrays

The patterning of colloid arrays is of paramount importance if these structures are to be used in nanoelectronic applications or to tailor addressable sensing domains. In recognition of this fact, methods for the patterning of colloid-functionalized surfaces have been developed, which can broadly be categorized into three paradigms: lithography, microcontact printing, and physical engineering. The direct engineering of surfaces by scanning microscopy tools, such as by STM and AFM tips, is intriguing but lies far from a cheap industrial or general laboratory process. Colloid particles have been electrodeposited,[155] "swept",[156] and even etched by CN^-[157] at the touch of a STM tip. Even so, the construction of large devices is unfeasible and even the manipulation of a single particle is currently seen as quite an achievement. Another approach is to adsorb nanoparticles onto a substrate that already bears a pattern. In one such example, a matrix of latex colloids was used as a mask for the evaporation of gold, after which gold colloids were attached to the pattern with a dithiol crosslinker.[127] Engineered colloidal films can also be produced by the exploitation of the monolayer formation reaction (Scheme 8).[158] A silanated substrate was slowly immersed in a solution of gold nanoparticles and was then washed. Since different points on the substrate had been exposed to the colloid for different periods of time, the colloid density varied across the sample. The sample was then rotated 90° and slowly dipped into a solution that deposited silver onto the gold. This procedure resulted in gradients of colloid size and composition across the film and, thus, no two points on the substrate had the same composition. This "combinatorial" surface was used to determine the optimum morphology for surface-enhanced Raman scattering (SERS; Section 4.1.2).

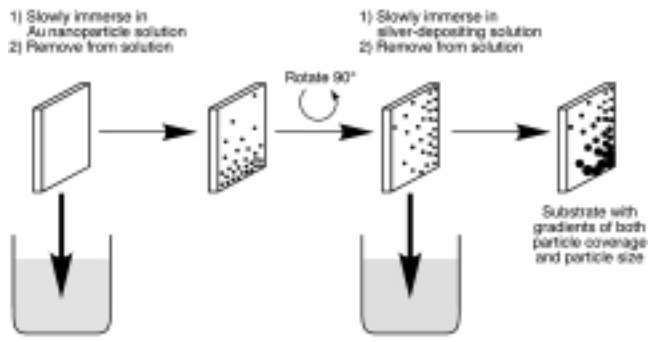

Scheme 8. *The synthesis of a "combinatorial" colloid array by the adsorption of two different colloidal materials in perpendicular concentration gradients across the substrate surface.*

The pattern engineering of the colloid monolayer after its formation has not been studied in any depth. This route would involve the construction of a colloid monolayer and its subsequent patterning by, for instance, scanning nanocapillaries filled with an "etching ink". In one example, a thin film of surfactant-covered palladium nanoparticles was patterned by an electron beam. In the exposed areas, the surfactant coating was removed from the particles, which allowed them to agglomerate into continuous metal. The remaining (unexposed) discrete nanoparticles were then washed away to leave the metal pattern.[78]

2.4.1. Photolithography-Based Patterning

Lithography provides a well known route to patterned substrates and a number of examples concerning colloidal systems are known. The most trivial of these relies on standard lithographic techniques to produce a poly(methylmethacrylate) (PMMA) pattern on a silica substrate.[159] The "windows" in the pattern can then be silanated and a colloid layer assembled by standard procedures (Figure 3 A). In other methods, the substrates have a functionalization which may adsorb colloids, dependent upon their exposure to the lithographic medium. Scheme 9 A shows the photolithographic patterning of a thiol-surfaced substrate.[160] Irradiation at 254 nm under air oxidizes the exposed thiol moieties to sulfonates, which are unable to bind gold colloids. Subsequently, treatment of the photolithographed surface with a gold nanoparticle solution results in the colloids adsorbing only in the areas that have not been irradiated (as seen in Figure 3 B). The system outlined in Scheme 9 B behaves in the converse fashion:[161] An amine monolayer is protected with the photolabile nitroveratryloxycarbonyl (NVOC) group and upon UV irradiation the neutral NVOC amines are photodeprotected, which exposes the positively charged amine.

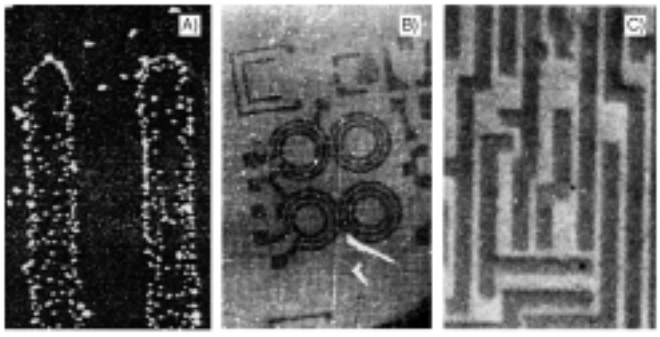

Figure 3. *Images of selectively adsorbed gold nanoparticles. A) Nanoparticles (20 nm) on amine-functionalized regions of a substrate. B) A SEM image of nanoparticles on nonirradiated areas of a thiol-functionalized substrate. C) An optical microscope image of nanoparticles on the photodeprotected regions of a protected amine-functionalized substrate. Images in (A), (B), and (C) are reproduced from refs. [159 – 161], respectively, with permission.*

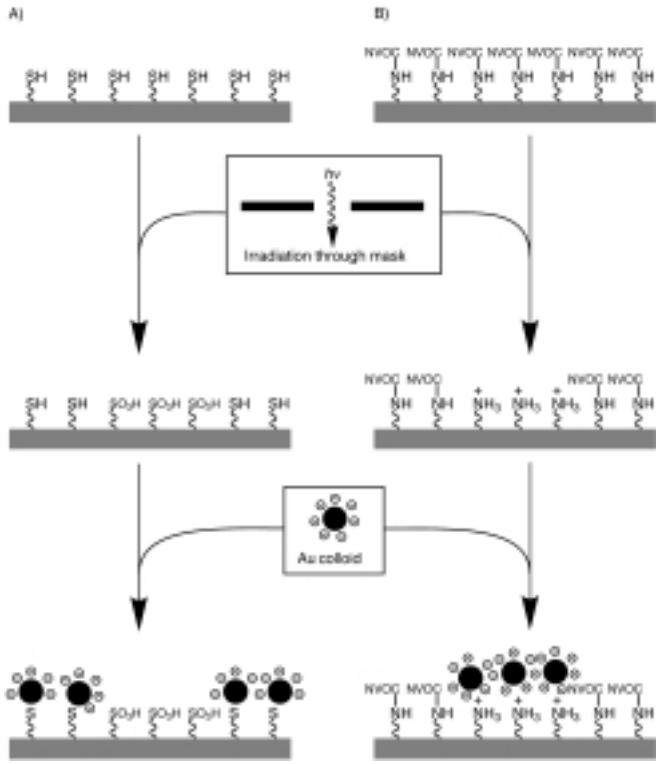

Scheme 9. *The construction of gold nanoparticle patterns by irradiative patterning methods. A) Nanoparticles only assemble on the nonirradiated parts of a thiol-surfaced substrate. B) Nanoparticles only assemble on the irradiated parts of an NVOC-amine-surfaced substrate.*

The colloid pattern is generated by immersing the pattern-irradiated substrate in a solution of negatively charged gold colloids, which adsorbs only to the amine. This pattern of gold colloids can also be intensified by the construction of further layers of colloids crosslinked by bisthiol molecules (the final pattern is shown in Figure 3C). Other lithographic methods have been used analogously and the final colloid pattern has been used for the deposition of other metals to create continuous metallic patterns.[162]

2.4.2. Printing-Based Patterning

Colloid patterns have also been achieved by the process of microcontact printing, often as a means to construct other architectures.[163, 164] This technique uses a microstructured "stamp" to form the nanoparticle pattern by one of two general routes (Scheme 10). In one of the these routes, the stamp is used to introduce a pattern of functionality onto the substrate, which may be either specifically chosen or of the well known hydrophobic/hydrophilic type (Scheme 10A). Self assembly of nanoparticles on the functionalized surface yields the colloid pattern. Figure 4A shows a pattern generated by the evaporation of a colloidal magnetite solution, which had selectively adsorbed to 2-mercaptoethanesulfonic acid functionalized areas, to leave hexadecanethiol-functionalized areas bare.[164] The other, simpler method is to use the stamp to introduce a colloid-containing "ink" directly on the surface (Scheme 10B). In one such example,

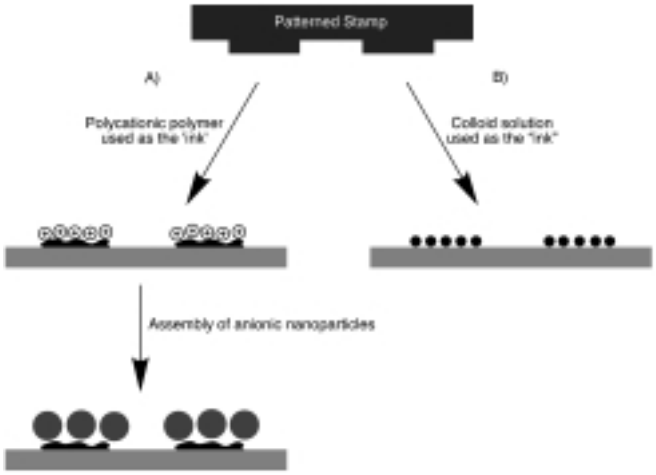

Scheme 10. *The construction of nanoparticle patterns by microcontact printing methods.*

a pattern of palladium nanoparticles was deposited on a siloxane-functionalized substrate by means of a poly(dimethylsiloxane) (PDMS) stamp.[163] The colloid domains were used to catalyze the electroless deposition of copper, to form a submicron-scale conductive pattern on the surface, as shown in Figure 4B.

2.4.3. DNA Template-Based Patterning

Recently, the ability to use DNA templates for the organization of nanometer-sized structures has been realized.[130] The possible methods for the preparation of DNA-based inorganic nanostructures can be divided into two categories: 1) The use of duplex DNA as a physical template for growing inorganic wires and organizing nonbiological building blocks into extended hybrid materials, and 2) the use of oligonucleotide (single-stranded DNA)-functionalized nanoparticles and sequence-specific hybridization reactions for organizing such particles into periodic, functional structures. In an early report, DNA was

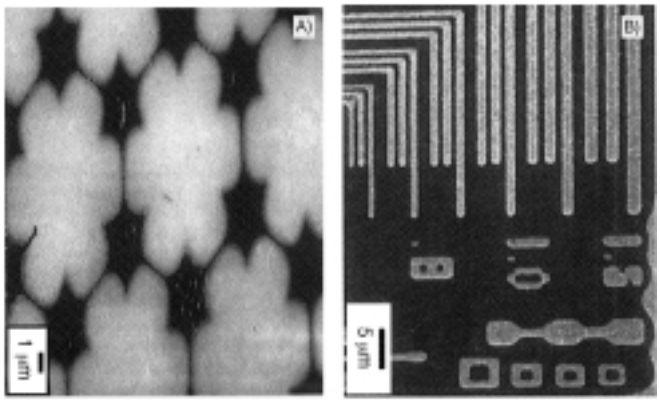

Figure 4. *A) A pattern of magnetite (dark areas) made by selective deposition on hydrophilic areas patterned by microcontact printing. B) Microstructure generated on a glass substrate by microcontact printing with palladium colloids, followed by the electroless deposition of copper. Images in (A) and (B) are reproduced from refs. [164] and [163], respectively, with permission.*

utilized as a stabilizer/template to form both CdS nanoparticles and mesoscopic aggregates from them.[165] These original efforts were based on the use of linear duplexes of DNA in solution as stabilizers for the formation of CdS nanoparticles from Cd^{2+} and S^{2-}. Further studies demonstrated that the DNA base sequence and, more specifically, the adenine content had a significant effect on the size and photophysical properties of the CdS particles thus formed.[166] More interesting for practical applications is a strategy for binding a template DNA strand to a solid substrate,[167] which has been used for the synthesis of a "ring" of CdS nanoparticles by employing the circular plasmid DNA molecule pUCLeu4 (3455 base pairs, 1.17 μm circumference). Initially, Cd^{2+} ions were added to a solution of the plasmid DNA to form a plasmid DNA/Cd^{2+} complex, which was subsequently bound to a polylysine-coated glass surface[168] (Scheme 11 A). Exposure to H_2S led to the formation of 5 nm CdS nanoparticles along the DNA ring backbone. This approach provides many

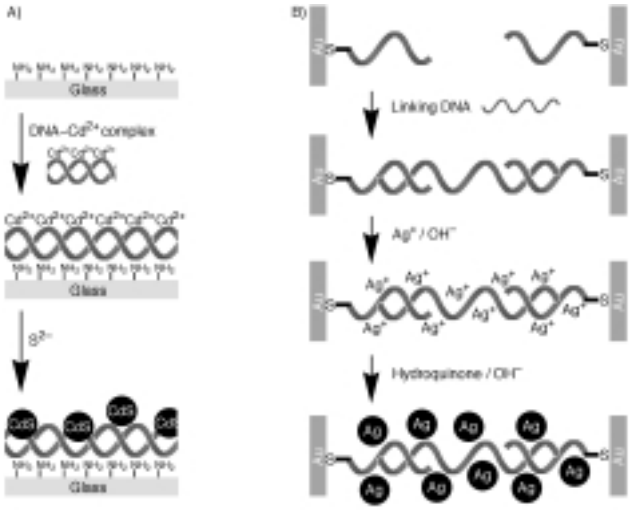

Scheme 11. *The synthesis of DNA-templated silver nanostructures. A) Synthesis of a silver ring immobilized on a glass substrate. B) Synthesis of a silver wire connecting two microelectrodes.*

possibilities for the synthesis of mesoscale structures, since the particle character (such as metallic or semiconductive) and the shape, length, and sequence of the DNA template can be controlled. DNA templates have also been used to grow nanometer-scale silver wires.[169] Two gold electrodes, separated by a defined distance (12 – 16 μm), were deposited onto a glass slide using photolithography and were subsequently modified with noncomplementary, hexane disulfide modified oligonucleotides (Scheme 11 B). Phage λ-DNA (16 μm in length) bearing "sticky ends" complementary to the oligonucleotides was introduced to the system and attached to the electrodes. After a single DNA bridge was assembled between the electrodes, silver ions were deposited onto the DNA and reduced with hydroquinone to form small silver aggregates along the DNA backbone. A contiguous silver wire was then formed by hydroquinone-catalyzed Ag^+ reduction onto the previously constructed silver aggregates. A wire 100 nm in diameter and 12 μm long could be synthesized reproducibly by this process. The wires comprised 30 – 50 nm silver grains that were contiguous along the DNA backbone. The nanowires had an extremely high resistance (more than 10^{13} Ω) and, thus, at low bias (about 10 V), no current was observed in the nanowires. However, at a higher bias the wires become conductive. By the deposition of more silver, the nonconductive threshold was reduced from about 10 V to 0.5 V, which demonstrated a crude control over the electrical properties of these systems. These examples demonstrate a new type of "biochemical lithography" to guide the formation of nanocircuitry for future nanosized electronic devices.[130]

3. Characterization of Nanoparticle Arrays

The study of functionalized surfaces is a relatively recent discipline and this reflects not only the recent interest in nanotechnology but also the advances in analytical methodology that allow us to characterize such constructions. Bulk and microscopic characterizations of nanoparticle arrays enable us to elucidate structural features, interparticle interactions, and superstructure functionality. Direct imaging on most substrates is now possible by various reliable, high resolution microscopies without prohibitive cost or time requirements. In addition, surface analysis techniques, such as X-ray photoelectron and Fourier-transform infrared spectroscopies (XPS, FTIR), provide tools to probe surface composition as well as to elucidate structural and geometric features at surfaces. These tools, along with others such as surface plasmon spectroscopy (SPS) and quartz crystal microgravimetry (QCM), complement traditional electrochemical and spectroscopic analyses to give us an unprecedented ability to characterize surface structures and functions.

3.1. Microscopic Methods

Microscopy is an invaluable method for the characterization of nanoparticles and their superstructures—only by direct observation can one ascertain an accurate picture of nanoparticle size and shape distributions and film morphologies. These methods do have their drawbacks, however. Sample preparation must conform to stringent requirements, while results can sometimes be difficult to interpret. It is not always certain whether an image is truly representative of the entire sample and whether imaging has affected the sample. Microscopy is used in almost all reports that discuss nanoparticle synthesis or nanoparticle monolayers and sometimes in the study of multilayer assemblies. Here, we will discuss electron and scanning probe techniques separately—a careful comparison has shown that these two methods have complementary features.[170]

3.1.1. Accelerated Electron Techniques

The most popular microscopic analyses of nanoparticles and their monolayers are scanning electron microscopy (SEM) and transmission electron microscopy (TEM). Of these, TEM provides the best images, even allowing the visualization of particle crystallinity and the surface-stabilizing layer (Figure 5 A).[30, 70]

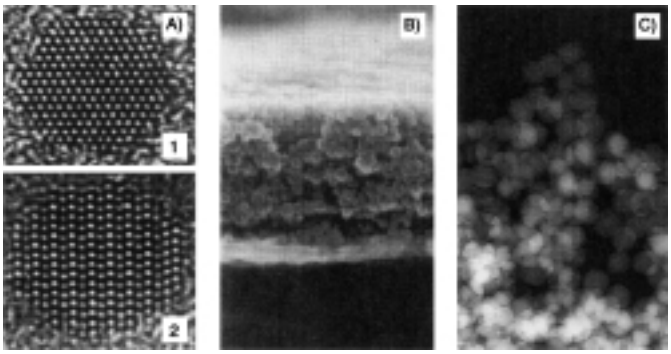

Figure 5. *A) High resolution TEM images of individual nanoparticles, which shows their crystallinity. B) Cross-sectional SEM of a SiO_2/PDDA multilayer. C) TEM of a SiO_2 aggregate, which shows how TEM reveals information through the entire thickness of the sample. Images in (A) and (B) are reproduced from refs. [12] and [113], respectively, with permission.*

Samples must be prepared on a suitable electron-transparent grid however, which makes it impossible to elucidate structural features formed on "everyday" substrates. SEM is capable of imaging layers formed on ordinary substrates but it is sometimes necessary to give the sample a thin conductive coating, which can result in a less defined image. Figure 5 B shows a SEM micrograph of the cross section of a silica-nanoparticle multilayer and Figure 5 C shows a TEM of a silica-nanoparticle aggregate. Consideration of these images reveals another complementary nature of the techniques: Whereas SEM gives an accurate picture of the surface, TEM allows visualization throughout a structure.

3.1.2. Scanning Probe Microscopies

Techniques such as atomic force microscopy (AFM), scanning nearfield optical microscopy (SNOM), and scanning tunneling microscopy (STM)[171, 172] allow visualization of thicker structures and can also provide some chemical information[170] but they suffer several drawbacks. The interpretation of AFM images can be problematic if the the underlying substrate is not completely flat and AFM resolution does not match that of electron microscopy. AFM and SNOM images of the same region of immobilized, 31 nm gold nanoparticles are shown in Figure 6. In gathering AFM data, precautions have to be taken to avoid "sweeping" loosely bound particles across the surface by the imaging tip.[157] Researchers overcome this restriction by various methods, such as the use of "tapping mode" imaging, low tip loads, and imaging under high ionic strengths to minimize electrostatic interactions between particles and the tip. Despite these drawbacks, AFM has great advantages in its ability to image almost any flat surface including multilayered assemblies and problematic substrates such as mica.[171] Scanning probe microscopies are generally not a good indicator of nanoparticle sizes, as the tip shape can cause an apparent particle enlargement. This distortion can be corrected by modeling the experiment with knowledge of the tip dimensions, however, and the particle height measurements remain unaffected.

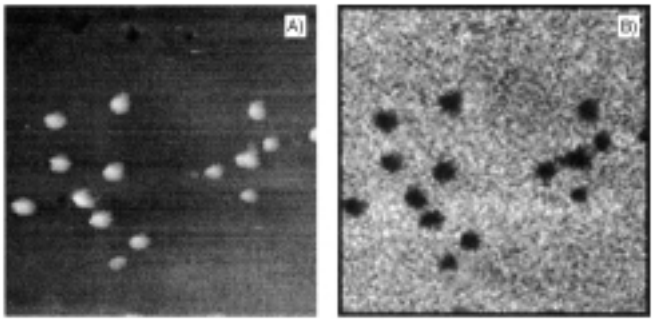

Figure 6. *A) AFM and B) SNOM images of the same region of 31 nm gold nanopaticles adsorbed on aminosilanated glass. Images reproduced from ref. [170] with permission.*

3.2. UV/Vis Spectroscopy

3.2.1. The Plasmon Absorbance

Solutions of colloidal gold particles have a very distinctive red color, which arises from their tiny dimensions.[10, 11, 173, 174] At nanometer dimensions, the electron cloud can oscillate on the particle surface and absorbs electromagnetic radiation at a particular energy. This resonance, known as plasmon absorbance, is a property characteristic of some mesoscale surfaces. Still smaller nanoparticles (quantum dimensions, $< 1-2$ nm) do not display this phenomenon, as their electrons exist in discrete energy levels, and bulk gold has a continuous absorbance in the UV/Vis/IR region (which is effectively collapsed into the single plasmon absorbance in the case of the nanoparticle). The plasmon absorbance of gold nanoparticles has been known for some considerable time and has been utilized since Roman times in the production of "ruby" glass. Other metal colloids also display plasmon absorbances in the visible region (for example, silver at about 350 nm for 10 nm particles) and semiconductor colloids display plasmon absorbances in the infrared region because of their lower density of free electrons. The exact wavelength and intensity of the absorbance maximum depends on factors such as surface functionality, temperature,[175] and the solvent (Figure 7), but the effect can be used to give a quick assessment of colloidal concentration and particle size in

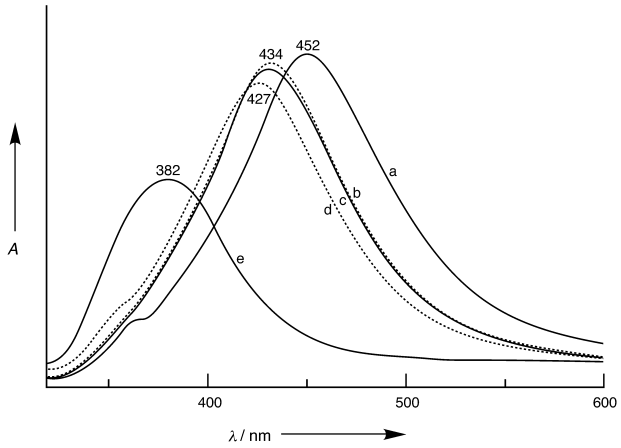

Figure 7. *The extinction spectra and peak wavelengths of a silver nanoparticle monolayer in various solvents: a) benzene, b) hexane, c) 2-propanol, d) water, e) air. Reproduced from ref. [71] with permission.*

solution if these conditions are known.[176] In gold colloid monolayers, the plasmon absorbance can be used as an analytical tool.

3.2.2. Interparticle Close Contact—Coupled Plasmon Absorbances

The close contact of optically absorbing nanoparticles leads to the appearance of an absorbance band attributed to the coupled plasmon absorbances of the particles. This property has been predicted theoretically[174] and has been shown with a Langmuir – Blodgett film of gold nanoparticles to emerge together with a loss of electrical resistivity at interparticle separations less than about 5 nm.[177] The more particles that are in contact, the longer the range of the plasmon coupling. Very long range coupling can lead to absorbances that are red-shifted several hundred nanometers from that of the individual particles. Integration of the spectral region containing coupled plasmon absorbances has been used as an empirical assay of the degree of coagulation within collidal gold solutions[178] and as the indicator in DNA sensors.[129] Spectral changes as a consequence of interparticle close contact have also been investigated for silver nanoparticles.[71, 179, 180] It was found that more densely packed films of silver nanoparticles display a much sharper absorbance and are blue shifted by up to 90 nm.

This characteristic absorbance also appears when multilayers of colloidal particles are constructed on surfaces as a consequence of their proximity to each other.[181] Figure 8 A shows the UV/Vis absorbance spectrum of a 13 nm gold nanoparticle superstructure, in which the layers are crosslinked with paraquat (**2**; *N*,*N*′-dimethyl-4,4′-bipyridyl).[151] As the number of layers increases, the plasmon absorbance ($\lambda \approx 520$ nm) of individual particles increases, while simutaneously an absorbance band at $\lambda \approx 650$ nm forms, strengthens, and shifts bathochromatically.

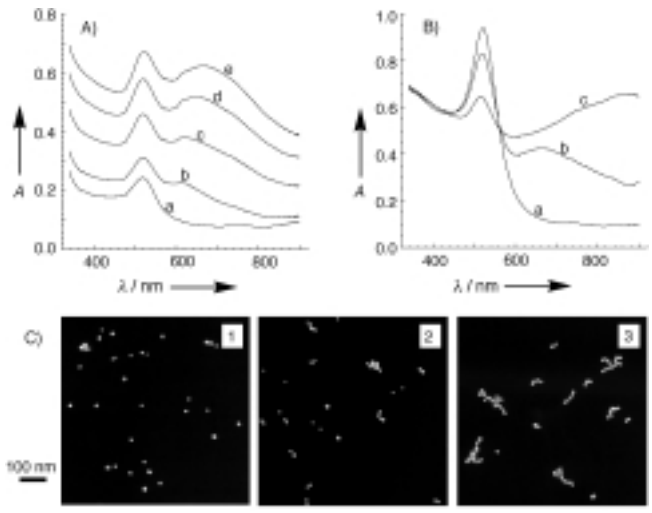

Figure 8. *A) Absorbance spectra of (a – e) 1 – 5 layers of Au colloid/**2** superstructures on a glass substrate. B) Absorbance spectra of a 12 nm colloidal gold solution a) 15, b) 50, and c) 165 min after the addition of methyl viologen (0.01 mM). C) TEM micrographs of representative aggregates from the same solution after 1) 15, 2) 50, and 3) 165 min.*

This energy is in the region expected for interparticle plasmon absorbances and the gradual increase in wavelength is indicative of increasing particle network size as the assembly grows. A similar feature is also evident in vapor-deposited, semicontinuous gold films but is absent in noncontinuous films.[173] Further evidence that these absorbance changes occur as a result of the close contact of gold particles is obtained by following the UV/Vis spectrum of a citrate-stabilized gold-nanoparticle solution upon the addition of **2**.[151] Figure 8 B shows the spectral changes after the addition of **2** (0.01 mM). Soon after the addition, the intensity of the plasmon absorbance at 520 nm reduces and a band at $\lambda \approx 650$ nm appears. With time, this absorbance intensifies at the expense of the plasmon absorbance from the individual particles and shifts to longer wavelengths and, ultimately, the particles precipitate. TEM micrographs of the aggregating solution over the same periods (Figure 8 C) show that as the absorbance at $\lambda \approx 650$ nm strengthens and shifts bathochromatically, the average size of particle aggregates increases.

3.2.3. Light Scattering and Reflectance

Some of the data recorded by UV/Vis spectroscopy of nanoparticle assemblies are artifacts of light scattering and reflectance. In particular, as the particle sizes increase and metallic regions appear (with increasing particle density or layer growth) these components become important. Light scattering contributions of gold-particle aggregates appear in the region of 650 – 800 nm[182, 183] and reflectance occurs over the entire frequency range. In combination, these effects cause the broadband feature that is observed with the generation of multilayers (Figure 8 A).

3.3. Electrochemistry

3.3.1. Redox Properties

When constructed on a suitable substrate, it is possible to estimate the surface coverage of a gold colloid by the assay of its surface area. By applying a cyclic potential (between 0.0 V and 1.5 V versus a saturated calomel electrode (SCE)) to the electrode, modified with colloidal gold in an acidic background electrolyte solution (0.5 M H_2SO_4), oxidation and reduction of the colloidal surface can be achieved.[150] Upon oxidation, a densely packed monolayer of hydroxide species is produced on the gold surface, that is reduced in the course of the cathodic wave of the cyclic voltammogram. The charge density associated with the reductive process on the gold electrode surface is well known (386 $\mu C\,cm^{-2}$ for the [100] plane and similar values for the other planes[184, 185] of a gold crystal). An electrochemical study performed on a glassy carbon electrode covered with gold nanoparticles showed that the charge density associated with the reduction of the oxide layer on the nanoparticles is similar to that of bulk gold electrodes.[186] Thus, the integral surface of the colloidal gold particles involved in the electrochemical process can be determined by measuring the charge associated with the cathodic peak in the cyclic voltammogram. Figure 9 shows cyclic

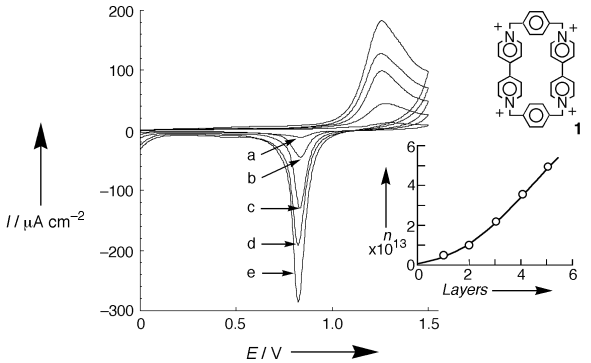

Figure 9. *Cyclic voltammograms of 1 – 5 layers of Au colloid/**1** assemblies corresponding to the electrochemical oxidation and reduction of the particle surface. Experiments were carried out in 1.0 M H_2SO_4 at a scan rate of 50 mV s^{-1}. Inset: Calibration curve corresponding to the surface coverage (measured as the number of of gold nanoparticles per square centimeter,* n*) against the number of layers.*

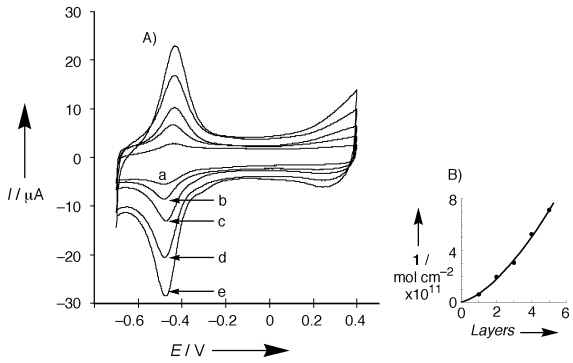

Figure 10. *A) Cyclic voltammograms correspsonding to the redox activity of the crosslinker (**1**) in arrays of 1 – 5 gold layers. Experiments were recorded under argon in 0.1 M buffer solution, at pH 7.2, and a scan rate of 100 mV s^{-1}. B) Calibration curve corresponding to the surface coverage of **1** against the number of layers, as determined by coulometric analysis.*

voltammograms of a gold colloid layered array upon construction of a **1**-crosslinked superstructure.[139] The characteristic cyclic voltammogram of gold is observed, consisting of an anodic wave corresponding to the oxidation of the colloid layer followed by a cathodic peak corresponding to the reductive stripping of the hydroxide layer formed on the gold surface at more positive potentials. The oxidation and reduction waves of the cyclic voltammograms of the gold particle surface increase almost linearly with the number of layers and, by the coulometric assay of the cathodic peak, the total gold surface area per nanoparticle layer can be estimated. Knowing the diameter of the gold particles and assuming that all of the particle surface is exposed to the electrochemical reaction, the surface density of the gold particles in this structure is estimated to have a lower limit of 0.8×10^{11} particles cm^{-2}, similar to the surface coverage of a colloid monolayer as determined by SEM (1.0×10^{11} particles cm^{-2}).[88] Another possiblity to estimate the integral area of the colloidal gold array exposed to an electrolyte solution is based on the capacitance measurements.[187] The double-layer capacitance obtained from the voltammograms is proportional to the integral area of the conductive array, so the area can be calculated if the capacitance per area is known (about 20 μF cm^{-2} for gold electrodes in aqueous solutions). A gold electrode functionalized by a layer of 42 nm gold nanoparticles assembled on a cystamine monolayer revealed an apparent capacitance of approximately 83 μF cm^{-2}, which gives an electrode roughness coefficient of about four.[188] More complex, three-dimensional systems were also characterized using capacitance measurements. For example, nanoporous filtration membranes (30 nm pore diameter, 6×10^8 pores cm^{-2}, 200 nm center-to-center average distance, 0.0042 fractional pore area) were filled with metal (gold) nanowires and the respective nanoelectrode assemblies were characterized by the capacitance measurements.[187] The fractional electrode area, 0.0045, was then derived from this measured capacitance value.

If the crosslinking species is electroactive, then its electrochemical response can reflect the buildup and formation of the particle superstructure. Figure 10 shows cyclic voltammograms of the molecular crosslinking units upon the construction of a **1**-crosslinked gold-colloid array. The cyclic voltammogram of **1** increases with the number of gold layers. This verifies that **1** indeed acts as a "crosslinker" for the particles, such that the formation of each additional gold layer requires its preassembly. By the coulometric analysis of the electrical responses of the crosslinker upon the buildup of the array, the crosslinker content was estimated to be about 1.5×10^{-11} moles cm^{-2} per layer. Knowing the surface coverage of the gold particles, it is estimated that, on average, about 100 crosslinking molecules are associated with each gold particle in the superstructure. Interestingly, this value is in excellent agreement with the number of molecules required to precipitate a gold colloid from solution.[150] The fact that the molecular crosslinker is electrochemically observable upon the buildup of the superstructure implies that the array exhibits three-dimensional conductivity and is porous to the electrolyte solution. A related experiment, in which a large number of layers were constructed, revealed that the response of the electroactive crosslinker reached a maximum, after which further layer growth had little effect.[189] In this case, only the top few layers were accessible to the electrochemical process. Potential-dependent changes of the redox-state of the linker can also result in variation of physicochemical (for example, spectral) properties of the nanoparticle array.[190]

3.3.2. Conductive and Semiconductive Properties

Apart from the vertical conductivity noted from cyclic voltammetry data, the transverse conductivity of colloid assemblies has also been measured. Monolayer films are found to be electrically insulating because individual particles are not in close contact but, when denser arrays are manufactured, electron transport through the matrix becomes possible. Networks consisting of gold nanoparticles connected through dithiols demonstrated a nonmetallic type of conductivity when the temperature was varied.[191] The resistance of gold nanoparticle arrays separated by organic crosslinkers varies with features such as the particle diameter, spacer length, and the number of particle layers. Samples consisting of 38 layers of gold particles separated by

alkanedithiols of various chain lengths demonstrated significantly different surface resistances: about 1500, 85, or 6.5 Ω (at room temperature) for structures with 12, 9, or 6 methylene units between the sulfur atoms, respectively.[190] Thus, the addition of three methylene units to the chain can increase the resistance by an order of magnitude. Only one particle array has approached the conductivity of pure gold (resistivity $= 2.4 \times 10^{-6}\ \Omega\,cm$)[192] but many exceed that of substrates, such as ITO. It has been found that colloidal gold multilayers undergo an insulator–conductor transition at a critical particle density.[144, 152] Samples containing up to 25×10^{11} particles cm^{-2} (11 nm) were found to insulate, with a resistance in excess of $10^7\ \Omega$, but further increases in the number of the gold layers resulted in an enormous decrease in resistance: By the time the gold particle density reached 50×10^{11} particles cm^{-2}, the resistance dropped below 100 Ω—a change of five orders of magnitude upon only doubling the particle content. Highly conductive nanoparticle aggregates can be generated when metallic nanowire connections, produced through electrochemical growth between the particles, are made.[193] Reversible metal–insulator transitions in ordered silver nanocrystal monolayers have been observed when 2D Langmuir–Blodgett films were compressed and decompressed.[194] The admittance of a 35 Å diameter silver nanoparticle film was reversibly modulated between values typical for an insulator and a conductive metal when the interparticle distance was changed from about 10 Å, in case of the uncompressed monolayer, to about 5 Å, when the monolayer is fully compressed. The conductivity change results from the change of the electron transfer mechanism: Quantum tunneling over the long distances between nanoparticles and a delocalized metallic mechanism over the short distances. Reversible optical changes, typical for continuous and discontinuous silver films, were also observed simultaneously with the conductivity changes.[195]

Mono- and multilayered constructions of semiconductor colloids (mainly CdS or TiO_2) have been well characterized by numerous spectral methods (UV/Vis spectroscopy, X-ray diffraction (XRD), resonance Raman scattering, TEM, electron diffraction, Rutherford backscattering, and so forth).[64, 76, 102] The evidence from a variety of characterization techniques indicates that semiconductive nanoparticles can be bound to metal surfaces using self-assembling monolayers. The nanocrystals are deposited intact, without fusion or aggregation, and at relatively high coverage—usually about half a monolayer.[102] The size distribution of nanoparticles on the solid support can be even narrower than the original size distribution of the particles in the solution before deposition. Such homogeneity of the nanoparticles is especially important for study of the electronic properties of the assembly. The samples are durable and may endure for months in air without degradation.

Tunneling spectroscopy (TS) of a single particle whose size was determined from a STM image has allowed the determination of the bandgap energy of the size-quantized particle. For this purpose, a current between a gold support and a TS tip, which passed through a CdS nanoparticle monolayer, was detected upon application of a variable potential difference.[64] The inset in Figure 11 shows the $I-V$ curve obtained for the nanoparticle monolayer (curve a) and that for bulk CdS particles (curve b). The $I-V$ curve obtained for the CdS nanoparticles is nearly symmetric against the potential axis, while that for the bulk CdS particle shows rectification and no appreciable current appears with positive bias. This difference results from the contribution of space charge effects, which are remarkable for the bulk CdS but not for the CdS nanoparticle, which is too small for any remarkable space charge layer to form.[196] The bandgap of the CdS nanoparticle was determined on the basis of a potential region where no appreciable current flow is observed.[64] For example, a bandgap of 2.9 eV was obtained for a 3.1 nm CdS nanoparticle. The TS measurements were carried out for other CdS nanoparticles of different sizes and their bandgap energies decreased with increased particle size (Figure 11). This result is in a good agreement with the theoretical predictions made by tight-binding approximations.[197]

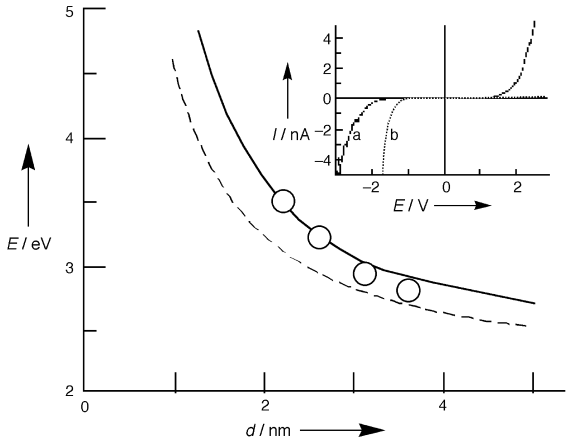

Figure 11. *Bandgap energies of CdS nanoparticles as a function of nanoparticle size. Circles represent experimental data and lines show theoretical calculations based on tight-binding approximations. Inset: the I–V curves obtained by TS measurements of a) a CdS nanoparticle and b) bulk CdS. Reproduced from ref. [64] with permission.*

Assemblies of semiconductive nanoparticles (CdS, CdSe, or TiO_2), upon appropriate illumination, have also been applied to photocurrent generation.[63, 65, 121, 198, 199] These systems demonstrate size-dependent photochemical properties different from those of bulk materials. Figure 12A shows the photocurrent potential of CdS nanoparticle films consisting of one to three

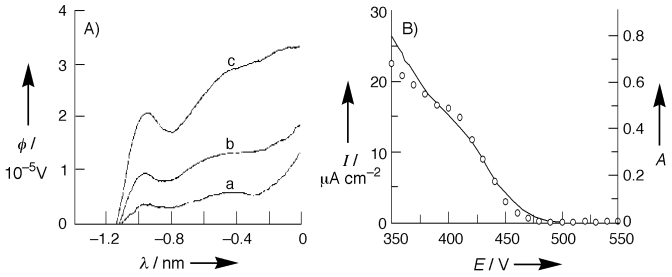

Figure 12. *A) Photocurrent potential of CdS nanoparticle electrodes consisting of a) one, b) two and c) three layers of crosslinked nanoparticles. B) Action spectra of the photocurrent acquired from a CdS nanoparticle film (circles) and the absorbance spectrum of CdS nanoparticles (solid line). Reproduced from ref. [121] with permission.*

monolayers. The photocurrent onset was observed at -1.15 V versus SCE, independent of the number of layers. Anodic photocurrent increases with the increasing anodic polarization, which is typical of n-type semiconductors. The magnitude of the anodic photocurrent increased almost linearly with the number of CdS layers, which indicates that all of the nanoparticles immobilized on the electrodes are photoelectrochemically active.[121] A similar dependence was observed for TiO_2 nanoparticles; however, beyond ten layers, a leveling-off (and even a decrease) of the photocurrent resulted. This phenomenon results from light absorbance by the TiO_2 layers located too far from the conductive support surface to pass electrons to the electrode.[65] Action spectra of the photocurrents (Figure 12B) demonstrate the same spectral shape as that of the absorption spectra, which indicates that all particles are active for the photocurrent generation and there is no significant energy transfer and redistribution.[121] The photocurrent measurements allowed determination of the potentials of the conduction-band edge, E_{CB}, and the valence-band edge, E_{VB}, of the CdS particles with size:[63] Both E_{CB} and E_{VB} are shifted toward negative and positive potentials, respectively, with a decrease of the CdS nanoparticle diameter. The experimental change of the potentials follows the theoretical prediction based on the finite depth potential model.[200] Approximate measurement of the CdSe bandgap was performed using photocurrent spectroscopy, applicable even for very small amounts of the material equivalent to a 2.5 nm thick film (less than a monolayer of the CdSe nanoparticles).[199] Intensity-modulated photoelectrochemical spectroscopy has been applied to determine the kinetics of charge transfer at an electrode modified with a monolayer of CdS nanoparticles.[57] An electrode modified with a CdS-nanoparticle monolayer was irradiated with light chopped at a frequency of about 17 Hz and the modulated current signal was recorded using a lock-in amplifier. The photocurrent response was analyzed in terms of impedance spectroscopy and the charge-transfer kinetics were determined; rate constants for hole and electron transfer were $2.8 \times 10^3\ s^{-1}$ and $5.1 \times 10^3\ s^{-1}$, respectively.

The unique features of the size-quantized semiconductive nanoparticles could result in the development of the novel photovoltaic, light-emitting, and sensory devices that will be discussed in Section 4.4.

3.4. Other Techniques

Of the other techniques used to characterize colloid superstructures, microgravimetric techniques stand out as the most important. With quartz-crystal microgravimetry, the construction of layers can be followed in great detail. Any particle material and crosslinker can be used, although the underlying substrate is usually gold, and construction may be followed for many layers. QCM can monitor the mass change upon the formation of layers, which allows the calculation of layer thicknesses, and can also show the homogeneity of layer thickness in repeating structures.[76, 89, 95, 113, 142, 201] The high mass of metallic colloidal particles means that their adsorption is followed very easily (the frequency decreases upon colloid assembly can be as much as 10000 Hz).[96] For example, colloidal gold particles of about 8 nm in diameter were deposited onto a QCM surface and nonane-1,9-dithiol was used as a linker between the gold layers.[95] Figure 13 shows the mass increase on the QCM surface upon deposition of several layers of the gold colloid. The measurements show clearly that saturated monolayers are

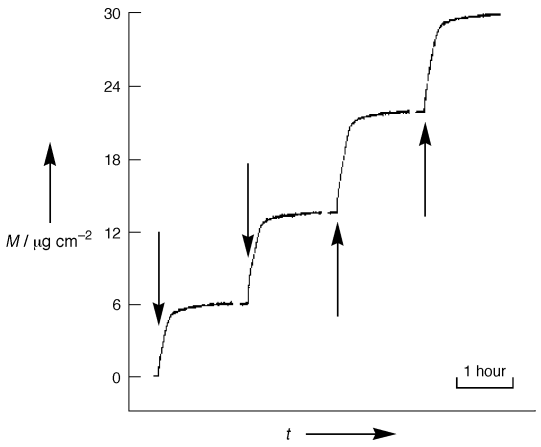

Figure 13. *The deposition of gold nanoparticle layers, as detected by QCM. Arrows show the times at which colloid was added. Reproduced from ref. [95] with permission.*

obtained, namely, the self-assembly process comes to saturation. The values obtained for the mass of the individual layers are in agreement with expected values. Assuming a particle radius of 4 nm and a maximum coverage of the surface, a mass increase of $9\ \mu g\ cm^{-2}$ can be expected. The measured value of $6\ \mu g\ cm^{-2}$ indicates about 50–60% coverage and is a more reasonable result for the first layer. The larger values, about $8\ \mu g\ cm^{-2}$, for the consecutive layers could be due to an increase in the surface roughness caused by the attachment of the first monolayer. Layer-by-layer deposition of particles formed from different materials (such as Au/CdS/Au[95]) or particles and polymers (such as SiO_2/PDDA/SiO_2[142]) have also been followed using QCM. Alternate layers can show different frequency changes, which translates into a different mass uptake resulting from various sizes and densities of the layer components. For example, the mass uptake in the course of building an Au/CdS/Au multilayer assembly is significantly higher for each gold-layer building step than that for CdS layer, since the CdS particles are lighter.[95]

The only other analyses that can provide related information are the much more troublesome ellipsometry[142, 153, 154, 157] and X-ray diffraction (XRD).[65] Sample preparation is important in these experiments and the interpretation of results can also be problematic. Finally, information about the array surface has also been gleaned from XPS[61, 149] (to verify the presence of certain compounds and their relative abundances), NMR spectroscopy,[202] and surface plasmon spectroscopy (SPS).[10]

4. Functional Nanoparticle Arrays

The ultimate aim of the nanoparticle engineer is the creation of materials and devices that have valuable functions in the real

world. The properties of colloidal particles are known to be of use in many disciplines but the challenge is to organize them with complete control. The integration of nanoparticles in composite structures as well as their interface with external inputs and outputs will be necessary to reach their full potential. Assemblies of disorganized nanoparticles have been used successfully to produce rudimentary sensors,[28] ultramicroelectrodes,[203] and unusual materials.[191] While these structures are able to demonstrate concepts, they do not give us access to the direct nanoengineering that is necessary for the development of the next generation of devices. Organized monolayers provide a route towards true nanoengineering. Organized nanoparticle monolayers have been used as masks for the evaporation of gold patterns.[84] If the individual particles in an organized monolayer are "stuck together" (for example, by the evaporation of a thin gold film), then the entire monolayer may be removed from the substrate in one piece.[85] This procedure allows the monolayer mask to be transferred to almost any substrate and provides access to colloid-templated patterning on curved surfaces and unusual materials. Electronic colloid-based devices have been built which take advantage of the precise placement and engineering of colloidal nanoparticles, while sensing matrices have been built which exploit the properties of both the colloidal and the crosslinking materials. As yet, the chemical[204] and catalytic properties of nanoparticles have not been used in functional arrays. Ultimately, it may be possible to integrate different colloid-based components to create highly functional electronic, sensor, and photoelectrochemical devices of nanoscale dimensions.

4.1. Arrays with Optical Functions

The intrinsic optical properties of metallic colloids has led to many applications exploiting their plasmon absorbance (Section 4.1.1) or their ability to enhance the Raman effect (Section 4.1.2). Other research has focused on their use as the components of diffraction gratings. The small size of nanoparticles means that if they are equally spaced in a lattice, the assembly can act as a diffraction grating. Because the properties of a diffraction grating depend on the unit spacing, an event that changes the interparticle spacing in a regular array can be detected optically. Thus, crystalline colloid arrays (CCAs) of polymer particles have been used to detect temperature and binding events.[205] In the latter example, a CCA was polymerized inside a hydrogel containing lead-binding crown ether moieties. The CCA/hydrogel absorbs any Pb^{2+} that is in solution and results in an osmotically driven swelling of the array. The optical consequences of this change are detectable by the naked eye at Pb^{2+} concentrations as low as 40 ppb.

4.1.1. Surface Plasmon Functions

The plasmon absorbance of nanoparticles is a consequence of their small size but it can be influenced by numerous factors. In particular, solvent and surface functionalization are important contributors to the exact frequency and intensity of the band.[10, 182, 183] This dependence on surface effects make the surface plasmon an ideal monitor of adsorption to the particle surface, which allows nanoparticle assemblies to be used as sensing devices. These effects are particularly pronounced for silver colloids and warrant their use in much of the research into SPS.[10]

The specific biochemical binding of biologically complementary pairs (for example, antigen – antibody, biotin – avidin, DNA – complementary DNA) can be performed at an interface and various physical means can be used to detect the corresponding change of the interfacial properties. A general approach includes the modification of a solid support with one component of the recognition pair and then the modified surface is allowed to react with the second complementary component, which produces a complex at the interface. When the applied solid support is electroconductive, electrochemical techniques (such as impedance spectroscopy,[206–208] chronopotentiometry,[207] or cyclic voltammetry[209, 210]) sensitive to an additional barrier against electron-transfer processes at the interface have been applied to detect the formation of these complexes. QCM,[208, 209, 211] ellipsometry,[212, 213] and surface plasmon resonance (SPR)[213, 214] have also been employed for the detection of the corresponding changes at the interface.

If an analyte is coupled to a metal nanoparticle, then the change in the interfacial properties resulting from the formation of the affinity complex at the interface can be greatly enhanced. SPR demonstrates the enhancement of the signal resulting from antigen – antibody complex formation (Figure 14).[215] In this paradigm, either antibody-functionalized nanoparticles bind to an antigen-functionalized surface (Figure 14 A) or antigen-functionalized colloids bind to an antigen-functionalized surface (Figure 14 B), for which a solution-state antibody acts as a linker.

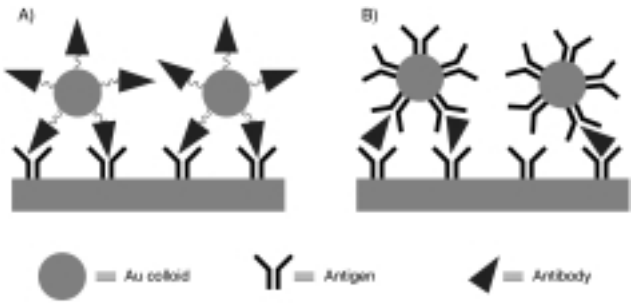

Figure 14. *Schematic representations of particle-enhanced biosensing architectures.*

Exposure of a gold film coated with an antibody (γ-chain-specific monoclonal goat anti-human immunoglobulin G; anti-IgG-γ) to a 1.0 mg mL^{-1} solution of human immunoglobulin G (IgG) results in a 0.1° shift in plasmon angle with no change in curve shape (Figure 15 A). In contrast, a significantly larger shift (1.5°), an approximately 2% increase in minimum reflectance, and noticeable broadening of the curve is observed (Figure 15 B) upon the exposure of an identically prepared surface to an electrostatically bound conjugate between IgG and 10 nm diameter colloidal gold.[215] Quantitative interpretation of the signal shows an almost linear change with the surface occupation of the

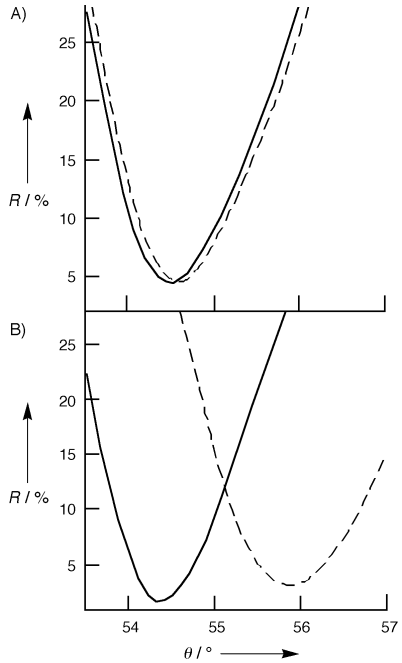

Figure 15. *In situ SPR curves of: A) An evaporated gold film, modified with anti-IgG-γ (——) and exposed to IgG (1.0 mg mL^{-1}; – – –); B) The same experiment, except that the IgG was conjugated with 10 nm gold nanoparticles.* R = *resonance enhancement. Reproduced from ref. [215] with permission.*

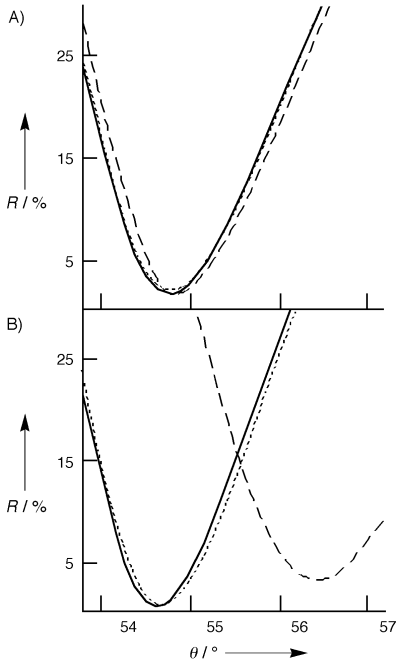

Figure 16. *In situ SPR curves of: A) An evaporated gold film, modified with anti-IgG-γ (——) and sequentially exposed to IgG (0.045 mg mL^{-1}; ····) then anti-IgG-F$_c$ (8.5 mg mL^{-1}; – – –). B) The same experiment, except that the final anti-IgG-F$_c$ was conjugated with 10 nm gold nanoparticles.* R = *resonance enhancement. Reproduced from ref. [215] with permission.*

analyte – gold conjugates. A similar SPR curve was observed using the primary interaction of the sensing interface with IgG followed by interaction with a secondary antibody (F_c-specific monoclonal goat anti-human immunoglobulin G; anti-IgG-F_c) conjugated with a gold colloid. Whereas little change in the surface plasmon was observed in the absence of gold colloids, (Figure 16 A), the application of the anti-IgG-F_c conjugated with a gold colloid greatly amplified the surface plasmon change (Figure 16 B). The colloidal gold particles introduced to the interface with the anti-IgG-F_c resulted in a 1.7° shift in plasmon angle (rather than 0.06° for pure anti-IgG-F_c), a 2% increase in minimum reflectance, and a noticeable broadening of the SPR curve. Both detection schemes clearly demonstrated enhancement of the signal as a result of gold colloids coming to the interface together with the biomaterial. This method can detect IgG to a concentration of about 7 nM.

4.1.2. Surfaced-Enhanced Raman Scattering Functions

When an adsorbate on a rough metal surface is subjected to Raman scattering spectroscopy, very high enhancements (several orders of magnitude) over a flat substrate are observed.[216] This SERS effect is a general analytical method for adsorbates on active metals such as gold, silver, and copper. The enhancement may extend tens of nanometers from the substrate surface and is at its highest for surfaces that are rough on the 10 – 100 nm scale—exactly the size of gold and silver colloids produced by the simple citrate reduction method. The mechanism of the enhancement is not fully understood but seems to stem from both an enhanced electromagnetic field as a consequence of surface plasmon resonance and the appearance of new electronic states in the adsorbate as a consequence of adsorption.

Solution-state SERS studies of pyridine on gold nanoparticles show that the enhancement occurs when the exciting radiation is coincident with the plasmon absorbance of the nanoparticles.[217] This result is consistent with the theory that the enhancement is caused by an enhanced local electromagnetic field. Later research studied aggregated nanoparticles, which have additional plasmon resonances associated with interparticle plasmon coupling. This work showed that the longer wavelength, interparticle plasmon resonances of nanoparticle aggregates provide an even better excitation frequency for SERS.[182, 183] The production of nanoparticle aggregates in solution can be problematic, however. Not only are the aggregates polydisperse in shape and size, but the process of aggregation is dynamic—the composition of an aggregating solution changes over time—and the particles ultimately precipitate (although there are ways to stabilize colloid aggregates in solution).[218]

Some of the first papers describing the assembly of nanoparticle monolayers were directed towards their use as SERS substrates.[71, 90] Previously, solid SERS substrates had been constructed by etching or deposition, which was both technically demanding and imprecise. The use of nanoparticles, which are easily synthesized to be monodisperse and were known to be excellent SERS substrates in solution, provided an elegant solution to these problems. In addition, immobilized particles are fixed in their morphology, so their aggregation state can be

carefully controlled. Monolayers of gold[90] or silver[71] nanoparticles were adsorbed onto silane-functionalized glass slides and were then treated with the analyte adsorbate. As expected, it was found that SERS activity is strongly dependent on the aggregation state of the particles (Figure 17). Enhancements

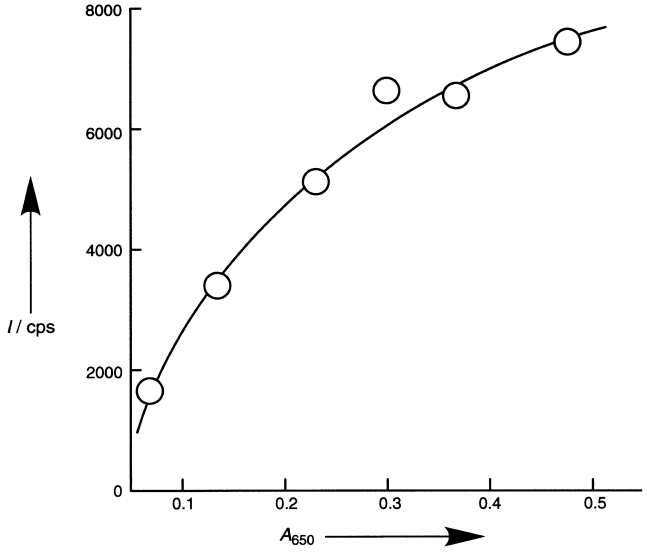

Figure 17. *The SERS intensity of the 1610 cm^{-1} band of* trans*-1,2-bis(4-pyridyl)-ethylene varies with the strength of the interparticle-coupled plasmon absorbance of a gold nanoparticle monolayer on which it is adsorbed (at 632.8 nm excitation). I = SERS intensity, A_{650} = absorbance at 650 nm. Reproduced from ref. [90] with permission.*

were comparable to those observed from electrochemically roughened electrodes. Even higher enhancements have been obtained by the use of silver-coated gold nanoparticles.[45, 56]

The high SERS enhancements observed on substrates of aggregated colloids are, in fact, an average of the very different enhancements at all the points on the film. Theoretical calculations predict that the variation is very pronounced,[219] which suggests that localized enhancements may be orders of magnitude higher than the (already high) average enhancement. This theory was checked by SERS studies on the tip of an atomic-force microscope.[220] Such a method allows the analysis of single particles and aggregates: If the adsorbate is added in a very low concentration of significantly less than one molecule per particle, then even single molecule analyses can be performed. This study focused on the analysis of rhodamine 6G on silver nanoparticles (of about 35 nm diameter). The dye was first adsorbed onto the surface of the nanoparticles, which were then immobilized on a polylysine-coated glass substrate. About one in 10 000 nanoparticles had a very high SERS activity and there seemed little to identify these nanoparticles in terms of size, shape, and aggregation state (Figure 18). The highly active "hot particles" often seemed to be larger or rod-shaped but other particles also displayed this property. Analysis showed that SERS enhancements of up to $\times 10^{15}$ were possible, which allows the detailed analysis of single molecules, even to the point of determining their orientation.

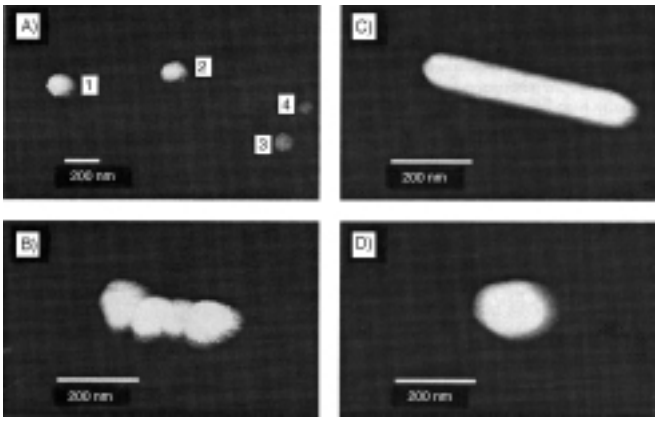

Figure 18. *Tapping mode AFM images of "hot" silver nanoparticles and their aggregates. A) Four particles, of which two show a high Raman enhancement (particles 1 and 2 are "hot") and two do not (particles 3 and 4). B) A "hot" four-particle linear aggregate. C) A "hot" rod-shaped particle. D) A single "hot" particle. Reproduced from ref. [220] with permission.*

4.2. Arrays with Electronic Functions

4.2.1. Colloids as Electrical Contacts

For the construction of colloid-based microelectronics, it is desirable to engineer two- and three-dimensional arrays of colloidal metal particles that can be used as wires and electrodes. The primary requirement for such applications is high electrical conductivity of the assembly, as can be attained by closely-packed colloid multilayers. The cyclic voltammetry of various redox probes (such as $K_3[Fe(CN)_6]$, hydroxymethylferrocene, and hydroquinone) has been studied on glass slides functionalized with different numbers of bisthiol-crosslinked colloidal gold layers.[144] At less than seven layers, the voltammetry is resistive and poorly defined, but at seven layers the voltammetry becomes sigmoid—such as that observed at a microelectrode due to radial diffusion of the redox species to the electrode surface. The electrode can be modeled as many small conductive "islands" with nonoverlapping diffusion layers and thus behaves as a microelectrode array. Cyclic voltammograms of electrodes with higher coverages exhibit the linear diffusion characteristics of planar macroelectrodes. Here, the electrode may be modeled either as a continuous metallic surface or as a microelectrode array, whose component diffusion layers overlap due to the higher density of gold "islands" on the electrode surface. Well defined diffusion-limited voltammograms were recorded, as demonstrated by a classical $t^{-1/2}$ current decay, linear plots of the peak current versus the square root of the potential sweep rate, and peak-to-peak separations (ΔE_{peak}) ranging from 85 mV ($K_3[Fe(CN)_6]$) to 133 mV (hydroquinone), and indicated nearly reversible to quasi-reversible electron-transfer kinetics. The electron-transfer rate constants of $[Fe(CN)_6]^{3-}$, measured at a ten-layer film of colloidal gold, were found to be close to those known for bulk gold electrodes: 7.6×10^{-3} cm s^{-1} and 7.9×10^{-3} cm s^{-1}, respectively.

Reversible and quasi-reversible electrochemical processes have been demonstrated at metal colloid multilayer arrays for many different, soluble redox probes, such as methyl viologen

(**2**),[90] ferrocene derivatives,[187] and $[Fe(CN)_6]^{3-/4-}$.[153, 188, 190] Direct, nonmediated electrochemical activity of cytochrome c was observed at a SnO_2 electrode modified with colloidal gold.[221] This is of particular interest as cytochrome c normally demonstrates reversible electrochemistry only at promoter-modified electrodes, at which favorable orientation of the hemoprotein towards electron transfer is provided.[222] Furthermore, the morphology of the nanoparticle surface is extremely important in the process—aggregated gold particles or particles of an inappropriate size fail to establish efficient electrical contact between the hemoprotein and the electrode.

When a multilayer of colloidal metal particles is organized onto a conductive support, one needs to determine the contributions of the external layer, internal layers, and the conductive support towards the heterogeneous electron-transfer process. A redox probe (*p*-nitrosodimethylaniline) that exhibits different cyclic voltammograms at SnO_2 and Au electrodes has been used to discriminate between the electrochemical responses from a SnO_2 support and the colloidal gold array organized onto it.[89] The recorded cyclic voltammogram clearly demonstrated that the main contribution to the electrochemical process is from the gold particles. Multilayer arrays of gold colloids linked through alkanedithiol bridging molecules were terminated with either the gold colloid or alkanedithiol as the external layer. The colloid-surfaced array demonstrated efficient electrochemical process in the presence of a soluble redox probe, whereas the alkanedithiol-terminated array was highly insulating and nonelectrochemically active.[153] Such electrochemical behavior can be observed if the redox probe does not penetrate inside the array so that the array surface is the only interface responsible for the heterogeneous electron-transfer process. In other cases, however, the array is porous so both the external and internal surfaces can participate in the electrochemical process.[139, 147, 150]

Monolayer (2D) and multilayer (3D) arrays of colloidal metal particles have been used as supports for the immobilization of redox-active molecules. Strong adsorption of $[Fe(CN)_6]^{3-/4-}$ ions onto gold colloids attached to a cystamine-functionalized gold electrode has been demonstrated.[188] Symmetrical anodic – cathodic peaks with very small peak-to-peak separations (3 mV), typical of Laviron-type electrochemistry,[223] were observed in the cyclic voltammograms when the gold colloid-modified electrode was probed in the presence of $[Fe(CN)_6]^{3-/4-}$. Laviron also reported a linear dependence on the potential scan rate, characteristic of adsorbed redox species. These peaks appear in addition to normal diffusional waves of the $[Fe(CN)_6]^{3-/4-}$ and are shifted by $+515$ mV from the diffusionally controlled redox waves. Such a large shift in potential is evidence of strong adsorption, which results in a significant change of the energetic properties of the redox ions. However, a colloidal gold electrode immersed in an electrolyte solution free of $[Fe(CN)_6]^{3-/4-}$ slowly loses the adsorbed redox-active anions because of their substitution with redox-inactive anions of the electrolyte. Much stronger adsorption of redox species, which results in their permanent immobilization onto conductive (or semiconductive) nanoparticles can be achieved if the adsorbed molecules have special "anchor" groups to provide binding to the solid support. Typical anchor groups used for coupling with gold nanoparticles (which can also be used with silver or platinum particles) are thiol and disulfide groups.[98] Redox-active modifiers (such as ferrocene units[224] or anthraquinones[225]) have been linked to gold colloids by spacers terminated with thiol anchor groups. The redox-functionalized gold nanoparticles can be later assembled on a solid support. Another approach includes the attachment of redox-active modifiers to gold nanoparticles already assembled on a solid support. For example, a ferrocene – thiol monolayer deposited on top of a colloidal gold layer demonstrated the Laviron-type electrochemical behavior typical for monolayers of redox materials on flat, continuous electrodes.[116] The small peak-to-peak separation in the cyclic voltammogram ($\Delta E = 6$ mV at a potential scan rate of 10 mV s^{-1}) demonstrates a fairly fast, reversible electrochemical process ($k_{et} = 4\ s^{-1}$) and a negligible contribution from the resistance between the colloid layer and the conductive support. More complex redox compounds, such as dyads comprising elements with pH-dependent (quinone) and pH-independent (bipyridinium) electrochemistries have been immobilized atop of nanoparticle 2D arrays.[88] For the first case, Equation (1) describes its behavior, where E^0_{pH} and $E^0_{pH\,7}$ are the redox potentials measured at any pH and pH 7; *m* and *n* are numbers of electrons and hydrogen ions involved in the reduction of a quinone molecule; and *R*, *T*, and *F* have their usual meanings of the gas constant, temperature, and Faraday constant, respectively.

$$E^0_{pH} = E^0_{pH\,7} - 2.3\left(\frac{m}{n}\right)\left(\frac{RT}{F}\right)(pH - 7) \quad (1)$$

4.2.2. Colloids in Single-Electron Devices

If metallic particles of a few nanometers in size are arranged within about 1 nm of each other, they build tunnel junctions with electrical capacitances as low as $10^{-19} - 10^{-18}$ F.[20] This allows controlled charge transport between the particles by single-electron tunneling (SET) events at room temperature, which has been recognized to be a fundamental requirement for the development of quantum electronics.[9] Charging energy (E_c) as well as capacitance depends on the size of the metallic nanoparticles and the distances between them. The charging energy (namely, the energy barrier that has to be overcome to transfer a single electron from an initially neutral cluster to a neutral nearest-neighboring cluster) is dependent on the interparticle capacitance *C*, as follows from Equation (2), where *e* is the charge of an electron.

$$E_c = \frac{e^2}{2C} \quad (2)$$

The use of interparticle spacers can be valuable in controlling capacitance. For instance, while the close packing of the $Pd_{561}(phen)_{36}O_{200}$ clusters (phen = 1,10-phenanthroline) produces a capacitance of 4.0×10^{-18} F, the insertion of 4,4′-diamino-1,2-diphenylethane spacers reduces it to 1.6×10^{-18} F.[226] The conductivity and capacitance of nanostructured materials have been studied using direct current (DC) measurements[20, 226] and impedance spectroscopy.[227] Cyclic voltammetry performed on a

single gold nanoparticle in contact with an STM tip has also been used to study single-electron transfer processes.[25]

SET devices range from a single conductive nanoparticle located between two microelectrodes[24, 26, 228] or in contact with an STM tip[25, 229] to 2D and 3D arrays that consist of nanoparticles which experience SET between them.[131, 229, 230] Scanning-tip microscopy techniques can be used to observe SET events and even to form the respective devices. For example, scanning tunneling spectroscopy (STS) has been applied to the observation of SET effects on nanoparticle monolayers of $Au_{55}(Ph_2C_6H_4\text{-}SO_3H)Cl_6$ in contact with a tip, to demonstrate "Coulomb staircase" behavior (single electron transfer steps in the current – potential curve) even to room temperature, where the capacitance of the cluster/substrate junction was calculated to be 3.9×10^{-19} F.[231] Similar results were obtained on application of STS to self-assembled gold nanoparticles (1.8 nm) on a dithiol-modified gold surface.[229, 232] A single-particle device was fabricated by AFM-assisted manipulation of a 20 nm gold nanoparticle between two metallic leads.[172] Two-dimensional lattices for SET devices can be prepared by self-assembly techniques.[70, 233] Layer-by-layer assembly has been used for the construction of metal-insulator-nanoparticle-insulator-metal ("MINIM") capacitors, which also demonstrate Coulomb staircase behavior.[131] The MINIM devices were made (Scheme 12) by first priming the surface of a gold substrate with cysteamine (2-aminoethanethiol). Insulating layers of α-$Zr(HPO_4)_2 \cdot H_2O$ (α-ZrP)

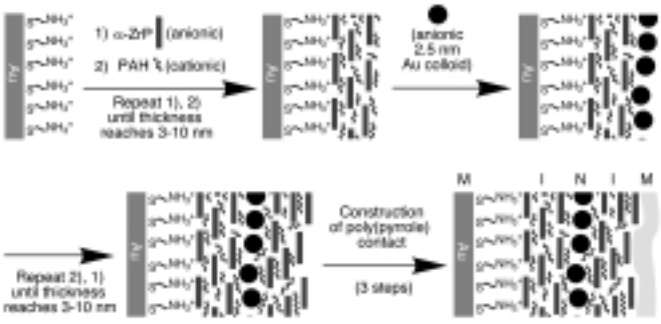

Scheme 12. *The stepwise construction of a MINIM device.*

and polyallylamine hydrochloride (PAH) were sequentially adsorbed, terminating with the cationic substance, until the desired thickness was obtained (typically 3 – 10 nm, as measured by ellipsometry). Subsequently, citrate-stabilized gold particles (about 2.5 nm) were immobilized on top of the insulating layer. The remaining half of the double junction was constructed by simply reversing the adsorption sequence described. For a junction thickness of 80 Å and a particle radius of 1.25 nm, the capacitance of a double-tunnel junction device is 4.5×10^{-19} F, as calculated from Equation (3), where μ_0 is the vacuum permittivity constant, μ_r is the dielectric constant of the insulator, a is the particle radius, and L is the junction thickness.[234] A Coulomb gap of 360 mV ($=e/C$) should be observed at room temperature, since it is substantially higher than values of kT.

$$C = 4\mu_0\mu_r[1 + \left(\frac{a}{2L}\right)] \quad (3)$$

A typical current – potential curve for such a MINIM structure is shown in Figure 19A. The high impedance region is observed on both sides of 0 V and represents the average charging potential ($\pm e/2C$) of each particle at the double junction array by a single

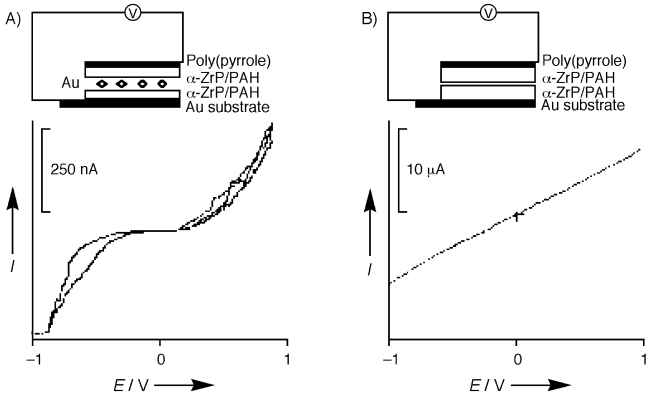

Figure 19. *Current – voltage curves for the MINIM device shown in Scheme 12. A) The properly constructed MINIM device. B) The curve for a device that was built without the nanoparticle layer. Reproduced from ref. [131] with permission.*

electron. When enough energy is supplied to charge a particle, electrons tunnel through the junction, which results in the square-law dependence of the current rise on either side of the gap. Figure 19B shows similar measurements on a device of similar thickness in the absence of the gold particles. A linear curve, typical for ohmic resistance, is observed.

In the next generation of single-electron devices,[235] "switchable" quantum dots and quantum channels with correlated electrons will offer components orders of magnitude smaller than classical electronic switches or semiconductor memories. This could result in a new generation of computers,[236] supersensitive electrometers, near-infrared receivers, and very simple miniature lasers.[9, 237] Recently, a single-electron transistor has been constructed using alkanedithiol-stabilized gold nanoparticles as tunnel junctions.[24, 26] Three colloidal gold particles (10 nm) were linked by 1,6-hexanedithiol, to produce a gold colloid chain. The particle chain was formed on a silica substrate with metallic source, drain, and gate electrodes defined by electron-beam lithography (Figure 20). The gold colloid chain bridged a 30 nm gap between the source and drain, which formed a single-electron transistor with a multitunnel junction in the particle chain. Electron conduction through the chain exhibited a clear Coulomb staircase and the periodic conductance oscillated as a function of gate voltage. A similar device was created using a single CdSe nanoparticle (5.5 nm) located between two gold microelectrodes that function as source and drain.[23, 27] Gold nanoparticles capped with dissociating modifier molecules, Au/galvinol, provided pH-dependent resistance to single-electron transfer processes, even if only about ten modifier molecules were present per gold nanoparticle.[238] Single-electron memory devices based on field-effect transistors (FETs), which consist of a single silicon particle[239] (or several particles[240]) embedded in a thin silica insulator, allows the control of current flow (on/off) by the injection of a single

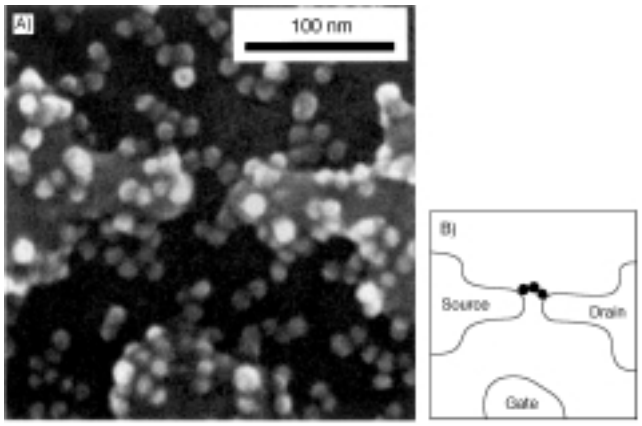

Figure 20. *A) An electron micrograph and B) schematic clarification of a three-nanoparticle bridge constructed between source and drain electodes. The gate electrode is seen in the lower part of the micrograph. Reproduced from ref. [24] with permission.*

electron into the gate. These SET devices displayed read/write times of about 20 ns, lifetimes in excess of 10^9 cycles, and charge retention times of days to weeks.

While single-electron computing continues to be the ultimate goal of SET technology, its most advanced practical application is currently the construction of a super-sensitive electrometer. FET devices with nanoparticles in the gate have provided a charge sensitivity of 600 pA per gate electron.[9] This electrometer could be used as an extremely sensitive tool for detection of the redox-state of a single molecule linked to the nanoparticle, thus allowing the detection of single-molecule chemical reactions.

Combining many SET elements together for the development of computing devices remains challenging. Even if it is not an unreasonable task to make electrical connections to a single nanotransistor, fabricating the 10^{12} transistor network that is required for computing is currently a far-off dream. Two independent approaches to connect many SET units have been suggested recently. The first approach involves the simple combination of SET units with well developed FET devices, in which a multigate FET device is used and each gate is associated with a single SET unit. The second, more novel approach is to forgo the connecting wires altogether.[241] This scheme, named quantum cellular automata (QCA), is based on the electrostatic interactions present between cells of connected clusters. In one possible design, the basic cell is a line of nanoclusters connected by insulating material (Figure 21 A). An electric field polarizes the string to give a "1" or "0" state, depending on the field direction. A similar design is produced from square cells of nanoclusters carrying the polarization states (Figure 21 B). Again, two states are possible, dependent upon the direction of the applied field. In either design, the cells can be connected in various configurations to make more complex logic circuits. Figure 21 C illustrates how the cells can be connected to form a logic gate. The dark and open circles correspond to one-electron rich and one-electron deficient clusters, respectively. The signals in QCA are rapidly transferred between interconnecting cells through electrostatic interactions at the speed of light. Fast intercell

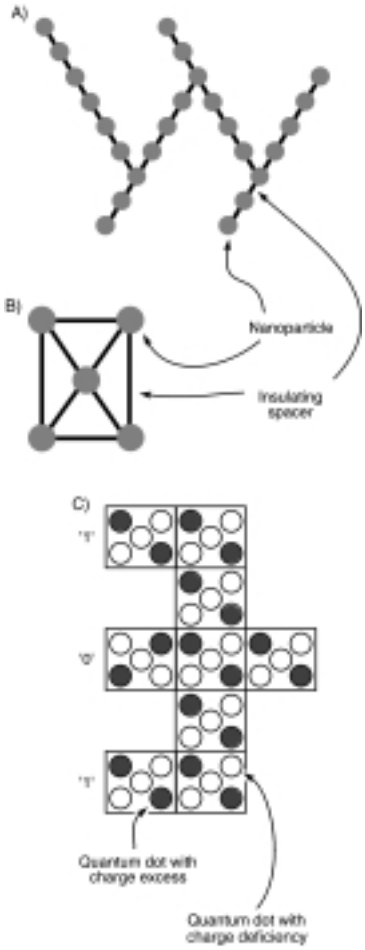

Figure 21. *Schematic representations of proposed "wireless" computation devices based on nanoparticle assemblies.*

interactions and the small size of each cell (as low as about 2.5 nm^2) hold excellent potential for ultrahigh density data storage and processing from this kind of device.

4.3. Arrays with Sensor Functions

The use of gold nanoparticle superstructures for the creation of electrochemical sensing devices is an extremely promising prospect. Multilayers of conductive particles give rise to a porous, high surface-area electrode, where the local micro-environment of the gold particles can be controlled by the crosslinking elements and may lead to specific and selective interactions with substrates.

4.3.1. Vapor Sensors

Chemiresistors are simple solid-state devices whose electrical resistance is changed by the presence of chemical species. The resistance of nanoparticle arrays depends on the colloid size, interparticle distance, and dielectric properties of the interparticle material. An array consisting of colloidal gold stabilized with hydrophobic long-chain alkyl thiols is a medium that can accommodate organic materials, such as hydrocarbons or

halogenated hydrocarbons, between the particles. Incorporation of the additional material can increase the interparticle distance and lower the relative (dielectric) permittivity of the medium, to result in a decrease of the electrical resistance of the array. This approach was recently applied for the detection of toluene and tetrachloroethylene vapors, which provided a detection threshold of approximately 1 ppm (v/v).[242] The device demonstrated a high sensitivity to these low polarity materials while being almost insensitive to materials with higher polarity (such as 1-propanol and water) at the same vapor pressure. Application of impedance spectroscopy could result in better understanding of the physical mechanisms of the sensing phenomenon, namely, finding which component of the resistance—faradaic or nonfaradaic—is mainly responsible for the resistance change.

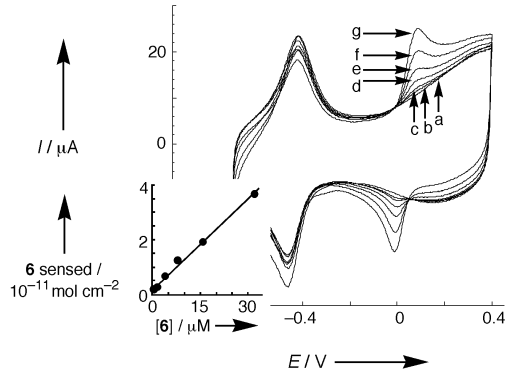

Figure 23. *Cyclic voltammograms of the five-layer electrode in the absence (a) and at various concentrations (b – g) of* ***6****. Inset: Calibration curve for the sensing of* ***6****. Recorded with conditions described in Figure 22.*

4.3.2. Sensing by a Receptor-Crosslinked Array

A series of electrochemical sensors were built by the electrostatic crosslinking of gold nanoparticles with the bipyridinium cyclophanes **1** or **3**, or the square-shaped oligocationic palladium(II)-ethylenediamine-bipyridine complex **4** (Scheme 6).[139, 147, 149, 150] The bipyridinium cyclophanes **1** and **3** act as receptors for the association of π-donor substrates in their cavities and the 3D conductivity of the gold nanoparticle array electrochemically senses π-donor substrates associated with the cyclophane units. The formation of π-donor acceptor complexes between the host receptor and the π-donor analyte enables the preconcentration of the analyte at the conductive surface. Furthermore, control of the number of gold particle layers associated with the ITO electrode allows the sensor sensitivity to be tuned. Figure 22 shows the electrochemical sensing of *p*-hydroquinone (**6**) at a

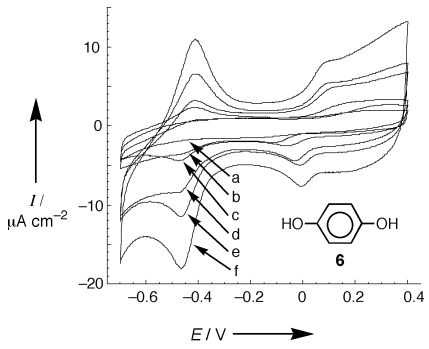

Figure 22. *Cyclic voltammograms of a bare ITO electrode (a) and 1 – 5 layer gold colloid/****1*** *arrays ((b) – (f), respectively) in the presence of hydroquinone (****6****; 1 × 10^−5^ M). Recorded under argon in 0.1 M phosphate buffer solution, pH 7.2, scan rate 100 mV s^−1^, SCE as reference electrode.*

bulk concentration of 1×10^{-5} M by an electrode functionalized with different numbers of **1**-crosslinked gold nanoparticle layers. The electrical responses of both the cyclophane (at $E^0 = -0.450$ V versus SCE) and the analyte increase with the number of layers, which implies that the array must be porous. Figure 23 shows the calibration curve for the electrochemical response of the five-layer electrode to **6**. The response, as indicated by the calibration curve, is approximately linear within the concentration range examined, which demonstrates that the sensor is not easily saturated. The electrochemical sensing of the hydroquinone is possible at concentrations as low as 1×10^{-6} M. In contrast, for a gold nanoparticle array crosslinked by the acyclic molecule *N*,*N*′-diaminoethyl-4,4′-bipyridinium (**5**), **6** is undetectable electrochemically within the range $10^{-5} - 10^{-6}$ M. These observations clearly reveal that the successful sensing of **6** by the **1**-crosslinked superstructure originates from a specific host–guest interaction rather than from the fabrication of a roughened interface. In addition to the enhanced sensitivity in the analysis of **6** with the number of layers, the electron transfer kinetics of the guest is vastly improved upon the buildup of the layers, as shown by the decrease in its peak-to-peak separation.

Other π-donor substrates, such as dihydroxyphenyl acetic acid and the neurotransmitters adrenaline (**7**) and dopamine (**8**), can also be sensed by the **1**-crosslinked gold nanoparticle electrode.[150] These substrates contain π-donor *ortho*-hydroquinone units but, in addition, include those with β-aminoalkyl substituents on the aromatic ring. The electrochemistry of these compounds has been examined and discussed for homogeneous aqueous solutions[243] and is summarized in Scheme 13. Oxidation of the *o*-hydroquinone residue to the quinone (**9**) is only partly reversible, since the amine substituent induces a Michael addition accompanied by a ring closure and the formation of **10**, which exhibits reversible or quasireversible electrochemical properties. Figure 24 shows the electrochemical sensing of different concentrations of adrenaline by a **1**-crosslinked gold nanoparticle electrode.[150] In addition to the cyclophane redox wave, an irreversible oxidation wave for adrenaline is observed (at 0.3 V versus SCE), as well as a quasireversible redox wave (at $E^0 = -0.28$ V versus SCE), which corresponds to the electrochemically induced cyclization product **10** (Scheme 13). Coulometric assay of the quasireversible redox wave of the electrogenerated product enables extraction of the calibration curve (Figure 24 inset).

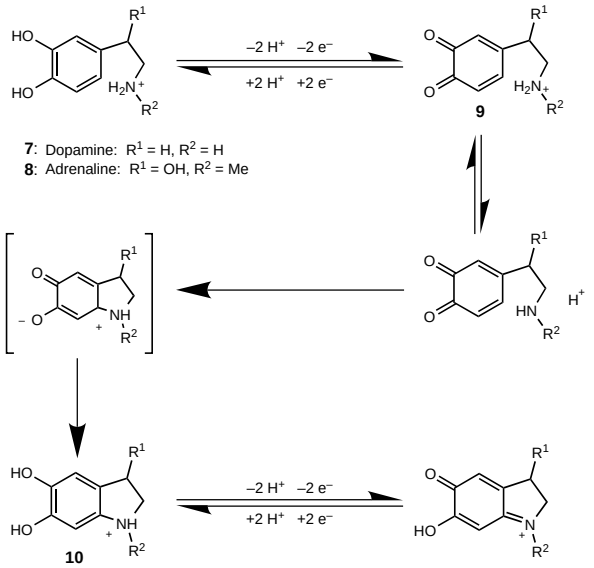

Scheme 13. *The electrochemically promoted intramolecular cyclization of 4-(β-aminoalkyl)1,2-benzohydroquinones.*

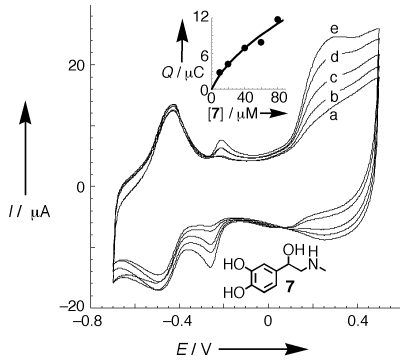

Figure 24. *Cyclic voltammograms of a 5-layer gold colloid/**1** electrode at various concentrations of adrenaline (**7**). Inset: Calibration curve for the signal of **7** from the reduction peak of its electrocatalysed Michael-type cyclization (Scheme 13). Recorded with conditions described in Figure 22.*

4.3.3. Receptor-Induced Selectivity

The selectivity of gold nanoparticle electrodes is controlled by the structure of the crosslinking receptor units. Application of the enlarged cyclophane **3** as a crosslinker for the gold particles enables the electrochemical sensing of *bis*-dihydroxymethylferrocene (**11**; Figure 25 A) but not of **6**, due to its large cavity dimensions.[139] Likewise, the **1**-crosslinked gold nanoparticle superstructure fails to sense **11** because the small receptor dimensions preclude the accommodation of the larger guest (Figure 25 B). The cationic Pd^{II} complex **4** enables the electrochemical sensing of both **6** and **11**, since its cavity is large enough for the former and the latter can associate with it in a diagonal orientation.[149] Lastly, the sensory features of the cyclophane–colloid electrodes are affected by the lattice morphology. A superstructure consisting of three inner layers of **1**-crosslinked gold nanoparticles then by three outer layers of **3**-crosslinked particles enables the electrochemical sensing of

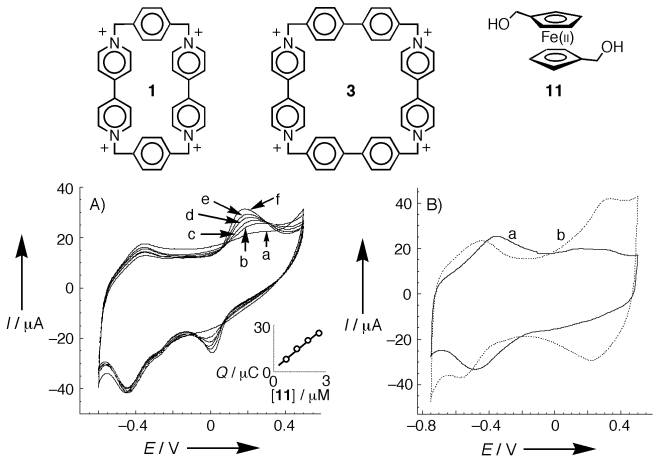

Figure 25. *A) Cyclic voltammograms of a **3**-crosslinked electrode (five layers) in the absence of and in various concentrations of **11**. Inset: Calibration curve for the signal of **11** from the amperometric reponses of the electrode. B) Cyclic voltammograms of five-layer electrodes crosslinked by **1** and **3** in the presence of **11** (1×10^{-6} M). Recorded with conditions described in Figure 22.*

both **6** and **11**. Conversely, a gold nanoparticle composite electrode, that consists of **3**-crosslinked gold nanoparticles then **1**-crosslinked gold nanoparticles, enables the electrochemical sensing of **6** only.[139] This phenomenon has been attributed to the porosity control of the gold nanoparticle array by the receptor crosslinking units—the superstructure consisting of **1**-crosslinked gold nanoparticles is porous to **6** but is impervious to the larger molecule **11**.

4.3.4. Nanoparticle Arrays as Ion-Sensitive Field-Effect Transistors

The receptor-based sensors described above are efficient in the concentration of the analyte at the substrate surface but, since the sensing is fundamentally electrochemical, the technique is limited to redox-active analytes. The same sensing principle can be used with a different sensing method, however, to allow the analysis of redox-inactive compounds. Ion-sensitive field-effect transistors (ISFETs) provide a means to detect charged species in close proximity to a gate surface. A charged species at the sensing interface (Figure 26 A) of such a device causes a change in the polarization of the underlying SiO_2/Si interface (a thin layer of a nonconductive material on the sensing interface, for example GaAs or Al_2O_3, is often used to ensure insulation). The conductance of electrons from the source electrode to the drain electrode through the semiconductor is highly sensitive to this gate polarization (which has the effect of either attracting or repelling charge carriers). By measuring either 1) the source–drain current at a given gate–source potential (V_{gs}) or 2) the gate–source potential required for a given source–drain voltage (V_{sd}) and source–drain current (I_{sd}), it is possible to determine the polarization of the sensing interface.

An ISFET-based sensor for small π-donors has been made by the fabrication of a **1**/gold nanoparticle surface at the Al_2O_3 sensing interface of an ISFET (Figure 26 B).[244] This assembly was built up by the stepwise deposition of polyethyleneimine, gold

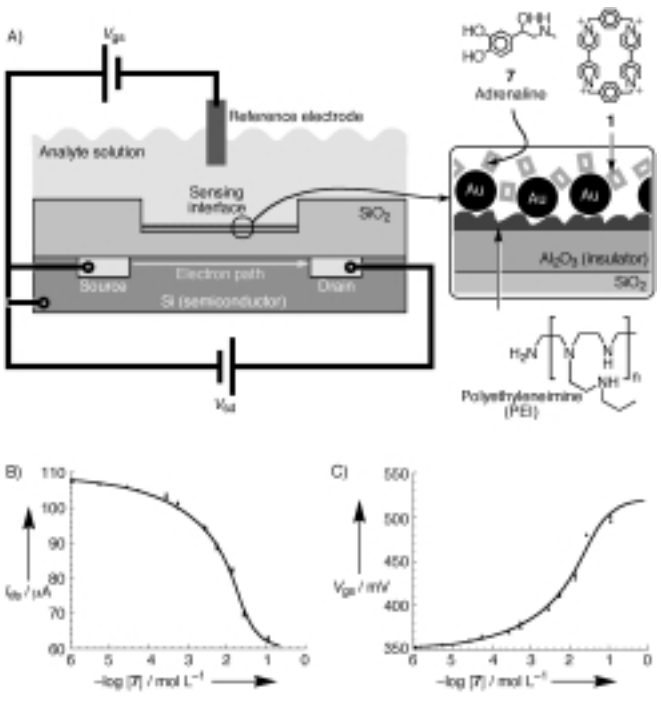

Figure 26. *A) Schematic diagram of a gold colloid/**1**-based ISFET sensor. B) Adrenaline (**7**) sensed by this ISFET by the source – drain current measurement mode. C) **7** sensed by the gate – source potential mode.*

nanoparticles, and **1** on the sensing interface. The resulting sensor is able to detect any charged molecule that complexes with the receptor **1**, including those that are not electrochemically active, such as serotonin. Figure 26C shows the results from a study of adrenaline. Reliable data for the detection of **7** can be obtained over six orders of magnitude of concentration, and Benesi – Hildebrand analysis[245] gave a calculated binding constant between **1** and **7** of $200 \pm 30\,M^{-1}$.

4.3.5. Nanoparticle – Enzyme Assemblies for Biosensing Applications

The possibility for direct electron transfer between conductive nanoparticles and redox proteins (such as cytochrome c[221]) paves the way for the construction of amperometric biosensors based on redox enzymes as sensing elements and nanoparticle arrays as the conductive matrix onto which the enzyme molecules are implanted. For example, a mixed layer of horseradish peroxidase (HRP) and colloidal gold particles (30 nm) was reported to be electrocatalytically active for hydrogen peroxide reduction without the need for electron-transfer mediators.[246] Although direct, nonmediated electron transfer is well known for some redox proteins and particularly for HRP,[247] it is usually very inefficient and is not generally used for practical biosensory devices. However, the small size of gold nanoparticles allows the conductive material to come into a close proximity of the active center of the enzyme, which facilitates the electron-transfer process and provides bioelectrocatalytic activity that can be utilized in biosensor devices. Another example of a biosensor exploring nonmediated, direct electron transfer is a D-fructose sensitive electrode based on D-fructose dehydrogenase encapsulated into a colloidal gold layer on a glassy carbon conductive support.[28] More attractive, but also more difficult from a nanoengineering point of view, is the organization of spatially ordered assemblies consisting of biocatalytic enzyme molecules and conductive nanoparticles, rather than their nonorganized composites. A thiol-terminated monolayer was prepared in a multistep procedure on a gold support (Scheme 14), to which colloidal gold (diameters of 16, 24, 42, or 51 nm) was added.[248] Finally, HRP was adsorbed onto the immobilized colloidal particles. Such a stepwise procedure provides some spatial organization of the system but the resulting array does not

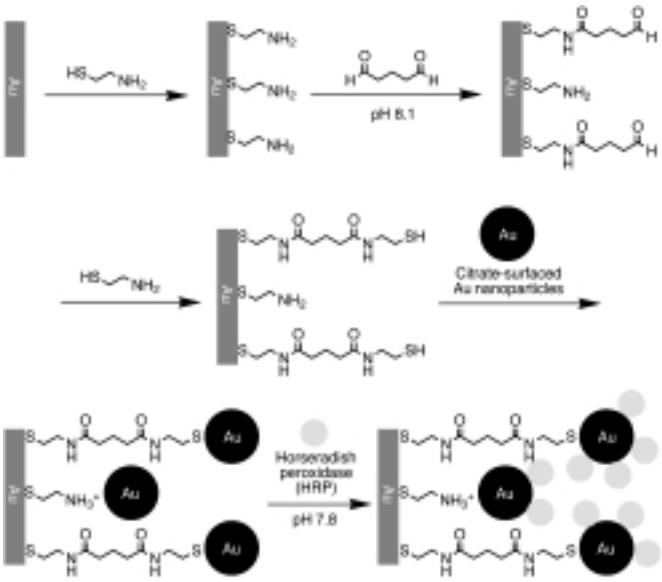

Scheme 14. *The preparation of a gold nanoparticle – horseradish peroxidase H_2O_2 sensor.*

operate in the absence of a diffusional electron-transfer mediator (catechol) because of the long nonconductive spacers used by the system. This problem can be solved by the application of conductive spacers, either with incorporated redox species, which function as intermediate stations for electron shuttling,[249] or with redox mediators tethered to enzyme molecules or nanoparticles.[250] In the case of small semiartificial biocatalyst molecules (for example, microperoxidase-11) that do not require electron-transfer mediators, a multilayer array with 3D-distributed bioelectrocatalysts has been created by a step-by-step deposition of the biomaterial and conductive nanoparticles.[251] The electrocatalytic current exhibited by the system was proportional to the number of biocatalytic layers in the multilayer array, thus all of the electrocatalyst molecules were accessible to the substrate (H_2O_2, in case of the colloidal gold/microperoxidase-11 3D array) and preserved their electrocatalytic activity.

Finally, the conductive properties of gold colloids can be used as an indicator for biosensing applications. A recent study detailed how arrays of individually tailored, addressable biosensors can be built up, where a "positive" signal results in the

short circuiting of two microelectrodes by gold nanoparticles (Scheme 15).[252] In the first step, an alternating current between two electrodes causes the collection of polymer-coated magnetic particles between them. These particles, which bear an IgG-binding protein coating, are covalently immobilized before the analyte (IgG) is added. After interaction with the analyte, the assembly is incubated with gold nanoparticles which bear anti-IgG. If IgG is present on the array, these gold colloids bind and provide conductivity between the electrodes (which can be enhanced by a further step of nonelectrochemical deposition of silver on the gold particles). An electron micrograph of two electrodes short circuited in this way is shown in Scheme 15.

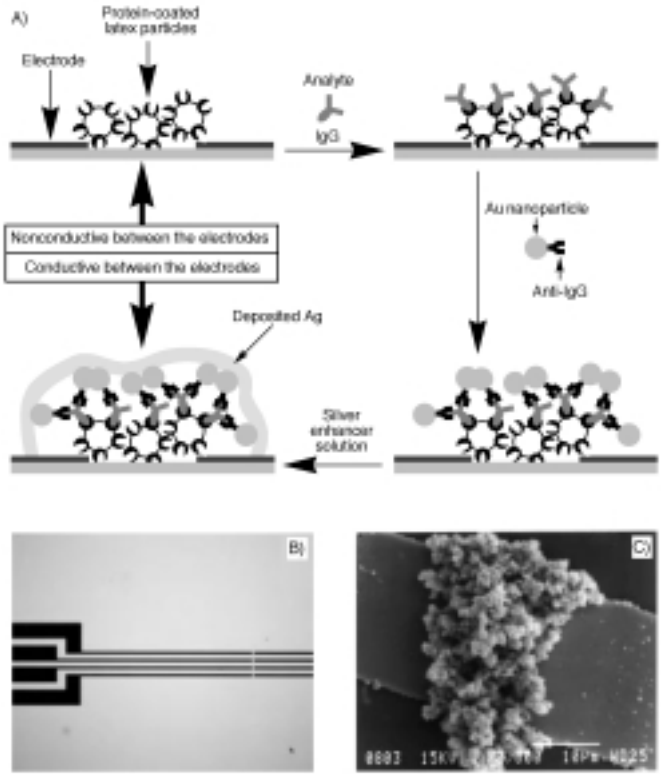

Scheme 15. *A) The assembly of the IgG sensor and its operation. B) An array of four 30 μm wide electrode pairs prior to sensor assembly. C) SEM image of a short-circuited electrode pair after the successful sensing of IgG. Reproduced from ref. [252] with permission.*

4.4. Arrays with Photoelectrochemical Functions

4.4.1. Photoelectrochemical Power To Generate Nanoparticle Superstructures

Photocurrent generation in semiconductor nanoparticle arrays has been used to characterize photoinduced charge separation and electron mobility in and between nanoparticles (see Section 3.3.2). The possibilities for the variation of nanoparticle architecture, for the construction of ordered mixtures of different components, and for the introduction of low-molecular mass additives make semiconductor nanoparticle arrays very attractive for the development of photocurrent generating elements.[253, 254] Lead sulfide based photosensitive nanoparticles capped with hydrophobic long-chain molecules (dioctyl sulfosuccinate) have been assembled onto gold electrode surfaces modified with long-chain thiols.[255] The hydrophobic interaction between the monolayer on the solid gold support and the capping material around the PbS nanoparticles provided immobilization of the particles at the electrode surface. A cathodic or anodic photocurrent was observed when an electron acceptor or donor, respectively, was added to the solution. Photoinduced, interparticle electron transfer between dissimilar semiconductive particles have been used to convert light into electricity. The coupling of two semiconductor particles may offer an opportunity to sensitize a wide bandgap semiconductor material by another with a narrower bandgap. Thus, interparticle conjugates of CdS/TiO_2, CdS/ZnO, CdS/Ag_2S, CdS/AgI, ZnS/AgI, ZnS/Ag_2S, ZnS/Cd_3P_2, ZnS/TiO_2, and ZnS/ZnO have been prepared and their interparticle electron transfer studied.[126, 256] Charge transfer from CdS to TiO_2 particles has been more extensively studied than the other systems. The conduction band of CdS lies above that of TiO_2 and, thus, CdS $\rightarrow$ TiO_2 electron transfer is energetically allowed. The possibility of using bifunctional bridging ligands to form rigid and well defined systems that consist of two kind of nanoparticles has been explored to build photosensitive mixed-particle aggregates.[126] Bifunctional linkers that contain both thiol and carboxylic acid groups to couple with CdS and TiO_2 particles, respectively, were applied to build mixed-particle assemblies. Optical and photochemical properties of these assemblies were studied and efficient photoinduced interparticle charge separation was demonstrated. These systems have not yet been used for photocurrent generation, however.

Spectral sensitization of wide bandgap semiconductors in photoelectrochemical cells is an attractive approach for conversion of the visible light from solar energy into electricity. Various organic dyes and metallocomplexes (for example, merocyanine-540[257] or ruthenium(II) polypyridyl species[253]) have been used as sensitizing dye molecules and facilitate an appreciable absorption of incident light. Although substantial effort has been directed towards the optimization of photochemical systems, the observed photocurrent efficiencies have generally been very low. A major factor responsible for the low photoconversion efficiency of an organic dye-sensitized solar cell is the formation of dye aggregates on the semiconductor surface. The photoinduced charge separation can be suppressed significantly because of intermolecular quenching in the dye aggregates. Different possibilities to prevent photosensitizer aggregation have been studied, such as incorporation of dye molecules into β-cyclodextrin cavities[258] and microencapsulation of dye molecules in surfactant systems.[257] Increased molecular spacing between photoexcited dye molecules can significantly diminish interconversion rates, which makes the deactivation pathways less competitive. The incident photon-to-photocurrent generation efficiency exhibited by the encapsulated monomeric dye (around 40%) was reported to be nearly five times larger than the corresponding efficiency of the dye aggregate (about 8%). A prototype solar cell "OTE/TiO_2/MC540/PVP", which consisted of a photoelectrode (photoanode) based on TiO_2 nanoparticles (as a 2–4 μm thick film), merocyanine-

540 dye encapsulated into a surfactant system (aerosol-OT), and a Pt wire gauge (counterelectrode), was studied.[257] Figure 27 shows the photovoltage versus photocurrent dependence (power characteristics) measured under different loading resistances. The maximum photovoltage (open circuit voltage, V_{oc}) and photocurrent (short circuit current, I_{sc}) were 200 mV and 165 μA cm^{-2}, respectively, while the maximum power output (P_{max}) was 19.6 μW cm^{-2} at an incident light intensity (W) of

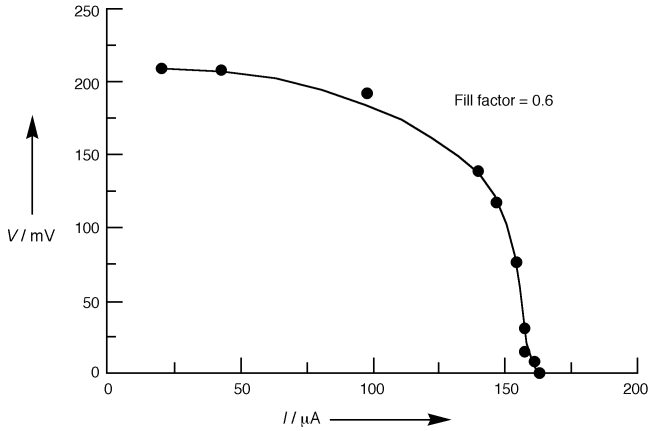

Figure 27. *The power characteristics of a OTE/TiO_2/MC540/PVP photosensitive electrode under 1.3 mW cm^{-2} illumination at 550 nm. A Pt counter electrode and 1 M LiI in 0.2 % CF_3COOH in CH_3CN electrolyte was employed. Reproduced from ref. [257] with permission.*

1.3 mW cm^{-2} (560 nm). The fill factor (f), obtained from Equation (4) and the results of Figure 27, was $f = 0.6$. These parameters yield, from Equation (5), a net power conversion efficiency (Δ) of 1.5 %.

$$f = \left(\frac{P_{max}}{V_{OC}\, I_{SC}}\right) \quad (4)$$

$$\Delta = 100\left(\frac{P_{max}}{W}\right) \quad (5)$$

The application of semiconductor particles associated with photosensitizing dyes allows the development of low cost, high efficiency solar cells which exhibit commercially realistic energy conversion efficiencies.[259] One such device was based on a 10 mm thick, optically transparent film of TiO_2 particles coated with a monolayer of a charge-transfer dye to sensitize the film for light harvesting.[259] Because of the high surface area of the semiconductor film and the ideal spectral characteristics of the dye, the device harvested a high proportion of the incident solar energy flux (46 %) and showed exceptional efficiencies for the conversion of incident photons to electrical current (> 80 %). The large current densities (> 12 mA cm^{-2}) and excellent stability of these constructions, as well as their low cost, make practical applications feasible. Sol – gel techniques[260] and electrophoretic deposition[261] of the colloids have been used successfully to improve the solar cell performance, which were well characterized by numerous methods.[262]

Substantial recent research efforts have been directed to the organization of porous high surface-area electrodes for photoelectrochemical applications and multilayer gold-nanoparticle architectures have been used for the construction of a photoelectrochemical device (Figure 28 A).[148] The multilayer gold-nanoparticle superstructure was assembled by the stepwise

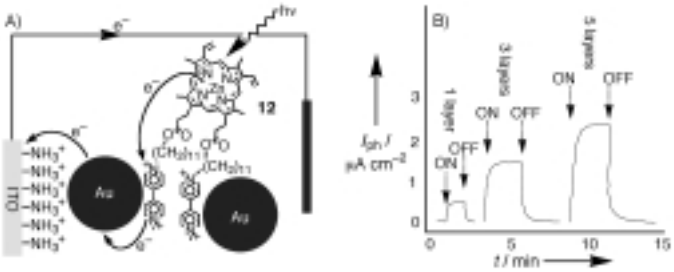

Figure 28. *A) Schematic representation of the functional part of the colloidal gold/**12** photoelectrochemical device showing the mechanism of photocurrent generation. B) The photocurrent generated by the irradiation of one-, three-, and five-layer arrays demonstrating the photocurrent dependence on assembly thickness.*

crosslinking of citrate-capped gold nanoparticles with the bis(bipyridinium)-Zn(II)/protoporphyrin IX dyad **12** acting as an electrostatic crosslinker. The presence of the photoactive porphyrin was detected in the absorbance spectrum of the array and other features were verified by cyclic voltammetry. Photoirradiation of the porphyrin component leads to electron transfer to the pendant bis(pyridinium) moieties. The gold array enables effective charge transport to the electrode, which generates a photocurrent that is controlled by the number of chromophore/acceptor and gold nanoparticle layers (Figure 28 B).

4.4.2. Electroluminescent Nanoparticle Superstructures

Semiconductor arrays have also been used for the fabrication of electroluminescent devices. In one case, a novel type of light-emitting diode (based on a CdS nanoparticle array) with two distinguishable emissions, that depend on the potential direction, was developed.[263] In another case, a hybrid organic/inorganic electroluminescent device was prepared using semiconductor nanocrystals and a conductive polymer (paraphenylene vinylene, PPV).[264] Five layers of CdSe nanoparticles, with hexanedithiol as a layer crosslinker, were deposited onto ITO/PPV plates. The overall thickness of the nanocrystal multilayer was a few hundred Ångströms and the composite was completed with a layer of magnesium on top of the nanoparticles. The close match between the emitting layer of nanocrystals with the work function of the metal contact lead to an operating voltage of only 4 V. Upon application of bias voltage, with the ITO positively biased with respect to magnesium, holes and excess electrons are created in the PPV and the CdSe nanocrystals, respectively, and the device emits light of approximately 100 cd m^{-2} intensity (visible under normal room light). Adjustment of the applied voltage varies the region (nanoparticles or conductive polymer) where the holes and electrons meet, which provides control over the color of the

emitted light. At lower voltages, emission occurs preferentially in the CdSe layer, whereas at higher voltages the green-colored PPV layer dominates (Figure 29). Such a phenomenon has not been observed in bilayer structures of organic polymers, even when similar carrier confinement properties are reported. Additional color control, from red to yellow, can be accomplished by changing the size of the CdSe nanoparticles. The quantum efficiency (emitted photons per passing electron) achieved in this system was in the range 0.001 – 0.01 %. In a similar CdS-nanocrystal system,[265] an overall quantum efficiency of about 1 % was achieved. Further, application of CdS allowed the use of the less active aluminium metal for the electron-injecting electrode while maintaining a very low threshold voltage (3 V). A stable electroluminescence with an intensity of 150 cd m^{-2} was achieved for 1200 hours when 10 V was applied.

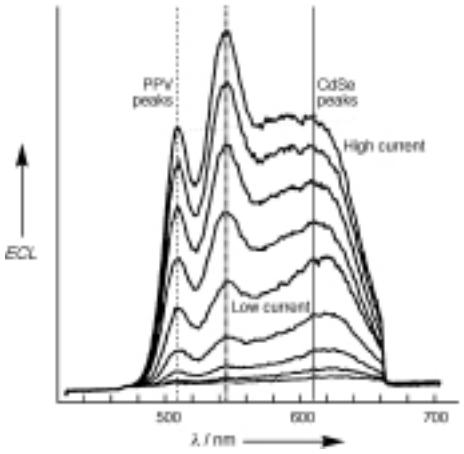

Figure 29. *Electroluminescence spectrum of the CdSe/PPV composite over a range of voltages and demonstrates a color change with the applied potential. ECL = electrochemically generated chemiluminescence intensity. Reproduced from ref. [264] with permission.*

Size-dependent photoemission of a quantum-dot system composed of CdS nanoparticles assembled onto thiol-terminated monolayers on metal surfaces (Au or Al) has been demonstrated.[266] A narrow, electroluminescent emission band was achieved when nearly monodisperse CdSe nanocrystals and a PPV layer were applied to an electroluminescence device.[267] The emission band was tunable with the size of nanoparticles. Conversely, a system composed of a PPV layer and several layers of CdSe particles with a broad size distribution generated a nearly white electroluminescent light (Figure 30) because of the broad fluorescence spectrum of the semiconductor layer.[268] Such a broad emission spectra results from both the deep trap sites at the particle surface and the defects within the particle. The broad particle size distribution also contributes to the inhomogeneous spectral broadening.

Dual properties of photocurrent generation and electroluminescence were found in hybrid devices, which consist of a nanoparticle semiconductor layer and a polymer layer.[269] Polymers such as poly(3-hexylthiophene), poly(2-methoxy-5-(2-ethylhexoxy)-1,4-phenylenevinylene), and poly(6-fluoro-dioxydecyl benzoxazole) covered wide spectral range with absorption

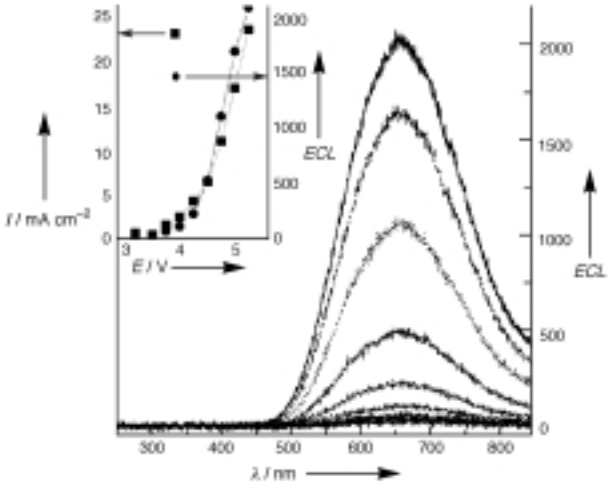

Figure 30. *Electroluminescence spectra of the CdSe/PPV device under ambient conditions and a positive bias on the ITO electrode. Inset: Electroluminescent intensity as a function of voltage. Reproduced from ref. [268] with permission.*

edges at 605, 560, and 495 nm, respectively. Monodisperse nanoparticles of CdS (mean size 4.4 and 2.2 nm) capped with 1-thioglycerol were spin coated on the polymer layer. The polymer/nanoparticle bilayer was sandwiched between an ITO plate (polymer side) and vacuum-evaporated aluminium (CdS side). It was observed that the spectral response and efficiency of the photocurrent in these multilayer devices are similar to that of the semiconductor component, whereas the spectral responses of the electroluminescence are closer to that of the polymer layer. Variation of the polymers and the sizes of CdS particles provided tunability of the photocurrent and electroluminescence spectra.

Composite materials consisting of electroluminescent polymers with implanted oxide nanoparticles were applied for the construction of light-emitting diodes. For example, a light-emitting diode based on PPV derivatives with incorporated mixed-oxide nanoparticles gives an enhancement of the current density and radiance by more than an order of magnitude at low voltage.[270] As a result, in these polymer/nanoparticle composite devices, radiances of 10 000 cd m^{-2} have been achieved at a drive voltage of only 5 V. Study of the mechanism responsible for this enhancement revealed that incorporation of nanoparticles into the electroluminescent polymer matrix results in the reduction of the effective layer thickness.[271] Both the magnitude and field dependence of the current are consistent with the assumption that the electrically effective thickness of a composite layer is about half of its physical thickness. Thus, the incorporation of nanoparticles into an electroluminescent polymer opens the possibility to combine the advantages of thick layers for mechanical strength and improved substrate coverage with the favorable electro-optic properties of a thin-layer device.

5. Conclusions, Perspectives, and Future Directions

It is clear that the unique properties of colloidal nanoparticles have much to contribute to the construction of surface-bound

nanostructures. Apart from their use as structural components, they have many useful properties which can be tuned by control over the particle size and can be utilized in the fabrication of nanostructured devices (e.g. surface morphology, electrochemical and photoelectrochemical activity, surface plasmon, surface-enhanced Raman scattering). Methods are available for the facile bulk-scale synthesis of monodisperse nanoparticles of many materials and surface functions, and the techniques for their analysis (for example, microscopy, light scattering, and spectroscopy) are now well developed.

The assembly of nanoparticles on solid substrates has been well studied and has given rise to a multitude of techniques for their immobilization on a wide range of conductive, semiconductive, and insulating substrates. Methods to produce patterned arrays of colloids and to organize colloid monolayers into close-packed or well spaced arrays have been found, leading the way towards the construction of addressable arrays of nanoparticle devices. Nanoparticle multilayers have been constructed using many different types of nanoparticle, even with different types in the same architecture. Other materials, such as polymers and molecular species, can also act as a functional part of the architecture, often while acting as a "glue" to hold the structure together. One factor that is missing from the synthesis of three-dimensional nanoparticle superstructures, however, is a high degree of three-dimensional organization. While superstructures may be composed of distinct layers, the exact alignment of each layer with respect to those around it (as well as the two-dimensional ordering within each layer) is an elusive goal. Perhaps this issue may be addressed by the further development of sophisticated fabrication methods that are already proving successful on the millimeter scale.[272]

It is very encouraging to consider the number and diversity of applications that have benefited from research into nanoparticle superstructures. In some cases, colloidal particles may be used in place of a bulk material, providing numerous advantages over the latter. In others, qualities specific to the nanoparticles may be used to create architectures for uses such as SERS or sensory applications. Electrically conducting or semiconducting colloids have been used for the construction of several components of electrical circuits, including wires, contacts, and single-electron components. Ultimately, these devices together with patterning and three-dimensional construction techniques could even lead to nanoparticle-based integrated circuits! Finally, nanoparticle assemblies have found great success in the construction of biosensing devices. With dimensions similar to those of biomaterials, nanoparticles are a natural choice for interfacing units, and have found use in both electrochemically and optically based sensors.

The current state of the art with respect to nanoparticle devices should be put into perspective, however. Nanoparticles are only likely to find commercially viable applications where they are either more convenient than current solutions (in terms of cost, ease of manufacture, performance, and so forth) or offer new opportunities as a consequence of their unique properties. In the construction of electronic nanocircuitry, for instance (see Section 4.2.1), patterned nanoparticle monolayers will face dificulties competing with photolithography, which can now produce feature of sizes approaching 50 nm with extreme-UV irradiation, or features as small as 5 nm by electron-beam lithography. Advantages may be found for the construction of three-dimensional electronic architectures or larger feature sizes, however, as colloid nanostructures may be constructed using very cheap and readily available facilities. In the construction of the next generation of electronic components, nanoparticles are of more interest. They are essential for the construction of single-electron devices (Section 4.2.2) and the self-assembling capabilities of solution-state nanoparticles are very useful in the development of simple fabrication techniques.[20] This field is in its infancy and industrial applications of the devices are unlikely to become apparent for many years.

One area where the outlook for nanoparticle architectures is particularly bright is in the development of SERS substrates (Section 4.1.2).[216] Nanoparticle substrates are cheap, easy, and reproducible to prepare and have even brought Raman spectroscopy into the select club of single-molecule spectroscopies.[220] There are still problems to overcome though—we still need to understand how the enhancement is dependent on factors such as the particular particle and the nature of the analyte.[218] The application of nanoparticle arrays with included receptor molecules for sensory applications has some advantages over other architectures (Sections 4.3.1 and 4.3.2). Immobilized receptor interfaces have the ability to act as selective sensors with an electrochemical[273] or microgravimetric[274] signal. The high surface area, conductive nanoparticle network gives a large surface density of the receptors compared to a single-monolayer array. The highly porous network allows the analyte to penetrate inside the matrix and interact with the receptor sites, although it should be noted that these assemblies do not yet rival the sensitivities of commercial devices. Such three-dimensional recognition matrices can be also organized in polymer layers but polymers rarely provide high porosity and stability. Sensors based on nanoparticle – enzyme assemblies (Section 4.3.5) are of particularly interest, as biosensors based on electrically "wired" enzymes have become very popular over the last two decades. While there are many methods of achieving electical communication with immobilized enzymes,[275] nanoparticles offer a particularly simple route. Nanoparticles can position themselves a short distance from the active sites of enzymes and provide direct, nonmediated electron transfer. Such direct electrical coupling of enzymes with the electrode support has the potential to be more efficient than even the most sophisticated multicomponent enzyme/relay systems, although, at present, few examples exist and the exact tailoring of the assembly is a matter of trial and error.

Photoelectrochemical and electroluminescent devices are becoming increasingly important with the growing need for renewable energy sources and display technologies. Organic and bioorganic light-energy transducers have gained a great deal of attention[276] but they suffer from relatively low stability. Much more stable photocurrent generating systems can be based on nanoparticles, allowing the combination of the very complex architectures of organic materials with the high stability of inorganic compounds (Section 4.4.1). A great deal of progress has been made recently in improving the performance of

organic electroluminescence (EL) devices, some of which are now adequate for many applications. The use of nanoparticles to design EL devices has brought novel capabilities to this area (Section 4.4.2). A very narrow or broad emission band, tunable emission band, and high quantum yield emission can become possible when nanoparticles are involved in the process.

The development of this very young field of nanoparticle superstructures has taken off rapidly and will surely continue to expand. While the exploitation of gold, silver, and cadmium sulfide colloids has gained much attention, there are many other functional materials from which nanoparticles can be synthesized. In addition, there is a whole world of materials (molecular and macromolecular) which may be incorporated into nanostructured composites in order to tailor properties to exact specifications. One challenging issue for further research is the ordered organization of nanoparticle arrays on solid supports. The use of biomaterials and specific binding events for the construction of superstructures may address this issue, perhaps along with new nanofabrication techniques such as particle manipulation by scanning microscopy tips. In essence, we should expect the unexpected in the near future. Nanoparticle superstructures are still in their infancy and already provide exciting outlooks for chemists, physicists, biologists, and materials scientists from theoretical, experimental, and practical perspectives.

Received: May 4, 2000 [A 1]

[1] a) *Nanosystems*, *Molecular Machinery, Manufacturing and Computation* (Ed.: K. E. Drexler), Wiley, New York, **1992**; b) J.-M. Lehn, *Angew. Chem.* **1990**, *102*, 1347 – 1362; *Angew. Chem. Int. Ed. Engl.* **1990**, *29*, 1304 – 1319; c) F. L. Carter, A. Schultz, D. Duckworth in *Molecular Electronic Devices* (Ed.: F. L. Carter), Marcel Decker, New York, **1987**, pp. 183 – 199; d) P. Ball, *Nature* **1993**, *362*, 123; e) A. C. Benniston, A. Harriman, V. M. Lynch, *J. Am. Chem. Soc.* **1995**, *117*, 5275 – 5291; f) D. Philp, J. F. Stoddart, *Angew. Chem.* **1996**, *108*, 1242 – 286; *Angew. Chem. Int. Ed. Engl.* **1996**, *35*, 1154 – 1196.

[2] a) A. P. DeSilva, H. Q. N. Gunazatne, C. P. McCoy, *Nature* **1993**, *364*, 42 – 44; b) P. Ball, L. Garwin, *Nature* **1992**, *355*, 761 – 766; c) *Molecular Electronics* (Ed.: G. J. Ashwell), Wiley, New York, **1992**; d) B. Tieke, *Adv. Mater.* **1990**, *2*, 222 – 231; e) R. W. Wagner, J. S. Lindsey, J. Seth, V. Palaniappan, D. F. Bocian, *J. Am. Chem. Soc.* **1996**, *118*, 3996 – 3997.

[3] a) W. Göpel, *Biosens. Bioelectron.* **1998**, *13*, 723 – 728; b) I. Willner, E. Katz, B. Willner in *Sensors Update*, *Vol. 5* (Eds.: H. Baltes, W. Göpel, J. Hesse), Wiley-VCH, Weinheim, **1999**, Chap. 2, pp. 45 – 102; c) I. Willner, *Acc. Chem. Res.* **1997**, *30*, 347 – 356; d) E. Katz, V. Heleg-Shabtai, I. Willner, H. K. Rau, W. Haehnel, *Angew. Chem.* **1998**, *110*, 3443 – 3447; *Angew. Chem. Int. Ed.* **1998**, *37*, 3253 – 3256; e) E. F. Bowden, *Interface* **1997**, *6*(4), 40 – 47; f) M. Brunozi, *Biosens. Bioelectron.* **1994**, *9*, 633 – 636; g) C. Ziegler, W. Göpel, H. Hämmezle, H. Hatt, G. Jung, L. Laxhuber, H.-L. Schmidt, S. Schütz, F. Vögtle, A. Zell, *Biosens. Bioelectron.* **1998**, *13*, 539 – 571.

[4] a) J.-M. Lehn, *Supramolecular Chemistry*, VCH, Weinheim, **1995**; b) J.-M. Lehn, *Angew. Chem.* **1988**, *100*, 91 – 116; *Angew. Chem. Int. Ed. Engl.* **1988**, *27*, 89 – 112; c) I. Willner, B. Willner in *Fronties in Supramolecular Organic Chemistry and Photochemistry* (Eds.: H.-J. Schneider, H. Dürr), VCH, Weinheim, **1991**, pp. 337 – 370; d) A. C. Benniston, *Chem. Soc. Rev.* **1996**, 427 – 435; f) M. Fujita, *Acc. Chem. Res.* **1999**, *32*, 53 – 61.

[5] a) C. M. Niemeyer, *Angew. Chem.* **1997**, *109*, 603 – 606; *Angew. Chem. Int. Ed. Engl.* **1997**, *36*, 585 – 587; b) M. Aizawa, T. Hazuyama, G. F. Khan, E. Kolatake, Y. Ikaziyama, *Biosens. Bioelectron.* **1994**, *9*, 601 – 610; c) F. A. Armstrong, H. A. Heezing, J. Hirst, *Chem. Soc. Rev.* **1997**, *26*, 169 – 179; d) H.-L. Schmidt, W. Schuhmann, *Biosens. Bioelectron.* **1996**, *11*, 127 – 135.

[6] a) O. A. Matthews, A. N. Shipway, J. F. Stoddart, *Prog. Polym. Sci.* **1998**, *23*, 1 – 56; b) D. A. Tomalia, A. M. Naylor, W. A. Goddard III, *Angew. Chem.* **1990**, *102*, 119 – 157; *Angew. Chem. Int. Ed. Engl.* **1990**, *29*, 138 – 175; c) G. R. Newkome, C. N. Moorefield, F. Vögtle, *Dendritic Molecules*, VCH, Weinheim, **1996**; d) A. W. Bosman, H. M. Janssen, E. W. Meijer, *Chem. Rev.* **1999**, *99*, 1665 – 1688; e) J.-P. Majoral, A.-M. Caminade, *Chem. Rev.* **1999**, *99*, 845 – 880; f) F. Zeng, S. C. Zimmerman, *Chem. Rev.* **1997**, *97*, 1681 – 1712.

[7] *Clusters and Colloids* (Ed.: G. Schmid), VCH, Weinheim, **1994**.

[8] R. F. Khairutdinov, *Colloid J.* **1997**, *59*, 535 – 548.

[9] "Single Charge Tunneling and Coulomb Blockade Phenomena in Nanostructures": *NATO ASI Ser. Ser. B* **1992**, 294.

[10] P. Mulvaney, *Langmuir* **1996**, *12*, 788 – 800.

[11] M. M. Alvarez, J. T. Khoury, T. G. Schaaff, M. N. Shafigullin, I. Vezmar, R. L. Whetten, *J. Phys. Chem. B* **1997**, *101*, 3706 – 3712.

[12] A. P. Alivisatos, *J. Phys. Chem.* **1996**, *100*, 13 226 – 13 329.

[13] L. E. Brus, *Appl. Phys. A* **1991**, *53*, 465 – 474.

[14] a) L. N. Lewis, *Chem. Rev.* **1993**, *93*, 2693 – 2730; b) V. Kesavan, P. S. Sivanand, S. Chandrasekaran, Y. Koltypin, A. Gedanken, *Angew. Chem.* **1999**, *111*, 3729 – 3730; *Angew. Chem. Int. Ed.* **1999**, *38*, 3521 – 3523; c) Y. Okahata, H.-J. Lim, G.-I. Nakamuza, S. Hachiya, *J. Am. Chem. Soc.* **1983**, *105*, 4855 – 4859; d) Y. Okahata, K. Aziga, T. Seki, *J. Am. Chem. Soc.* **1988**, *110*, 2495 – 2500; e) R. Ahuja, P.-L. Caruso, D. Möbius, W. Paulus, H. Ringsdorf, G. Wildburg, *Angew. Chem.* **1993**, *105*, 1082; *Angew. Chem. Int. Ed. Engl.* **1993**, *32*, 1033 – 1036.

[15] A. P. Alivisatos, *Science* **1996**, *271*, 933 – 937.

[16] A. P. Alivisatos, K. P. Johnsson, X. Peng, T. E. Wilson, C. J. Loweth, M. P. Bruchez, Jr., P. G. Schultz, *Nature* **1996**, *382*, 609 – 611.

[17] a) X. Peng, T. E. Wilson, A. P. Alivisatos, P. G. Schultz, *Angew. Chem.* **1997**, *109*, 113 – 115; *Angew. Chem. Int. Ed. Engl.* **1997**, *36*, 145 – 147; b) L. C. Brousseau III, J. P. Novak, S. M. Marinakos, D. L. Feldheim, *Adv. Mater.* **1999**, *11*, 447 – 449.

[18] a) S. M. Marinakos, L. C. Brousseau III, A. Jones, D. C. Feldheim, *Chem. Mater.* **1998**, *10*, 1214 – 1219; b) G. Hornyak, M. Kröll, R. Pugin, T. Sawitowski, G. Schmid, J.-O. Bovin, G. Karsson, H. Hofmeister, S. Hopfe, *Chem. Eur. J.* **1997**, *3*, 1951 – 1956; c) S.-W. Chung, G. Markovich, J. R. Heath, *J. Phys. Chem. B* **1999**, *102*, 6685 – 6687; M. Sano, A. Kamino, S. Shinkai, *Langmuir* **1999**, *15*, 13 – 15.

[19] M. Antonietti, C. Göltner, *Angew. Chem.* **1997**, *109*, 944 – 964; *Angew. Chem. Int. Ed. Engl.* **1997**, *36*, 910 – 928.

[20] D. L. Feldheim, C. D. Keating, *Chem. Soc. Rev.* **1998**, *27*, 1 – 12.

[21] a) S. L. Westcott, S. J. Oldenburg, T. R. Lee, N. J. Halas, *Langmuir* **1998**, *14*, 5396 – 5401; b) T. Sato, H. Ahmed, *Appl. Phys. Lett.* **1997**, *70*, 2759 – 2761; c) L. Cusack, R. Rizza, A. Gorelov, D. Fitzmaurice, *Angew. Chem.* **1997**, *109*, 887 – 890; *Angew. Chem. Int. Ed. Engl.* **1997**, *36*, 848 – 851; d) R. L. Whetten, J. T. Khoury, M. M. Alvarez, S. Murthy, I. Vezmar, Z. L. Wang, P. W. Stephens, C. L. Cleveland, W. D. Luedke, U. Landman, *Adv. Mater.* **1996**, *8*, 428 – 433; e) A. Chemseddine, H. Jungblut, S. Boulmaaz, *J. Phys. Chem.* **1996**, *100*, 12 546 – 12 551; f) X. M. Lin, C. M. Sorensen, K. J. Klabunde, *Chem. Mater.* **1999**, *11*, 198 – 202; g) W. Shenton, S. A. Davis, S. Mann, *Adv. Mater.* **1999**, *11*, 449 – 452; h) Z. L. Wang, *Adv. Mater.* **1998**, *10*, 13 – 30; i) M. Li, H. Schnablegger, S. Mann, *Nature* **1999**, *402*, 393 – 395.

[22] R. C. Mucic, J. L. Storhoff, C. A. Mirkin, R. L. Letsinger, *J. Am. Chem. Soc.* **1998**, *120*, 12 674 – 12 675.

[23] D. L. Klein, R. Roth, A. K. L. Kim, A. P. Alivisatos, P. L. McEuen, *Nature* **1997**, *389*, 699 – 701.

[24] T. Sato, H. Ahmed, D. Brown, B. F. G. Johnson, *J. Appl. Phys.* **1997**, *82*, 696 – 701.

[25] R. S. Ingram, M. J. Hostetler, R. W. Murray, T. G. Schaaff, J. T. Khoury, R. L. Whetten, T. P. Bigioni, D. K. Guthrie, P. N. First, *J. Am. Chem. Soc.* **1997**, *119*, 9279 – 9280.

[26] T. Sato, H. Ahmed, *Appl. Phys. Lett.* **1997**, *70*, 2759 – 2761.

[27] H. Weller, *Angew. Chem.* **1998**, *110*, 1748 – 1750; *Angew. Chem. Int. Ed.* **1998**, *37*, 1658 – 1659.

[28] S. Yabuki, F. Mitzutani, *Electroanalysis* **1997**, *9*, 23 – 25.

[29] a) M. P. Pileni, *New J. Chem.* **1998**, 693 – 702; b) G. Schmid, L. F. Chi, *Adv. Mater.* **1998**, *10*, 515 – 526; c) C. R. Martin, *Science* **1994**, *266*, 1961 – 1966; d) J. H. Fendler, F. C. Meldrum, *Adv. Mater.* **1995**, *7*, 607 – 632.

[30] a) G. Schmid, *Chem. Rev.* **1992**, *92*, 1709 – 1727; b) N. Toshima, T. Yonezawa *New J. Chem.* **1998**, *11*, 1179 – 1201.

[31] D. A. Handley in *Colloidal Gold. Principles*, *Methods*, *and Applications*, *Vol. 1* (Ed.: M. A. Hayat), Academic Press, New York, **1989**, pp. 13 – 32.

[32] T. S. Ahmadi, Z. L. Wang, T. C. Green, A. Henglein, M. A. El-Sayed, *Science* **1996**, *272*, 1924 – 1925.
[33] J. Turkevich, P. C. Stevenson, J. Hiller, *Discuss. Faraday Soc.* **1951**, *11*, 55 – 75.
[34] C. Yee, M. Scotti, A. Ulman, H. White, M. Rafailovich, J. Sokolov, *Langmuir* **1999**, *15*, 4314 – 4316.
[35] T. Teranishi, M. Hosoe, T. Tanaka, M. Miyake, *J. Phys. Chem.* **1999**, *103*, 3818 – 3827.
[36] a) M. J. Hostetler, J. E. Wingate, C.-J. Zhong, J. E. Harris, R. W. Zashet, M. R. Clark, J. D. Londono, S. J. Green, J. J. Stokes, G. D. Wignall, G. L. Glish, M. D. Porter, N. D. Evans, R. W. Murray, *Langmuir* **1998**, *14*, 17 – 30; b) G. Frens, *Nat. Phys. Sci.* **1973**, *241*, 20 – 22.
[37] T. Cassagneau, J. H. Fendler, *J. Phys. Chem. B* **1999**, *103*, 1789 – 1793.
[38] a) R. M. Bright, M. D. Musick, M. J. Natan, *Langmuir* **1998**, *14*, 5695 – 5701; b) J. Turkevich, G. Kim, *Science* **1970**, *169*, 873 – 879; c) L. D. Rampino, F. F. Nord, *J. Am. Chem. Soc.* **1941**, *63*, 2745 – 2749.
[39] C. D. Keating, K. K. Kovaleski, M. J. Natan, *J. Phys. Chem. B* **1998**, *102*, 9404 – 9413.
[40] C. Roos, M. Schmidt, J. Ebenhoch, F. Baumann, B. Deubzer, J. Weis, *Adv. Mater.* **1999**, *11*, 761 – 766.
[41] R. H. Morriss, L. F. Collins, *J. Chem. Phys.* **1964**, *41*, 3357 – 3363.
[42] P. V. Kamat, B. J. Shanghavi, *J. Phys. Chem. B* **1997**, *101*, 7675 – 7679.
[43] R. M. Bright, D. G. Walter, M. D. Musick, M. A. Jackson, K. J. Allison, M. J. Natan, *Langmuir* **1996**, *12*, 810 – 817.
[44] K. R. Brown, M. J. Natan, *Langmuir* **1998**, *14*, 726 – 728.
[45] R. G. Freeman, M. B. Hommer, K. C. Grabar, M. A. Jackson, M. J. Natan, *J. Phys. Chem.* **1996**, *100*, 718 – 724.
[46] P. A. Buining, B. M. Humbel, A. P. Philipse, A. J. Verkleij, *Langmuir* **1997**, *13*, 3921 – 3926.
[47] a) S. R. Johnson, S. D. Evans, R. Brydson, *Langmuir* **1998**, *14*, 6639 – 6647; b) M. Brust, J. Fink, D. Bethell, D. J. Schiffrin, C. Kiely, *J. Chem. Soc. Chem. Commun.* **1995**, 1655 – 1666.
[48] M. Brust, M. Walker, D. Bethell, D. J. Schiffrin, R. Whyman, *J. Chem. Soc. Chem. Commun.* **1994**, 801 – 802.
[49] a) K. Esumi, A. Suzuki, N. Aihara, K. Usui, K. Torigoe, *Langmuir* **1998**, *14*, 3157 – 3159; b) M. E. Garcia, L. A. Baker, R. M. Crooks, *Anal. Chem.* **1999**, *71*, 256 – 258.
[50] T. Teranishi, I. Kiyokawa, M. Miyake, *Adv. Mater.* **1998**, *10*, 596 – 599.
[51] T. Teranishi, M. Hosoe, M. Miyake, *Adv. Mater.* **1997**, *9*, 65 – 67.
[52] W. P. Wuelfing, S. M. Gross, D. T. Miles, R. W. Murray, *J. Am. Chem. Soc.* **1998**, *120*, 12696 – 12697.
[53] J. P. Spatz, A. Roescher, M. Möller, *Adv. Mater.* **1996**, *8*, 337 – 340.
[54] S. Bharathi, O. Lev, *Chem. Commun.* **1997**, 2302 – 2304.
[55] L. A. Porter, Jr., D. Ji, S. L. Westcott, M. Graupe, R. S. Czernuszewicz, N. J. Halas, T. R. Lee, *Langmuir* **1998**, *14*, 7378 – 7386.
[56] N. Félidj, G. Lévi, J. Pantigny, J. Aubard, *New J. Chem.* **1998**, 725 – 732.
[57] S. G. Hickey, D. J. Riley, *J. Phys. Chem.* **1999**, *103*, 4599 – 4602.
[58] F. C. Meldrum, J. Flath, W. Knoll, *Langmuir* **1997**, *13*, 2033 – 2049.
[59] L. Spanhel, H. Weller, A. Fojtik, A. Henglein, *Ber. Bunsen-Ges. Phys. Chem.* **1987**, *91*, 88 – 94.
[60] E. Stathatos, P. Lianos, F. Del Monte, D. Levy, D. Tsiourvas, *Langmuir* **1997**, *13*, 4295 – 4300.
[61] R. Rizza, D. Fitzmaurice, S. Hearne, G. Hughes, G. Spoto, E. Ciliberto, H. Kerp, R. Schropp, *Chem. Mater.* **1997**, *9*, 2969 – 2982.
[62] a) M. L. Steigerwald, A. P. Alivisatos, J. M. Gibson, T. D. Harris, R. Kortan, A. J. Muller, A. M. Thayer, T. M. Duncan, D. C. Douglass, L. E. Brus, *J. Am. Chem. Soc.* **1988**, *110*, 3046 – 3050; b) P. Lianos, J. K. Thomas, *Chem. Phys. Lett.* **1986**, *125*, 299 – 302.
[63] M. Miyake, T. Torimoto, T. Sakata, H. Mori, H. Yoneyama, *Langmuir* **1999**, *15*, 1503 – 1507.
[64] M. Miyake, H. Matsumoto, M. Nishizawa, T. Sakata, H. Mori, S. Kuwabata, H. Yoneyama, *Langmuir* **1997**, *13*, 742 – 746.
[65] N. A. Kotov, I. Dékány, J. H. Fendler, *J. Phys. Chem.* **1995**, *99*, 13065 – 13069.
[66] X. Li, J. R. Fryer, D. J. Cole-Hamilton, *J. Chem. Soc. Chem. Commun.* **1994**, 1715 – 1716.
[67] C. B. Murray, D. J. Norris, M. G. Bawendi, *J. Am. Chem. Soc.* **1993**, *115*, 8706 – 8715.
[68] Y. Xie, Y. Qian, W. Wang, S. Zhang, Y. Zhang, *Science* **1996**, *272*, 1926 – 1927.
[69] S. D. Burnside, V. Shklover, C. Barbé, P. Comte, F. Arendse, K. Brooks, M. Grätzel, *Chem. Mater.* **1998**, *10*, 2419 – 2425.
[70] R. P. Andres, J. D. Bielefeld, J. I. Henderson, D. B. Janes, V. R. Kolagunta, C. P. Kubiak, W. J. Mahoney, R. G. Osifchin, *Science* **1996**, *273*, 1690 – 1693.
[71] G. Chumanov, K. Sokolov, B. W. Gregory, T. M. Cotton, *J. Phys. Chem.* **1995**, *99*, 9466 – 9471.
[72] J. Nedderson, G. Chumanov, T. M. Cotton, *Appl. Spectrosc.* **1993**, *47*, 1959 – 1964.
[73] T. R. Jensen, G. C. Schatz, R. P. Van Duyne, *J. Phys. Chem. B* **1999**, *103*, 2394 – 2401.
[74] J. C. Hulteen, D. A. Treichel, M. T. Smith, M. L. Duval, T. R. Jensen, R. P. Van Duyne, *J. Phys. Chem. B* **1999**, *103*, 3854 – 3863.
[75] a) D.-L. Lu, K. Tanaka, *J. Phys. Chem.* **1996**, *100*, 1833 – 1837; b) S. E. Gilbert, O. Cavalleri, K. Kern, *J. Phys. Chem.* **1996**, *100*, 12123 – 12130.
[76] R. S. Urquhart, D. N. Furlong, T. Gengenbach, N. J. Geddes, F. Grieser, *Langmuir* **1995**, *11*, 1127 – 1133.
[77] a) G. Sberveglieri, L. E. Depero, M. Ferroni, V. Guidi, G. Martinelli, P. Nelli, C. Perego, L. Sangaletti, *Adv. Mater.* **1996**, *8*, 334 – 337; b) H. Xiong, M. Cheng, Z. Zhou, J. Shen, *Adv. Mater.* **1998**, *10*, 529 – 532.
[78] M. T. Reetz, M. Winter, *J. Am. Chem. Soc.* **1997**, *119*, 4539 – 4540.
[79] M. Nagtegaal, R. Seshadri, W. Tremel, *Chem. Commun.* **1998**, 2139 – 2140.
[80] J. R. Heath, R. S. Williams, J. J. Shiang, S. J. Wind, J. Chu, C. D'Emic, W. Chen, C. L. Stanis, J. J. Bucchignano, *J. Phys. Chem.* **1996**, *100*, 3144 – 3149.
[81] a) H. Yanagi, T. Ohno, *Langmuir* **1999**, *15*, 4773 – 4776; b) Y. Plyuto, J.-M. Berquier, C. Jacqinod, C. Ricolleau, *Chem. Commun.* **1999**, 1653 – 1654; c) H. Kind, A. M. Bittner, O. Cavalleri, K. Kern, *J. Phys. Chem. B* **1998**, *102*, 7582 – 7589.
[82] I. Moriguchi, F. Shibata, Y. Teraoka, S. Kagawa, *Chem. Lett.* **1995**, 761 – 762.
[83] K. C. Grabar, R. G. Freeman, M. B. Hommer, M. J. Natan, *Anal. Chem.* **1995**, *67*, 735 – 743.
[84] a) F. Burmeister, C. Schäfle, B. Keilhofer, C. Bechinger, J. Boneberg, P. Liederer, *Adv. Mater.* **1998**, *10*, 495 – 497; b) F. Burmeister, W. Badowsky, T. Braun, S. Wieprich, J. Boneberg, P. Liederer, *Appl. Surf. Sci.* **1999**, *144 – 145*, 461 – 466.
[85] F. Burmeister, C. Schäfle, T. Matthes, M. Böhmisch, J. Boneberg, P. Leiderer, *Langmuir* **1997**, *13*, 2983 – 2987.
[86] F. Remacle, C. P. Collier, G. Markovich, J. R. Heath, U. Banin, R. D. Levine, *J. Phys. Chem. B* **1998**, *102*, 7727 – 7734.
[87] T. Sato, D. Brown, B. F. G. Johnson, *Chem. Commun.* **1997**, 1007 – 1008.
[88] A. Doron, E. Katz, I. Willner, *Langmuir* **1995**, *11*, 1313 – 1317.
[89] K. C. Grabar, K. J. Allison, B. E. Baker, R. M. Bright, K. R. Brown, R. G. Freeman, A. P. Fox, C. D. Keating, M. D. Musick, M. J. Natan, *Langmuir* **1996**, *12*, 2353 – 2361.
[90] R. G. Freeman, K. C. Grabar, K. J. Allison, R. M. Bright, J. A. Davis, A. P. Guthrie, M. B. Hommer, M. A. Jackson, P. C. Smith, D. G. Walter, M. J. Natan, *Science* **1995**, *267*, 1629 – 1632.
[91] W. J. Albery, A. J. Hillman, *Annu. Rep. Prog. Chem. Sect. C* **1981**, *78*, 377 – 437.
[92] R. W. Murray in *Electroanalytical Chemistry, Vol. 13* (Ed.: A. J. Bard), Marcel Dekker, New York, **1984**, pp. 191 – 368.
[93] J. Schmitt, P. Mächtle, D. Eck, H. Möhwald, C. A. Helm, *Langmuir* **1999**, *15*, 3256 – 3266.
[94] R. A. Hayes, M. R. Böhmer, L. G. J. Fokkink, *Langmuir* **1999**, *15*, 2865 – 2870.
[95] M. Brust, R. Etchenique, E. J. Calvo, G. J. Gordillo, *Chem. Commun.* **1996**, 1949 – 1950.
[96] T. Yonezawa, S. Onoue, T. Kunitake, *Adv. Mater.* **1998**, *10*, 414 – 416.
[97] K. C. Grabar, P. C. Smith, M. D. Musick, J. A. Davis, D. G. Walter, M. A. Jackson, A. P. Guthrie, M. J. Natan, *J. Am. Chem. Soc.* **1996**, *118*, 1148 – 1153.
[98] a) H. O. Finklea in *Electroanalytical Chemistry, Vol. 19* (Eds.: A. J. Bard, I. Rubinstein), Marcel Dekker, New York, **1996**, pp. 109 – 335; b) J. Xu, H.-L. Li, *J. Colloid Interface Sci.* **1995**, *176*, 138 – 149.
[99] K. V. Sarathy, P. J. Thomas, G. U. Kulkarni, C. N. R. Rao, *J. Phys. Chem. B* **1999**, *103*, 399 – 401.
[100] T. Zhu, X. Zhang, J. Wang, X. Fu, Z. Liu, *Thin Solid Films* **1998**, *327 – 329*, 595 – 598.
[101] K. Bandyopadhyay, V. Patil, K. Vijayamohanan, M. Sastry, *Langmuir* **1997**, *13*, 5244 – 5248.

[102] V. L. Colvin, A. N. Goldstein, A. P. Alivisatos, *J. Am. Chem. Soc.* **1992**, *114*, 5221 – 5230.

[103] a) M. Giersig, P. Mulvaney, *Langmuir* **1993**, *9*, 3408 – 3413; b) M. Giersig, P. Mulvaney, *J. Phys. Chem.* **1993**, *97*, 6334 – 6336.

[104] A. C.Templeton, D. E. Cliffel, R. W. Murray, *J. Am. Chem. Soc.* **1999**, *121*, 7081 – 7089.

[105] a) A. Milchev, E. Vassileva, V. Kertov, *J. Electroanal. Chem.* **1980**, *107*, 323 – 336; b) A. Milchev, E. Vassileva, V. Kertov, *J. Electroanal. Chem.* **1980**, *107*, 337 – 352; c) G. Gunawardena, G. Hills, I. Montenegro, B. Scharifker, *J. Electroanal. Chem.* **1982**, *138*, 225 – 239; d) G. Gunawardena, G. Hills, I. Montenegro, *J. Electroanal. Chem.* **1982**, *138*, 241 – 254; e) G. Gunawardena, D. Pletcher, A. Razaq, *J. Electroanal. Chem.* **1984**, *164*, 363 – 367; f) G. Gunawardena, G. Hills, I. Montenegro, *J. Electroanal. Chem.* **1985**, *184*, 357 – 369; g) G. Gunawardena, G. Hills, I. Montenegro, *J. Electroanal. Chem.* **1985**, *184*, 371 – 389; h) K. Shimazu, D. Weisshaar, T. Kuwana, *J. Electroanal. Chem.* **1987**, *223*, 223 – 234; i) K. Shimazu, K. Uosaki, H. Kita, Y. Nodasaka, *J. Electroanal. Chem.* **1988**, *256*, 481 – 487; j) N. Georgolios, D. Jannakoudakis, P. Karabinas, *J. Electroanal. Chem.* **1989**, *264*, 235 – 245; k) J. V. Zoval, P. R. Biernacki, R. M. Penner, *Anal. Chem.* **1996**, *68*, 1585 – 1592; l) J. V. Zoval, R. M. Stiger, P. R. Biernacki, R. M. Penner, *J. Phys. Chem.* **1996**, *100*, 837 – 844; m) J. V. Zoval, J. Lee, S. Gorer, R. M. Penner, *J. Phys. Chem. B* **1998**, *102*, 1166 – 1175; n) Z. Chen, J. Li, E. Wang, *J. Electroanal. Chem.* **1994**, *373*, 83 – 87; o) B. U. Yoon, K. Cho, H. Kim, *Anal. Sci.* **1996**, *12*, 321 – 326.

[106] M. O. Finot, G. D. Braybrook, M. T. McDermott, *J. Electroanal. Chem.* **1999**, *466*, 234 – 241.

[107] a) S. Gorer, G. S. Hsiao, M. G. Anderson, R. M. Stiger, J. Lee, R. M. Penner, *Electrochim. Acta* **1998**, *43*, 2799 – 2809; b) S. Gorer, J. C. Ganske, J. C. Hemminger, R. M. Penner, *J. Am. Chem. Soc.* **1998**, *120*, 9584 – 9593; c) M. A. Anderson, S. Gorer, R. M. Penner, *J. Phys. Chem. B* **1997**, *101*, 5895 – 5899.

[108] a) G. S. Hsiao, M. G. Anderson, S. Gorer, D. Harris, R. M. Penner, *J. Am. Chem. Soc.* **1997**, *119*, 1439 – 1448; b) R. M. Nyffenegger, B. Craft, M. Shaaban, S. Gorer, R. M. Penner, *Chem. Mater.* **1998**, *10*, 1120 – 1129.

[109] S. Gorer, R. M. Penner, *J. Phys. Chem. B* **1999**, *103*, 5750 – 5753.

[110] S. Peschel, G. Schmid, *Angew. Chem.* **1995**, *107*, 1568 – 1569; *Angew. Chem. Int. Ed. Engl.* **1995**, *34*, 1442 – 1443.

[111] J. Schmitt, G. Decher, W. J. Dressick, S. L. Brandow, R. E. Geer, R. Shashidhar, J. M. Calvert, *Adv. Mater.* **1997**, *9*, 61 – 65.

[112] M. A. Correa-Duarte, M. Giersig, N. A. Kotov, L. M. Liz-Marzán, *Langmuir* **1998**, *14*, 6430 – 6435.

[113] K. Ariga, Y. Lvov, M. Onda, I. Ichinose, T. Kunitake, *Chem. Lett.* **1997**, 125 – 126.

[114] a) Y. Hotta, K. Inukai, M. Taniguchi, A. Yamagishi, *Chem. Lett.* **1997**, 83 – 84; b) G. S. Ferguson, E. R. Kleinfeld, *Adv. Mater.* **1995**, *7*, 414 – 416.

[115] A. R. Hillman in *Electrochemical Science and Technology of Polymers*, *Vol. 1*, (Ed.: R. G. Linford), Elsevier, New York, **1987**, pp. 103 – 239.

[116] S. Rubin, G. Bar, T. N. Taylor, R. W. Cutts, T. A. Zawodzinski, Jr., *J. Vac. Sci. Technol. A* **1996**, *14*, 1870 – 1877.

[117] G. Bar, S. Rubin, R. W. Cutts, T. N. Taylor, T. A. Zawodzinski, *Langmuir* **1996**, *12*, 1172 – 1179.

[118] M. Gao, X. Zhang, B. Yang, J. Shen, *J. Chem. Soc. Chem. Commun.* **1994**, 2229 – 2230.

[119] K. S. Mayya, M. Sastry, *Langmuir* **1999**, *15*, 1902 – 1904.

[120] a) M. Sastry, K. S. Mayya, V. Patil, D. V. Paranjape, S. G. Hegde, *J. Phys. Chem. B* **1997**, *101*, 4954 – 4958; b) V. Patil, M. Sastry, *Langmuir* **1998**, *14*, 2707 – 2711.

[121] T. Torimoto, N. Tsumura, M. Miyake, M. Nishizawa, T. Sakata, H. Mori, H. Yoneyama, *Langmuir* **1999**, *15*, 1853 – 1858.

[122] a) M. Sastry, K. S. Mayya, V. Patil, *Langmuir* **1998**, *14*, 5921 – 5928; b) Y. Tian, J. H. Fendler, *Chem. Mater.* **1996**, *8*, 969 – 974.

[123] J. H. Fendler, *Chem. Mater.* **1996**, *8*, 1616 – 1624.

[124] S. Drouard, S. G. Hickey, D. J. Riley, *Chem. Commun.* **1999**, 67 – 68.

[125] C. D. Keating, K. K. Kovaleski, M. J. Natan, *J. Phys. Chem. B* **1998**, *102*, 9414 – 9425.

[126] D. Lawless, S. Kapoor, D. Meisel, *J. Phys. Chem. B* **1995**, *99*, 10329 – 10335.

[127] H. Takei, N. Shimizu, *Langmuir* **1997**, *13*, 1865 – 1868.

[128] a) M. Sastry, N. Lala, V. Patil, S. P. Chavan, A. G. Chittiboyina, *Langmuir* **1998**, *14*, 4138 – 4142; b) M. Li, K. K. W. Wong, S. Mann, *Chem. Mater.* **1999**, *11*, 23 – 26.

[129] a) R. Elghanian, J. J. Storhoff, R. C. Mucic, R. L. Letsinger, C. A. Mirkin, *Science* **1997**, *277*, 1078 – 1081; b) J. J. Storhoff, R. Elghanian, R. C. Mucic, C. A. Mirkin, R. L. Letsinger, *J. Am. Chem. Soc.* **1998**, *120*, 1959 – 1964; c) C. A. Mirkin, R. L. Letsinger, R. C. Mucic, J. J. Storhoff, *Nature* **1996**, *382*, 607 – 609.

[130] a) J. J. Storhoff, C. A. Mirkin, *Chem. Rev.* **1999**, *99*, 1849 – 1862; b) G. P. Mitchell, C. A. Mirkin, R. L. Letsinger, *J. Am. Chem. Soc.* **1999**, *121*, 8122 – 8123.

[131] D. L. Feldheim, K. C. Grabar, M. J. Natan, T. E. Mallouk, *J. Am. Chem. Soc.* **1996**, *118*, 7640 – 7641.

[132] T. Hatakeyama, K. Murakami, Y. Miyamoto, N. Yamasaki, *Anal. Biochem.* **1996**, *237*, 188 – 192.

[133] J. Liu, S. Mendoza, E. Román, M. J. Lynn, R. Xu, A. F. Kaifer, *J. Am. Chem. Soc.* **1999**, *121*, 4304 – 4305.

[134] a) L. Motte, F. Billoudet, E. Lacaze, J. Douin, M. P. Pileni, *J. Phys. Chem. B* **1997**, *101*, 138 – 144; b) M. T. Reetz, M. Winter, B. Tesch, *Chem. Commun.* **1997**, 147 – 148.

[135] a) C. B. Murray, C. R. Kagan, M. G. Bawendi, *Science* **1995**, *270*, 1335 – 1338; b) G. Schmid, M. Bäumle, N. Beyer, *Angew. Chem.* **2000**, *112*, 177 – 179; *Angew. Chem. Int. Ed.* **2000**, *39*, 181 – 183.

[136] P. V. Braun, P. Osenar, S. I. Stupp, *Nature* **1996**, *380*, 325 – 328.

[137] W. Shenton, D. Pum, U. B. Sleytr, *Nature* **1997**, *389*, 585 – 587.

[138] R. Blonder, L. Sheeney, I. Willner, *Chem. Commun.* **1998**, 1393 – 1394.

[139] M. Lahav, A. N. Shipway, I. Willner, M. Nielsen, J. F. Stoddart, *J. Electroanal. Chem.*, **2000**, *482*, 217 – 221.

[140] a) N. I. Kotyukhova, P. J. Ollivier, B. R. Martin, T. E. Mallouk, S. A. Chizhik, E. V. Buzaneva, A. D. Gorchinskiy, *Chem. Mater.* **1999**, *11*, 771 – 778; b) S. Pethkar, R. C. Patil, J. A. Kher, K. Vijayamohanan, *Thin Solid Films* **1999**, *349*, 105 – 109.

[141] T. Yonezawa, H. Matsune, T. Kunitake, *Chem. Mater.* **1999**, *11*, 33 – 35.

[142] Y. M. Lvov, J. F. Rusling, D. T. Thomsen, F. Papadimitrakopoulos, T. Kawakami, T. Kunitake, *Chem. Commun.* **1998**, 1229 – 1230.

[143] J. Tien, A. Terfort, G. M. Whitesides, *Langmuir* **1997**, *13*, 5349 – 5355.

[144] M. D. Musick, D. J. Peña, S. L. Botsko, T. M. McEvoy, J. N. Richardson, M. J. Natan, *Langmuir* **1999**, *15*, 844 – 850.

[145] a) E. Hao, B. Yang, J. Zhang, X. Zhang, J. Sun, J. Shen, *J. Mater. Chem.* **1998**, 1327 – 1328; b) R. Iler, *J. Colloid. Interface Sci.* **1996**, *21*, 569 – 594.

[146] M. Brust, C. J. Kiely, D. Bethell, D. J. Schiffrin, *J. Am. Chem. Soc.* **1998**, *120*, 12367 – 12368.

[147] A. N. Shipway, M. Lahav, R. Blonder, I. Willner, *Chem. Mater.* **1999**, *11*, 13 – 15.

[148] M. Lahav, T. Gabriel, A. N. Shipway, I. Willner, *J. Am. Chem. Soc.* **1999**, *121*, 258 – 259.

[149] M. Lahav, R. Gabai, A. N. Shipway, I. Willner, *Chem. Commun.* **1999**, 1937 – 1938.

[150] M. Lahav, A. N. Shipway, I. Willner, *J. Chem. Soc. Perkin Trans. 2* **1999**, 1925 – 1931.

[151] A. N. Shipway, M. Lahav, R. Gabai, I. Willner, *Langmuir*, in press.

[152] M. D. Musick, C. D. Keating, M. H. Keefe, M. J. Natan, *Chem. Mater.* **1997**, *9*, 1499 – 1501.

[153] T. Baum, D. Bethell, M. Brust, D. J. Schiffrin, *Langmuir* **1999**, *15*, 866 – 871.

[154] M. Brust, D. Bethell, C. J. Kiely, D. J. Schiffrin, *Langmuir* **1998**, *14*, 5425 – 5429.

[155] F. P. Zamborini, R. M. Crooks, *J. Am. Chem. Soc.* **1998**, *120*, 9700 – 9701.

[156] a) R. Resch, C. Baur, A. Bugacov, B. E. Koel, A. Madhukar, A. A. G. Requicha, P. Will, *Langmuir* **1998**, *14*, 6613 – 6616; b) S. L. Brandow, W. J. Dressick, C. S. Dulcey, T. S. Koloski, L. M. Shirey, J. Schmidt, J. M. Calvert, *J. Vac. Sci. Technol. B* **1997**, *15*, 1818 – 1824.

[157] A. Doron, E. Joselevich, A. Schlittner, I. Willner, *Thin Solid Films* **1999**, *340*, 183 – 188.

[158] B. E. Baker, N. J. Kline, P. J. Treado, M. J. Natan, *J. Am. Chem. Soc.* **1996**, *118*, 8721 – 8722.

[159] T. Sato, D. G. Hasko, H. Ahmed, *J. Vac. Sci. Technol. B* **1997**, *15*, 45 – 48.

[160] a) J.-F. Liu, L.-G. Zhang, P.-S. Mao, D.-Y. Chen, N. Gu, J.-Y. Ren, Y.-P. Wu, Z.-H. Lu, *Chem. Lett.* **1997**, 1147 – 1148; b) J.-F. Liu, L.-G. Zhang, J.-Y. Ren, Y.-P. Wu, Z.-H. Lu, P.-S. Mao, D.-Y. Chen, *Thin Solid Films* **1998**, *327 – 329*, 176 – 179.

[161] T. Vossmeyer, E. Delonno, J. R. Heath, *Angew. Chem.* **1997**, *109*, 1123 – 1125; *Angew. Chem. Int. Ed. Engl.* **1997**, *36*, 1080 – 1083.

[162] a) W. J. Dressick, C. S. Dulcey, S. L. Brandow, H. Witschi, P. F. Neeley, *J. Vac. Sci. Technol. A* **1999**, *17*, 1432 – 1440; b) S. L. Brandow, M.-S. Chen, R.

Aggarwal, C. S. Dulcey, J. M. Calvert, W. J. Dressick, *Langmuir* **1999**, *15*, 5429 – 5432.
[163] P. C. Hidber, W. Helbig, E. Kim, G. M. Whitesides, *Langmuir* **1996**, *12*, 1375 – 1380.
[164] S. Palacin, P. C. Hildber, J.-P. Bourgoin, C. Miramond, C. Fermon, G. M. Whitesides, *Chem. Mater.* **1996**, *8*, 1316 – 1325.
[165] J. L. Coffer, S. R. Bigham, R. F. Pinizzotto, H. Yang, *Nanotechnology* **1992**, *3*, 69 – 76.
[166] S. R. Bigham, J. L. Coffer, *Colloid Surf. A* **1995**, *95*, 211 – 219.
[167] J. L. Coffer, S. R. Bigham, X. Li, R. F. Pinizzotto, Y. G. Rho, R. M. Pirtle, I. L. Pirtle, *Appl. Phys. Lett*. **1996**, *69*, 3851 – 3853.
[168] J. L. Coffer, *J. Cluster Sci.* **1997**, *8*, 159 – 179.
[169] E. Braun, Y. Eichen, U. Sivan, G. Ben-Yoseph, *Nature* **1998**, *391*, 775 – 778.
[170] K. C. Grabar, K. R. Brown, C. D. Keating, S. J. Stranick, S.-L. Tang, M. J. Natan, *Anal. Chem*. **1997**, *69*, 471 – 477.
[171] G. Schmid, S. Peschel, *New J. Chem*. **1998**, 669 – 675.
[172] G. S. McCarty, P. S. Weiss, *Chem. Rev.* **1999**, *99*, 1983 – 1990.
[173] a) S. Norman, T. Andersson, C. G. Granqvist, O. Hunderi, *Phys. Rev. B* **1978**, *18*, 674 – 695; b) R. H. Dormeus, *J. Appl. Phys*. **1996**, *37*, 2775 – 2781.
[174] M. Quinten, U. Kreibig, *Surf. Sci.* **1986**, *172*, 557 – 577.
[175] S. Link, M. A. El-Sayed, *J. Phys. Chem. B* **1999**, *103*, 4212 – 4217.
[176] N. G. Khlebtsov, V. A. Bogatyrev, L. A. Dyknman, A. G. Melnikov, *J. Colloid Interface Sci*. **1996**, *180*, 436 – 445.
[177] C. P. Collier, R. J. Saykally, J. J. Shiang, S. E. Henrichs, J. R. Heath, *Science* **1997**, *277*, 1978 – 1981.
[178] C. S. Weisbecker, M. V. Merritt, G. M. Whitesides, *Langmuir* **1996**, *12*, 3763 – 3772.
[179] G. Chumanov, K. Sokolov, T. M. Cotton, *J. Phys. Chem*. **1996**, *100*, 5166 – 5168.
[180] J. J. Shiang, J. R. Heath, C. P. Collier, R. J. Saykally, *J. Phys. Chem*. *B* **1998**, *102*, 3425 – 3430.
[181] K. C. Grabar, K. J. Allison, B. E. Baker, R. M. Bright, K. R. Brown, R. G. Freeman, A. P. Fox, C. D. Keating, M. D. Musick, M. J. Natan, *Langmuir* **1996**, *12*, 2353 – 3261.
[182] C. G. Blatchford, J. R. Campbell, J. A. Creighton, *Surf. Sci*. **1982**, *120*, 435 – 455.
[183] L. A. Lyon, D. J. Peña, M. Natan, *J. Phys. Chem. B* **1999**, *103*, 5826 – 5831.
[184] a) R. Woods in *Electroanalytical Chemistry, Vol. 9* (Ed.: A. J. Bard), Marcel Dekker, New York, **1976**, pp. 1 – 162; b) D. A. J. Rand, R. Woods, *J. Electroanal. Chem*. **1971**, *31*, 29 – 38.
[185] B. E. Conway, *Prog. Surf. Sci*. **1995**, *49*, 331 – 452.
[186] M. O. Finot, G. D. Braybrook, M. T. McDermott, *J. Electroanal. Chem*. **1999**, *466*, 234 – 241.
[187] V. P. Menon, C. R. Martin, *Anal. Chem*. **1995**, *67*, 1920 – 1928.
[188] X.-Y. Hu, Y. Xiao, H.-Y. Chen, *J. Electroanal. Chem*. **1999**, *466*, 26 – 30.
[189] D. L. Gittins, D. Bethell, R. J. Nichols, D. J. Schiffrin, *Adv. Mater.* **1999**, *11*, 737 – 740.
[190] D. Bethell, M. Brust, D. J. Schiffrin, C. Kiely, *J. Electroanal. Chem*. **1996**, *409*, 137 – 143.
[191] M. Brust, D. Bethell, D. J. Schiffrin, C. J. Kiely, *Adv. Mater.* **1995**, *7*, 795 – 797.
[192] Y. J. Liu, Y. X. Wang, R. O. Claus, *Chem. Phys. Lett*. **1998**, *298*, 315 – 319.
[193] J.-C. Bradley, H.-M. Chen, J. Crawford, J. Eckert, K. Ernazarova, T. Kurzeja, M. Lin, M. McGee, W. Nadler, S. G. Stephens, *Nature* **1997**, *389*, 268 – 271.
[194] G. Markovich, C. P. Collier, J. R. Heath, *Phys. Rev. Lett*. **1998**, *80*, 3807 – 3810.
[195] C. P. Collier, R. J. Saykally, J. J. Shiang, S. E. Henrichs, J. R. Heath, *Science* **1997**, *277*, 1978 – 1981.
[196] W. J. Albery, N. Bartlett, *J. Electrochem. Soc*. **1984**, *131*, 315 – 325.
[197] P. E. Lippens, M. Lannoo, *Phys. Rev. B* **1989**, *39*, 10935 – 10942.
[198] S. Ogawa, F.-R. F. Fan, A. J. Bard, *J. Phys. Chem*. **1995**, *99*, 11182 – 11189.
[199] B. Alperson, H. Demange, I. Rubinstein, G. Hodes, *J. Phys. Chem. B* **1999**, *103*, 4943 – 4948.
[200] Y. Nosaka, *J. Phys. Chem*. **1991**, *95*, 5054 – 5058.
[201] T. Serizawa, H. Takeshita, M. Akashi, *Chem. Lett*. **1998**, 487 – 488.
[202] H. Schmitt, A. Badia, L. Dickinson, L. Reven, R. B. Lennox, *Adv. Mater.* **1998**, *10*, 475 – 479.
[203] C. Demaille, M. Brust, M. Tsionsky, A. J. Bard, *Anal. Chem*. **1997**, *69*, 2323 – 2328.
[204] M. S. Sibbald, G. Chumanov, T. M. Cotton, *J. Electroanal. Chem*. **1997**, *438*, 179 – 185.
[205] a) J. M. Weissman, H. B. Sunkara, A. S. Tse, *Science* **1996**, *274*, 959 – 960; b) J. H. Holtz, S. A. Asher, *Nature* **1997**, *389*, 829 – 832.
[206] a) F. Patolsky, B. Filanovsky, E. Katz, I. Willner, *J. Phys. Chem. B* **1998**, *102*, 10359 – 10367; b) A. Bardea, F. Patolsky, A. Dagan, I. Willner, *Chem. Commun*. **1999**, 21 – 22.
[207] L. Alfonta, A. Bardea, O. Khersonsky, E. Katz, I. Willner, *Biosens. Bioelectron.*, in press.
[208] A. Bardea, A. Dagan, I. Willner, *Anal. Chim. Acta* **1999**, *385*, 33 – 43.
[209] R. Blonder, S. Levi, G. Tao, I. Ben-Dov, I. Willner, *J. Am. Chem. Soc*. **1997**, *119*, 10467 – 10478.
[210] a) I. Willner, S. Rubin, Y. Cohen, *J. Am. Chem. Soc*. **1993**, *115*, 4937 – 4938; b) P. Skládal, *Electroanalysis* **1997**, *9*, 737 – 745.
[211] a) A. Bardea, A. Dagan, I. Ben-Dov, A. Amit, I. Willner, *Chem. Commun*. **1998**, 839 – 840; b) A. L. Ghindilis, P. Atanasov, M. Wilkins, E. Wilkins, *Biosens. Bioelectron*. **1998**, *13*, 113 – 131.
[212] D. D. Schlereth, *J. Electroanal. Chem*. **1999**, *464*, 198 – 207.
[213] W. Göpel, P. Heiduschka, *Biosens. Bioelectron*. **1995**, *10*, 853 – 883.
[214] a) E. Kaganer, R. Pogreb, D. Davidov, I. Willner, *Langmuir* **1999**, *15*, 3920 – 3923; b) B. Liedberg, C. Nylander, I. Lundström, *Biosens. Bioelectron*. **1995**, *10*, i – ix.
[215] L. A. Lyon, M. D. Musick, M. J. Natan, *Anal. Chem*. **1998**, *70*, 5177 – 5183.
[216] a) A. Campion, P. Kambhampati, *Chem. Soc. Rev.* **1998**, *27*, 241 – 250; b) M. Moskovits, *Rev. Mod. Phys*. **1985**, *57*, 783 – 826.
[217] J. A. Creighton, C. G. Blatchford, M. G. Albrecht, *J. Chem. Soc. Faraday Trans. 2* **1979**, *75*, 790 – 798.
[218] J. C. Jones, C. McLaughlin, D. Littlejohn, D. A. Sadler, D. Graham, W. E. Smith, *Anal. Chem*. **1999**, *71*, 596 – 601.
[219] D. P. Tsai, J. Kovacs, Z. Wang, M. Moskovits, V. M. Shalaev, J. S. Suh, R. Botet, *Phys. Rev. Lett*. **1994**, *72*, 4149 – 4152.
[220] S. Nie, S. R. Emory, *Science* **1997**, *275*, 1102 – 1106.
[221] K. R. Brown, A. P. Fox, M. J. Natan, *J. Am. Chem. Soc*. **1996**, *118*, 1154 – 1157.
[222] a) F. A. Armstrong, H. A. O. Hill, N. J. Walton, *Q. Rev. Biophys*. **1986**, *18*, 261 – 322; b) F. A. Armstrong, H. A. O. Hill, N. J. Walton, *Acc. Chem. Res*. **1988**, *21*, 407 – 413.
[223] E. J. Laviron, *Electroanal. Chem*. **1979**, *101*, 19 – 28.
[224] J. Liu, R. Xu, A. E. Kaifer, *Langmuir* **1998**, *14*, 7337 – 7339.
[225] R. S. Ingram, R. W. Murray, *Langmuir* **1998**, *14*, 4115 – 4121.
[226] U. Simon, R. Flesch, H. Wiggers, G. Schön, G. Schmid, *J. Mater. Chem*. **1998**, *8*, 517 – 518.
[227] a) U. Simon, G. Schön, G. Schmid, *Angew. Chem. Int. Ed. Engl*. **1993**, *32*, 250 – 254; *Angew. Chem*. **1993**, *105*, 264; b) G. Schmid in *Clusters and Colloids. From Theory to Applications*, (Ed.: G. Schmid), VCH, Weinheim, **1994**, pp. 178 – 211.
[228] D. L. Klein, P. L. McEuen, J. E. Bowen Katari, R. Roth, A. P. Alivisatos, *Appl. Phys. Lett*. **1996**, *68*, 2574 – 2576.
[229] R. P. Andres, T. Bein, M. Dorogi, S. Feng, J. I. Henderson, C. P. Kubiak, W. Mahoney, R. G. Osifchin, R. Reifenberger, *Science* **1996**, *272*, 1323 – 1325.
[230] a) S. J. Green, J. J. Stokes, M. J. Hostetler, J. Pietron, R. W. Murray, *J. Phys. Chem. B* **1997**, *101*, 2663 – 2668; b) B. Sweryda-Krawiec, T. Cassagneau, J. H. Fendler, *Adv. Mater.* **1999**, *11*, 659 – 664.
[231] L. F. Chi, M. Hartig, T. Drechsler, T. Schaak, C. Seidel, H. Fuchs, G. Schmid, *Appl. Phys. Lett*. **1998**, *66*, S187-S190.
[232] U. Simon, *Adv. Mater.* **1998**, *10*, 1487 – 1492.
[233] a) J. R. Tucker, *J. Appl. Phys*. **1992**, *71*, 4399 – 4404; b) A. N. Korotkov, R. H. Chen, K. Likharev, *J. Appl. Phys*. **1995**, *78*, 2520 – 2530.
[234] J. B. Barner, S. T. Ruggerio, *Phys. Rev. Lett*. **1987**, *59*, 807 – 810.
[235] K. K. Likharev, T. Claeson, *Sci. Am*. **1992**, *266*(6), 50 – 55.
[236] R. F. Service, *Science* **1997**, *275*, 303 – 304.
[237] E. Corcoran, *Sci. Am*. **1990**, *263*(11), 74 – 83.
[238] L. C. Brousseau III, Q. Zhao, D. A. Shultz, D. L. Feldheim, *J. Am. Chem. Soc*. **1998**, *120*, 7645 – 7646.
[239] L. Guo, G. Lingjie, E. Leobandung, S. Y. Chou, *Science* **1997**, *275*, 649 – 651.
[240] S. Tiwari, F. Rana, H. Hanafi, A. Hartstein, E. F. Crabbe, K. Chan, *Appl. Phys. Lett*. **1996**, *68*, 1377 – 1379.
[241] a) M. S. Montemerlo, J. C. Love, G. J. Opiteck, D. Goldhaber-Gordon, J. C. Ellenbogen, *Technologies and Designs for Electronic Nanocomputers*, Mitre Corp., McLean, VA (USA), **1996**; b) A. O. Orlov, I. Amlani, G. H. Berstein, C. S. Lent, G. L. Snider, *Science* **1997**, *277*, 928 – 930.
[242] H. Wohltjen, A. W. Snow, *Anal. Chem*. **1998**, *70*, 2856 – 2859.
[243] T. E. Young, B. W. Babbit, *J. Org. Chem*. **1983**, *48*, 562 – 566.

[244] a) A. B. Kharitonov, A. N. Shipway, I. Willner, *Anal. Chem.* **1999**, *71*, 5441 – 5443; b) A. B. Kharitonov, A. N. Shipway, E. Katz, I. Willner, *Rev. Anal. Chem.* **1999**, *18*, 255 – 260.

[245] H. Tsukube, H. Furuta, A. Odani, Y. Takeda, Y. Kudo, Y. Inoue, Y. Liu, H. Sakamoto, K. Kimura in *Comprehensive Supramolecular Chemistry, Vol. 8* (Eds.: J.-M. Lehn, J. L. Atwood, J. E. D. Davies, D. D. MacNicol, F. Vögtle), Pergamon Press, Oxford, **1996**, pp. 425 – 482.

[246] J. Zhao, R. W. Henkens, J. Stonehuerner, J. P. O'Daly, A. L. Crumbliss, *J. Electroanal. Chem*. **1992**, *327*, 109 – 119.

[247] a) S. D. Varfolomeev, I. N. Kurochkin, A. I. Yaropolov, *Biosens. Bioelectron*. **1996**, *11*, 863 – 871; b) A. L. Ghindilis, P. Atanasov, E. Wilkins, *Electroanalysis* **1997**, *9*, 661 – 674.

[248] Y. Xiao, H.-X. Ju, H.-Y. Chen, *Anal. Chim. Acta* **1999**, *391*, 73 – 82.

[249] E. Katz, H.-L. Schmidt, *J. Electroanal. Chem*. **1993**, *360*, 337 – 342.

[250] a) Y. Degani, A. Heller, *J. Phys. Chem*. **1987**, *91*, 1285 – 1289; b) W. Schuhmann, T. J. Ohara, H.-L. Schmidt, A. Heller, *J. Am. Chem. Soc*. **1991**, *113*, 1394 – 1397.

[251] F. Patolsky, T. Gabriel, I. Willner, *J. Electroanal Chem.* **1999**, *479*, 69 – 73.

[252] O. D. Velev, E. W. Kaler, *Langmuir* **1999**, *15*, 3693 – 3698.

[253] M. Grätzel, *Nanocrystalline Electronic Junctions*, in *Semiconductor Nanoclusters—Physical, Chemical and Catalytic Aspects* (Eds.: P. V. Kamat, D. Meisel), Elsevier, Amsterdam, **1997**, p. 353.

[254] P. V. Kamat in *Nanoparticles and Nanostructural Films* (Ed.: J. Fendler), Wiley-VCH, Weinheim, **1998**, p. 207.

[255] S. Ogawa, K. Hu, F.-R. F. Fan, A. J. Bard, *J. Phys. Chem.* **1997**, *101*, 5707 – 5711.

[256] a) L. Spanhel, H. Weller, A. Henglein, *J. Am. Chem. Soc*. **1987**, *109*, 6632 – 6635; b) K. R. Godipas, M. Bohorquez, P. V. Kamat, *J. Phys. Chem*. **1990**, *94*, 6435 – 6440; c) N. Serpone, E. Borgarello, M. Grätzel, *J. Chem. Soc. Chem. Commun*. **1984**, 342 – 344; d) P. Pichat, E. Borgarello, J. Disdier, J.-M. Herrmann, E. Pelizzetti, N. Serpone, *J. Chem. Soc. Faraday Trans. 1* **1988**, *84*, 261 – 274; e) N. Serpone, E. Borgarello, E. Pelizzetti, *J. Electrochem. Soc.* **1988**, *135*, 2760 – 2766.

[257] A. C. Khazraji, S. Hotchandani, S. Das, P. V. Kamat, *J. Phys. Chem. B* **1999**, *103*, 4693 – 4700.

[258] I. Willner, Y. Eichen, B. Willner, *Res. Chem. Intermed*. **1994**, *20*, 681 – 700.

[259] a) B. O'Regan, M. Grätzel, *Nature* **1991**, *353*, 737 – 740; b) U. Bach, D. Lupo, P. Comte, J. E. Moser, F. Weissortel, J. Salbeck, H. Spreitzer, M. Grätzel, *Nature* **1998**, *395*, 583 – 585.

[260] S. D. Burnside, V. Shklover, C. Barbé, P. Comte, F. Arendse, K. Brooks, M. Grätzel, *Chem. Mater.* **1998**, *10*, 2419 – 2425.

[261] D. Matthews, A. Kay, M. Grätzel, *Aust. J. Chem.* **1994**, *47*, 1869 – 1877.

[262] a) L. Kavan, M. Grätzel, J. Rathousky, A. Zukal, *J. Electrochem. Soc.* **1996**, *143*, 394 – 400; b) V. Shklover, M.-K. Nazeeruddin, S. M. Zakeeruddin, C. Barbé, A. Kay, T. Haibach, W. Steurer, R. Hermann, H.-U. Nissen, M. Grätzel, *Chem. Mater.* **1997**, *9*, 430 – 439.

[263] T. Cassagneau, T. E. Mallouk, J. H. Fendler, *J. Am. Chem. Soc*. **1998**, *120*, 7848 – 7859.

[264] V. L. Colvin, M. C. Schlamp, A. P. Alivisatos, *Nature* **1994**, *370*, 354 – 357.

[265] N. D. Kumar, M. P. Joshi, C. S. Friend, P. N. Prasad, R. Burzynski, *Appl. Phys. Lett*. **1997**, *71*, 1388 – 1390.

[266] a) V. L. Colvin, A. P. Alivisatos, J. G. Tobin, *Phys. Rev. Lett*. **1991**, *66*, 2786 – 2789; b) B. O. Dabbousi, C. B. Murray, M. F. Rubner, M. G. Bawendi, *Chem. Mater.* **1994**, *6*, 216 – 219.

[267] B. O. Dabbousi, M. G. Bawendi, O. Onitsuka, M. F. Rubner, *Appl. Phys. Lett*. **1995**, *66*, 1316 – 1318.

[268] M. Gao, B. Richter, S. Kirstein, *Adv. Mater.* **1997**, *9*, 802 – 805.

[269] K. S. Narayan, A. G. Manoj, J. Nanda, D. D. Sarma, *Appl. Phys. Lett*. **1999**, *74*, 871 – 873.

[270] S. A. Carter, J. C. Scott, P. J. Brock, *Appl. Phys. Lett*. **1997**, *71*, 1145 – 1147.

[271] P. W. M. Blom, H. F. M. Schoo, M. Matters, *Appl. Phys. Lett*. **1998**, *73*, 3914 – 3916.

[272] A. Terfort, N. Bowden, G. M. Whitesides, *Nature* **1997**, *386*, 162 – 164; N. Bowden, A. Terfort, J. Carbeck, G. M. Whitesides, *Science* **1997**, *276*, 233 – 235; W. T. Huck, J. Tien, G. M. Whitesides, *J. Am. Chem. Soc.* **1998**, *120*, 8267 – 8268; J. Tien, T. L. Breen, G. M. Whitesides, *J. Am. Chem. Soc.* **1998**, *120*, 12670 – 12671.

[273] a) P. He, J. Ye, Y. Fang, I. Suzuki, T. Osa, *Electroanalysis* **1997**, *9*, 68 – 73; b) M. T. Rojas, R. Königer, J. F. Stoddart, A. E. Kaifer, *J. Am. Chem. Soc.* **1995**, *117*, 336 – 343.

[274] J. Rickert, T. Weiss, W. Kraas, G. Jung, W. Göpel, *Biosens. Bioelectron.* **1996**, *11*, 591 – 598.

[275] I. Willner, E. Katz, *Angew. Chem.* **2000**, *112*, 1230 – 1269; *Angew. Chem. Int. Ed.* **2000**, *39*, 1180 – 1218.

[276] a) J.-P. Collin, A. Harriman, V. Heitz, F. Odobel, J.-P. Sauvage, *J. Am. Chem. Soc.* **1994**, *116*, 5679 – 5690; b) A. C. Benniston, A. Harriman, *J. Am. Chem. Soc.* **1994**, *116*, 11 531 – 11 537; c) H. Imahori, Y. Sakata, *Adv. Mater.* **1997**, *9*, 537 – 546; d) X. Marguerettaz, D. Fitzmaurice, *J. Am. Chem. Soc.* **1994**, *116*, 5017 – 5018; e) K. Uosaki, T. Kondo, X.-Q. Zhang, M. Yanagida, *J. Am. Chem. Soc.* **1997**, *119*, 8367 – 8368; f) S. Yamada, Y. Koide, T. Matsuo, *J. Electroanal. Chem.* **1997**, *426*, 23 – 26; g) H. Imahori, H. Yamada, S. Ozawa, K. Ushida, Y. Sakata, *Chem. Commun.* **1999**, 1165 – 1166; h) E. Katz, *J. Electroanal. Chem.* **1994**, *365*, 157 – 164; i) E. Katz, A. Y. Shkuropatov, O. I. Vagabova, V. A. Shuvalov, *Biochim. Biophys. Acta* **1989**, *976*, 121 – 128; j) A. A. Solov'ev, E. Katz, V. A. Shuvalov, Y. E. Erokhin, *Bioelectrochem. Bioenerg.* **1991**, *26*, 29 – 41.

[277] *Note Added in Proof (July 12, 2000):* The topic of nanoparticle expands rapidly and, in the course of the publication of this review, important advances have been made. In particular, the organization and patterning of nanoparticle arrays has received attention leading to evaporation-driven self-assembly,[278] templated nanoparticle deposition,[279] and increased attention in CCAs[280] and the use of nanoparticle arrays as templates.[281] Patterning by scanning probe microscopy[282] and stamping[283] techniques have been developed further, as has the understanding of the physical properties of nanoparticle arrays.[284] New functions of nanoparticle arrays have been developed, such as ion-gating recognition.[285] Most notable, biomolecule-linked nanoparticle assemblies have gained significant research efforts.[286] Multilayer and dendron-like structures of DNA-linked nanoparticles have been constructed on gold and glass surfaces and the construction procedure has been used for the detection of DNA analytes.[287]

[278] a) S. Maenosono, C. D. Dushkin, S. Saita, Y. Yamaguchi, *Langmuir* **1999**, *15*, 957 – 965; b) C. J. Kiely, J. Fink, G. Zheng, M. Brust, D. Bethell, D. J. Schiffrin, *Adv. Mater.* **2000**, *12*, 640 – 643.

[279] J. P. Spatz, S. Mossmer, C. Hartmann, M. Möller, T. Herzog, M. Krieger, H. G. Boyen, P. Ziemann, B. Kabius, *Langmuir* **2000**, *16*, 407-415.

[280] a) Y. Xia, B. Gates, Y. Yin, Y. Lu, *Adv. Mater.* **2000**, *12*, 693 – 713; b) A. Rogach, A. Sucha, F. Caruso, G. Sukhorokov, A. Kornowski, S. Kershaw, H. Möhwald, A. Eychmüller, H. Weller, *Adv. Mater.* **2000**, *12*, 333 – 337.

[281] a) Z. Zhong, Y. Yin, B. Gates, Y. Xia, *Adv. Mater.* **2000**, *12*, 206 – 209; b) J. E. G. J. Wijnhoven, S. J. M. Zevenhuizen, M. A. Hendriks, D. Vanmaekelbergh, J. J. Kelly, W. L. Vos, *Adv. Mater.* **2000**, *12*, 888 – 890; c) K. M. Kulinowski, P. Jiang, H. Vaswani, V. L. Colvin, *Adv. Mater.* **2000**, *12*, 833 – 837.

[282] a) J. W. Zheng, Z. H. Zhu, H. F. Chen, Z. F. Liu, *Langmuir* **2000**, *16*, 4409 – 4412; b) R. Resch, D. Lewis, S. Meltzer, N. Montoya, B. E. Koel, A. Madhukar, A. A. G. Requicha, P. Will, *Ultramicroscopy* **2000**, *82*, 135 – 139; c) R. Maoz, E. Frydman, S. R. Cohen, J. Sagiv, *Adv. Mater.* **2000**, *12*, 424 – 429.

[283] a) H. X. He, H. Zhang, Q. G. Li, T. Zhu, S. F. Y. Li, Z. F. Liu, *Langmuir* **2000**, *16*, 3846 – 3851.

[284] a) N. Del Fatti, F. Vallee, C. Flytzanis, Y. Hamanaka, A. Nakamura, *Chem. Phys.* **2000**, *251*, 215 – 226; b) J. P. Novak, D. L. Feldheim, *J. Am. Chem. Soc.* **2000**, *122*, 3979 – 3980; c) F. P. Zamborini, J. F. Hicks, R. W. Murray, *J. Am. Chem. Soc.* **2000**, *122*, 4514 – 4515; d) D. M. Kolb, G. E. Engelmann, J. C. Ziegler, *Angew. Chem. Int. Ed.* **2000**, *39*, 1123 – 1125.

[285] W. Zheng, M. M. Maye, F. L. Leibowitz, C.-J. Zhong, *Anal. Chem.* **2000**, *72*, 2190 – 2199.

[286] S. Mann, W. Shenton, M. Li, S. Connolly, D. Fitzmaurice, *Adv. Mater.* **2000**, *12*, 147 – 150.

[287] a) F. Patolsky, K. T. Ranjit, A. Lichtenstein, I. Willner, *Chem. Commun.* **2000**, 1025 – 1026; b) T. A. Taton, R. C. Mucic, C. A. Mirkin, R. L. Letsinger, *J. Am. Chem. Soc.* **2000**, *122*, 6305 – 6306.